Growth of the Preserved Continental Crust

Integrated U-Pb, O, and Hf isotopic systematics of detrital zircons from Australia and Antarctica

Bei Chen

A thesis submitted for the degree of Doctor of Philosophy of

The Australian National University

December 2021

Declaration

The work presented in this thesis was carried out while I was a full-time student at the Research School of Earth Sciences, at the Australian National University, Canberra, Australia, between November 2016 and November 2021. Except where acknowledged in the text, the research described here is, to the best of my knowledge, original and has not been submitted in whole or part for a degree in any university.

Bei Chen

Canberra, December 2021

Acknowledgements

Throughout these several years of my PhD study, I have received lots of support and help to finish this long but self-developing journey in Australia.

Firstly, I would like to express my sincere gratitude to my supervisor panel members. Thank Prof. Ian Williams for his sincere help and generous support in both life and research. I am profoundly grateful for his encouragement and guidance to help me through many hard times. Thank Prof. Ian H. Campbell for his help and suggestions for my PhD lab work and research projects. His academic guidance greatly helped me in all these years of study and writings. I am also greatly grateful to have wonderful comments and suggestions from Prof. Richard Arculus about my manuscripts. And Prof. Richard Armstrong provided his generous assistance of lab work and data processing, and many valuable suggestions to my project in all study stages. Without their aid and invaluable supports, my research would have been impossible. They provided me not only lots of useful comments and encouragement but also important questions on my research topic leading me to expand my horizons and enhance my logical thinking in multiple dimensions.

I also would like to thank the China Scholarship Council (File No. 201604910679) and RSES for financial support to study abroad, which made this expedition happen.

Heartfelt thanks to my amazing adviser Charlotte Allen who teaches me how to conduct lab works from scratch when I first arrived in Australia. Her passion for science and nature as well tells me how to enjoy the exploration of scientific questions and wildlife. I truly appreciated all her help and suggestions during my whole PhD journey.

My sincere thanks to the lab managers in RSES: Shane Paxton, Peter Holder, Janaina Ávila, Bin Fu, Leslie Kinsley, Gabriel Enge and Brett Knowles. They provided enormous help for all my lab works. Without the completion of experiments, this research is never going to be accomplished.

My thanks also go to my research group members: Mimi Chen, Hongda Hao, Monika Misztela, Zhijie Huang, Jessica Lowczak, Carlos Carrasco Godoy and Yamila Cajal

Contreras. I have received huge supports and love from them to help me to overcome the difficulties on research and life issues.

I felt extremely lucky that while studying in Australia, I met all the great friends from all over the world. They made my PhD life so wonderful and amazing and comforted me while I was struggling. I greatly enjoyed the fabulous time with them.

And last but by no means the least, I would like to thank my family: my parents and friends in China for supporting me spiritually throughout writing this thesis, my whole PhD study, and my life. When I was frustrated by obstacles of study, their encouragement and accompany made me stronger to face difficulties and solve problems. With their sincere love and backup, I become more confident to conquer the challenges in the future and ready to welcome the amazing future ahead of me!

Abstract

A fundamental question concerning Earth's evolution is when and how the continental crust has formed. Multiple models (steady-state, episodic, continuous, or early growth followed by crustal recycling) have been proposed to explain the growth of Earth's continental crust, but without consensus. The resistant mineral zircon has been widely used to study crust-mantle evolution. This thesis reports the results of an integrated U-Pb, O and Lu-Hf isotopic study of detrital zircons carried out to better understand the evolutionary history of the preserved continental crust on both continental and global scales.

Detrital zircons from glacial deposits derived from the Antarctic continent were analyzed for U-Pb, O and Lu-Hf isotopic compositions. To minimize sampling bias, the U-Pb age distributions were weighted according to the land area within Antarctica sampled by the particular ice flow feeding each deposit. The use of weighting provided a more accurate and realistic detrital zircon record for the Antarctic continent than raw numbers. The overwhelming abundance of Pan-African-aged zircons (650–450 Ma) in those deposits shows that the assembly of Gondwana was the most important tectonic event that profoundly impacted the detrital zircon record. The detritus shed from the Pan-African collisional orogens fed the source materials for magmatism during 650–450 Ma, resulting in a high abundance of zircons with sediment-dominated (S-type magma) signatures. The zircon Hf model age results were also weighted according to the previously weighted distributions of the U-Pb age groups, reducing the inherent bias of selecting zircons for Lu-Hf isotopic analyses during data collection. The weighted results of both U-Pb ages and Hf model ages show that Archean terranes are a smaller component of Antarctica than previous studies supposed. The significant growth of the Antarctic continental crust was one billion years later than that of other well-studied continents. The detrital zircon records according to the successive weighting approach show that only 8% of the Antarctic continental crust had formed by the end of the Archean, with the significant growth peaking between 2.2 and 1.1 Ga.

A similar detailed integrated detrital zircon study was also conducted for the Australian continent, applying similar successive weighting procedures. Weighted

according to the catchment area, the U-Pb age peaks from many detrital zircons are consistent with the magmatic events in Australia. However, the exotic detritus transported from Antarctica to Australia during the Gondwana assembly has resulted in the overestimation of the amount of Pan-African-aged (650–450 Ma) and Grenvillian-aged (1.20–0.95 Ga) detrital zircons derived from the Australian sources. The O and Lu-Hf isotopic systematics show that the period of the highest rate of crustal reworking was during Gondwana assembly, accompanied by high sedimentary input into source magmas. The weighted zircon Hf model age growth curve for Australia matches well with the whole-rock Nd model age growth curve. The former indicates that the Australian continent began to form at 4.1 Ga, followed by a high rate of crustal growth during 3.1 to 1.1 Ga. The growth curves from other continents (including Antarctica, contiguous USA, Russia, and Africa) were also reassessed by adopting the same methodology for comparison.

By compiling similar data sets from five continents (the contiguous USA, Russia, Africa, Australia, and Antarctica), a new growth curve for the preserved continental crust on a global scale is proposed. Weighted by the relative surface areas of the five continents, the new growth curve supports a continuous growth model and shows that very little continental crust formed during the Hadean era. Earth's continental crust began to form at 4.1 Ga, grew slowly until about 3.3 Ga, faster through the period of 3.3–2.2 Ga, and even faster from 2.2 to 1.0 Ga. Following a slowing growth from 1.0 to 0.6 Ga, rapid growth resumed for 600–300 Ma, after which growth slowed significantly to the present-day rate. At least 25% of the preserved continental crust was produced by the end of Archean, and ca. 90% was formed by 0.9 Ga.

Finally, two proxies in detrital zircons were applied to the revised global detrital zircon database from the five continents to explore the major periods of high-mountain formation associated with high-grade metamorphism and sediment-derived felsic magmatism on a global scale. The results weighted according to the sampling areas confirm that the collision between West and East Gondwana led to the formation of ultra-high mountains—the Transgondwanan Supermountains. The giant eastern turbidite fan produced due to the rapid erosion of the ultra-high Supermountains extended across Antarctica into south-eastern Australia. The volume of the detritus from the Antarctic section is comparable to the size of 5 Bengal Fans. More importantly,

nearly half of the 550–510 Ma zircons in the weighted global database were contributed from the Antarctic section, which may be critical for the development of complex animals during the Cambrian.

Table of Contents

List of tables:

All the tables are presented in Electronic Supplementary Information

Chapter 1

Introduction

1.1. Background and motivation

Continental crust is the principal archive of Earth's history. It is the outermost layer of Earth's lithosphere and forms nearly all of Earth's land surface. Continental crust is much thicker (mostly ca. 30–40 km) than oceanic crust (ca. 6 km). It has been extracted from the mantle and evolved compositionally and tectonically over a period of 4.5 Ga. Crust formation not only profoundly modified the composition of the mantle, but also produced major changes in the atmosphere, hydrosphere, and biosphere. Continental crust, therefore, plays a key role in our understanding of the origin of life, the evolution and oxygenation of the atmosphere, climate change, the thermal evolution of the Earth and the interactions between the surficial and deep Earth. Important as these questions are, the most debated and fundamental questions concerning the continental crust are when and how it has formed. Numerous studies have investigated the growth of the continental crust (e.g., Taylor, 1967; Armstrong, 1981; Taylor and Mclennan, 1995; Albarède, 1998; Rino et al., 2004; Hawkesworth and Kemp, 2006a; Kemp et al., 2006; Poupinet and Shapiro, 2009; Belousova et al., 2010; Condie and Aster, 2010; Dhuime et al., 2012; Arndt and Davaille, 2013; Cawood et al., 2013; Roberts and Spencer, 2015; Iizuka et al., 2017; Hawkesworth et al., 2019), but no consensus has been reached.

Models for the growth of the continental crust are constrained by estimates of the rates of crustal growth: the relative volume (%) of the present continental crust versus geological time (Fig. 1.1). These models can be classified into three groups, according to their assumptions of continental growth and methods of calculation. The first is based on the distributions of exposed rocks or basement rocks of different ages (e.g., Hurley and Rand, 1969; Goodwin, 1996), proposing gradual continental growth since the Archean, then significant growth in the Phanerozoic. The second group is dependent on the distribution of rocks with different model ages (e.g., Allegre and Rousseau, 1984) or rocks with juvenile features from Nd and Hf isotopic data (e.g., Condie and Aster, 2010). The curve from Condie and Aster (2010) emphasized the episodicity of continental crustal growth, in contrast to the first group models. However, in the third, some researchers applied more constraints by adding isotopic information (such as Ar and O isotopes) to estimate the volumes of crust formed through the Earth's history, even though some of that crust is no longer preserved (e.g., Armstrong, 1981; Belousova et al., 2010; Dhuime et al., 2012; Pujol et al., 2013; Iizuka et al., 2017). Considering whether

the records from rocks presently preserved on Earth can represent the relative volumes of crust present during the Archean or Hadean, for instance, Dhuime et al. (2012) used oxygen isotopes in zircon as a proxy to assess crustal reworking rate and thus estimated the growth of newly formed crust through time. They proposed that a large proportion of continental crust was produced before ca. 3.0 Ga, followed by slow crustal growth due to enhanced crustal reworking. Iizuka et al. (2017), however, placed a lower-bound on the net growth of the continental crust, showing the opposite. The wide variety of proposed models for the growth of the continental crust highlights the complexity of continental growth.

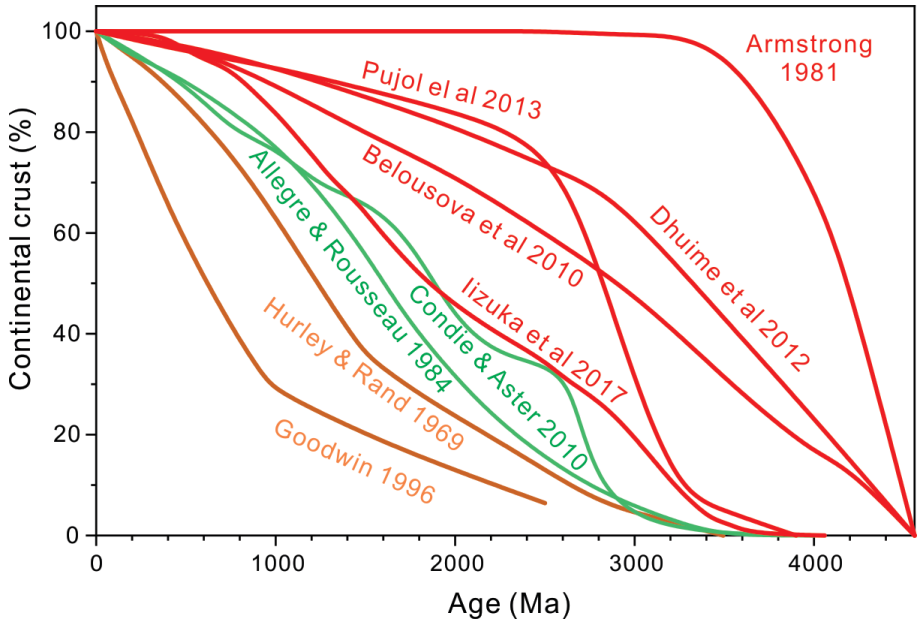

Fig. 1.1 Selected growth models for the continental crust. The three main groups of models are marked by different colours: brown (Hurley and Rand, 1969; Goodwin, 1996), green (Allegre and Rousseau, 1984; Condie and Aster, 2010) and red (Armstrong, 1981; Belousova et al., 2010; Dhuime et al., 2012; Pujol et al., 2013; Iizuka et al., 2017).

One cause for the disagreements surrounding continental growth results from the lack of available geological material from the first 1–2 billion years of Earth history (Cawood et al., 2013). The incomplete early Earth record makes it necessary to use a variety of tectonic, mineralogical, geochemical, and geophysical evidence to trace the early evolution of the continents. Many studies have shown that global tectonic processes have changed through Earth history, for example, igneous whole-rock geochemistry (Campbell and Griffiths, 1993; Campbell, 2003; Arndt and Davaille, 2013), inclusions in diamonds (Shirey and Richardson, 2011), atmospheric oxidation (Holland, 2002), osmium isotopes (Pearson et al., 2007), changing P-T conditions of

metamorphism (Stern, 2005; Brown, 2006), and associated with tectonics, changes in the rates of growth and erosion of the continental crust. Another important cause for the disagreements is the type of samples on which their assumptions and models are based—igneous whole-rocks (e.g., Hurley and Rand, 1969; Goodwin, 1996) or minerals (e.g., quartz and zircon) from sediments (e.g., Dhuime et al., 2012; Pujol et al., 2013; Iizuka et al., 2017).

An important method for determining the evolution of continental crust through time is the isotopic age and composition of zircon as quantitative proxies for crustal growth (Iizuka et al., 2005; Hawkesworth and Kemp, 2006a; Campbell and Allen, 2008; Wang et al., 2009; Belousova et al., 2010; Wang et al., 2011; Dhuime et al., 2012; Cawood et al., 2013; Iizuka et al., 2013; Payne et al., 2015; Spencer et al., 2015; Van Kranendonk et al., 2015). Zircon ($ZrSiO_4$) is a common accessory mineral occurring in various types of igneous, sedimentary, and metamorphic rocks and is one of the most durable minerals, being highly resistant to both chemical and physical weathering (Kowalewski and Rimstidt, 2003). Zircon hosts a significant fraction of the whole-rock abundance of U, Th, Hf and rare earth elements (REE) (O'Hara et al., 2001). These elements are geochemically essential as process indicators or parent isotopes for age determination. The very high closure temperature for the U-Pb system in crystalline zircon (> 900°C) (Lee† et al., 1997; Cherniak and Watson, 2003) makes its radiometric system more resistant to metamorphic, magmatic, and other thermal processes. Consequently, zircon is a key mineral for dating events in the geological record and preserving isotopic characteristics of its source magmas through most sedimentary and metamorphic processes.

Zircon is ubiquitous in felsic to intermediate igneous rocks (e.g., granitoids), but rarely present in mafic rocks (e.g., basalts). Mafic magmas are commonly zircon under-saturated, unless saturation (based on temperature and composition) is reached during late stage fractional crystallization (Watson and Harrison, 1983). Detrital zircon therefore records information mainly from felsic crust primarily generated in continental, continental arc or mature island arc settings (Lee et al., 2016). This makes zircon a superior mineral for investigating the growth of continental crust that formed primarily at subduction zones along destructive plate margins (Dhuime et al., 2011).

Zircon U-Pb and Lu-Hf isotopic systematics can constrain global evolution for the growth, differentiation, and recycling of the continental crust. Improvements in micro-analytical techniques now make possible a rapid determination of the U-Pb age and Hf isotopic composition of the same zircon grain, resulting in large amounts of data being available to investigate the evolution of continental crustal (e.g., Fisher et al., 2014a). This potent approach has been widely used, not only in zircons from known rocks (e.g., Chen et al., 2015), but also in zircons from detritus (e.g., Iizuka et al., 2010).

Zircons from large rivers are likely to be representative of the age distribution of continental crust (Bodet and Schärer, 2000; Rino et al., 2004), which can be used to obtain continental growth rates. Zircons from outcrops of basement rocks, however, identify specific regional events. There are five main advantages in using zircons collected from river sands: i) large rivers erode surficial continental crust over an extensive area, effectively sampling an entire river basin (Wang et al., 2009); ii) detritus eroded from various rocks is well-mixed by several erosion cycles during transport from bedrocks to the river mouths (Campbell et al., 2005); iii) prolonged sediment-sediment recycling through the time allows zircons from the rocks, which have been eroded and are no longer exposed on the continental surface, to be preserved in sedimentary records; iv) most metamict zircons, which are susceptible to Pb loss and thus isotopically discordant, are destroyed by natural abrasion during transport (Delattre et al., 2007); and v) the sampling area (i.e., drainage area) can be estimated, making sample weighting available.

Following the great advances in analytical methodology in the past few decades and large differences in data treatment methods, recognizing the limitations and potential pitfalls in interpreting detrital zircon ages is important in fully understanding the behavior of this provenance proxy when drawing any conclusions. There are several potential biases in sampling detrital zircons: i) The differential zircon fertility of felsic basement rocks can potentially bias the record from detrital zircons (e.g., Moecher and Samson, 2006). As Zr-enriched rocks mostly have high zircon fertility, erosion of Zr-enriched source rocks, in general, would produce disproportionately large volumes of detrital zircons compared to zircon-poor source rocks; ii) A tendency of young basement rocks to be more accessible to sampling than old basement rocks; iii) The preference for

extracting and analyzing relatively large zircon crystals for U-Pb dating, especially when dating cores and rims; iv) The intensive studies of detrital zircons from geologically interesting or significant areas; v) A natural bias, due to the absence of detrital zircon records from areas where sampling is impossible (e.g., ice-covered Antarctica), cannot be avoided.

In the present study, a weighting method based on the extensive sampling areas (see details in Chapters 4, 5 and 6) was adopted to decrease the sampling biases significantly, especially that introduced by ii and iv. The method of sample preparation (e.g., random selection zircon for dating) and analytical approach (e.g., rim-piercing method) in this study (Chapter 2) helped to circumvent problem iii. It should be noted that the sampling bias from differential zircon fertility and erosion of source rocks was difficult to overcome, as were the effects of prolonged sediment-sediment recycling through time.

To verify the credibility of detrital zircon records, I have examined the provenance of detrital zircon populations within different U-Pb age peaks in two case studies (Antarctica and Australia in Chapters 4 and 5). Any zircon population from detrital zircons, which fails to represent the magmatic events identified by previous studies, will be removed from the estimation for the crustal growth. Although the detrital zircon record is biased in favor of the felsic crust, the growth curves derived from the detrital zircon record and the igneous rock record (including felsic and mafic rocks) for the preserved Australian continent are consistent with each other (Chapter 5). Therefore, detrital zircons from the world's major rivers are particularly useful for investigating the evolution of the preserved continental crust on a continental scale.

The U-Pb age of zircon records the time of crystallization of the source magma or occasionally of high-grade metamorphism (i.e., anatexis). Lu-Hf isotopes in zircon can be used to calculate a model age for the source magma from which the zircon crystallized: the time when the source material was extracted from the mantle. O isotopes in magmatic rocks are highly sensitive to the incorporation of supracrustal material that has been subjected to low-temperature processes, especially clays produced by weathering, into a magma source region, or the involvement of fluid-rock alteration. O isotopes thus can be used to estimate the importance of these processes, which

influence the choice of Lu/Hf ratio of the source region, required for model age calculations. In combination, in-situ analyses of U-Pb, Lu-Hf, and O isotopic compositions of detrital zircons from large riverine systems in a continent can be used to identify major periods of crustal reworking and to reconstruct the growth of the continental crust on a continental scale (Kemp et al., 2006; Lancaster et al., 2011; Iizuka et al., 2013). A similar methodology has been applied to North America, Russia, and Africa (Wang et al., 2009; Wang et al., 2011; Iizuka et al., 2013). The integrated data of detrital zircons derived from Antarctica and Australia are presented in this study, to investigate the growth of the Antarctic and Australian continental crust and thus to obtain clearer insights into the growth of the preserved continental crust on a global scale.

Aside from zircon isotopic geochemistry, trace element geochemistry has been applied in zircon to investigate the composition of source magmas (e.g., Barbey et al., 1995; Johnson et al., 2017) or the provenance of zircon crystals (e.g., Hoskin and Ireland, 2000). REE composition of zircons can be used to study metamorphic conditions (Peucat et al., 1995; Hoskin and Black, 2000; Villaseca et al., 2003), by reflecting the concurrent growth of minerals, such as garnet (zircon with HREE-depletion; Schaltegger et al., 1999) or feldspars (zircon with negative Eu anomaly; Peucat et al., 1995). And different substitution mechanisms for REE in zircon can provide insights into the nature of its source magmas, for example, distinguishing peraluminous magmas via the co-existence of accessary minerals (i.e., monazite and xenotime) formed in these magmas. (e.g., Burnham and Berry, 2017). The REE patterns and trace element composition of zircon, therefore, can monitor the coexisting paragenesis to offer information on geological tectonic settings. Two geochemical proxies in zircons were applied to a revised global detrital zircon database proposed in the present research, to explore the nature of the assembly of Gondwana and identify the role of Antarctica on a global scale during the massive Pan-African continent-continent collision.

1.2. Thesis objectives

My PhD project focuses on the topic of “Growth of the Preserved Continental Crust” using an integrated study of U-Pb, O and Lu-Hf isotopes in detrital zircons from the World's major rivers. In my work, I analyzed U-Pb, O and Lu-Hf isotopic compositions of detrital zircons derived from two continents, Antarctica and Australia, to investigate the

crustal growth of those continents and the major tectonic events that have affected them. Combined with other data sets from other continents, this work sheds new light on the growth of the preserved continental crust on a global scale and the nature of the assembly of Gondwana.

My work included the following objectives:

1. Integrate the U-Pb, O and Lu-Hf isotopic data from detrital zircons derived from Antarctica to identify the major tectonic events that affected that continent and estimate the growth of the Antarctic continental crust.

2. Integrate the U-Pb, O and Lu-Hf isotopic data from detrital zircons derived from Australia to investigate the major periods of crustal growth of the Australian continent.

3. Reconstruct a more accurate model for the growth of the preserved continental crust on a global scale by compiling similar data sets from detrital zircons from other continents.

4. Investigate the relationship between Antarctica and Australia and identify the role of Antarctica during the assembly of Gondwana.

1.3. Thesis outline

The methodology used is presented in Chapter 2. The strength and reliability of zircon Hf model ages, which mark the time when the crustal source material was extracted from the mantle, is demonstrated in Chapter 3. The case studies on Antarctica and Australia are presented in Chapters 4 and 5 respectively. In Chapter 6, several geochemical proxies have been used to illustrate the connection between Antarctica and Australia. By placing Antarctica into a centre stage on a global scale, Chapter 6 also illustrates the essential role of Antarctica in the Gondwana jigsaw and provides new insights into the nature of the Pan-African continent-continent collision. The last, Chapter 7 comprises the overall conclusions of these studies and provides suggestions for further work.

Chapter 2

Methods

2.1 Sample collection

This study focuses on samples collected from Antarctica and Australia specifically.

Because over 99.5% of Antarctica is covered by ice, sedimentary samples from the International Ocean Discovery Program (IODP) surrounding Antarctica are ideal for the aims of this study and one of the limited available samples for studying the Antarctic continent, instead of inaccessible river samples. Analyzed samples from IODP sites were strictly chosen. First, to avoid sampling bias, all closest IODP sites around Antarctica were selected. Second, because detrital zircons are potentially found in the lithological composition consisting of diamict, sand/sandstone, sandy silt, terrigenous sediments or clay/claystone, potential drill holes with these lithological compositions in certain depths were preferred. Finally, 12 samples from IDOP drill holes around Antarctica (Fig. 2.1) were requested and then obtained from the Gulf Coast Repository of IODP for the following procedures and isotopic analyses. The sample list is shown in Tables 2.1.

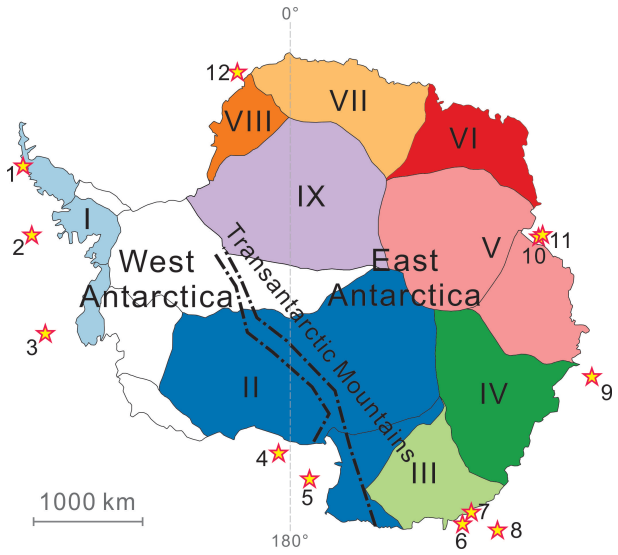

Fig. 2.1 Sample location of selected IODP sites around Antarctica showing the sampling areas which are based on the area of ice flow of Antarctic ice sheet (Rignot et al., 2011).

For Australian samples, the sand samples from major rivers (Murray and Murrumbidgee) and other rivers (Bega, Shaw, Ord, and De Grey) were collected around 100 km away from their estuary. Duplicated samples from Murray and Murrumbidgee rivers were also collected within at least 3 km apart from the first sampling location. More than 1 kg sands were collected in the field first. Because zircons have a higher density (4.6–4.7 g/cm^3) than other objects (i.e., quartz, clay), heavy minerals (zircon and

magnetite, etc.) then were concentrated after panning with tap water by using the gold panning kits in the lab. Ideally, less than 30 g heavy minerals of each sample are obtained after dried thoroughly for further zircon mineral separation. However, because over one-third of the Australian continent is covered by desert, larger rivers are lacking in these arid areas. To minimize the sampling bias, 10 sand samples of sand dune fields were carefully selected based on the study of Pell (1994) to cover the desert area especially in western and central Australia, and those samples collected by Dr Stephen. D Pell were obtained from the sample archive at ANU. In addition, the soil samples from flood plains that potentially collect the detritus from their surrounding areas were also selected according to their high abundance of zirconium (> 150 ppm Zr in the topsoil analyzed by ICP-MS) according to the study of Cooper et al. (2010) to better cover the whole continent. 19 raw topsoil samples (catchment outlet sediments) collected by the National Geochemical Survey of Australia (NGSA; www.ga.gov.au/ngsa) were obtained from Dr Patrice de Caritat (De Caritat and Cooper, 2011, 2016). The sample list is presented in Table 2.2 and sample locations are shown in Fig. 2.2.

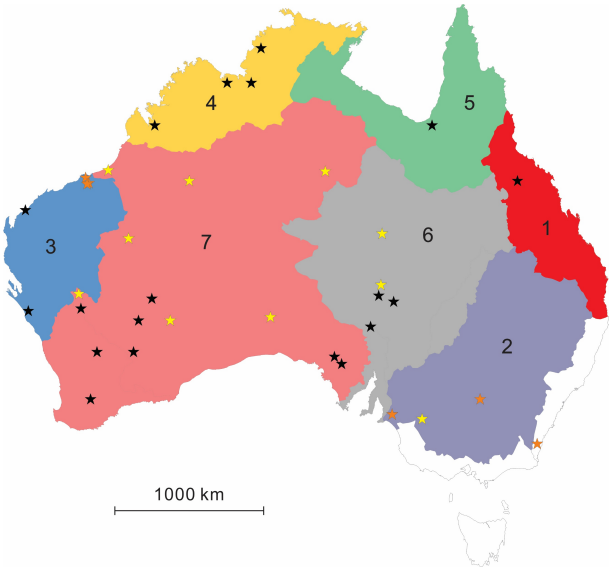

Fig. 2.2 Locations of analyzed samples from Australia showing the sampling areas. The orange, black and yellow stars represent sand samples from rivers, topsoils and sand dunefields, respectively. The sampling area is based on the drainage divisions and river basins of Australia modified after Stein et al. (2014).

2.2 Zircon separation

All samples were sieved to filter the grains with a size less than 420 µm. Heavy minerals were separated from sieved sand samples using tetrabromoethane ($C_2H_2Br_4$:

2.96 g/cm^3) for separating felsic minerals (e.g., quartz, feldspar, and muscovite) and subsequently with diiodomethane (CH_2I_2: 3.3 g/cm^3) for separating mafic minerals (e.g., biotite, amphibole, and hornblende). A hand-magnet was used to remove the minerals with high magnetic susceptibility (such as magnetite) or any other metallic materials in the heavy mineral concentration to reduce the time for further magnetic separation. By using a Frantz Isodynamic Magnetic Separator, which induces magnetic fields at various electric current settings, heavy minerals were further separated as they passed through the magnets at a set slope and tilt according to their magnetic susceptibility. This also potentially discriminated grains with surface slick, smears, coatings, cracks, magnetic inclusion, and internal fractures. Non-magnetic remains with high-quality zircons were separated using a 1-1.5 Amp electric current setting on the Frantz Isodynamic Magnetic Separator. Zircon grains were randomly handpicked for the following isotopic analyses.

2.3 Isotope analyses

2.3.1 U-Pb isotopic dating

Randomly handpicked unknown zircons and reference zircons (91500, Temora 2, R33 and Plešovice) were annealed at 900 ℃ for 48 h in the aluminium oxide ceramic crucible cups (Fig. 2.2a) in the air to minimize the “matrix effect” induced by alpha-dose of samples when measuring $^{206}Pb/^{238}U$ via Laser Ablation Inductively Coupled Plasma Mass Spectrometry (LA-ICP-MS) (Allen and Campbell, 2012). To avoid sampling bias, clear zircon grains were randomly chosen under a binocular microscope, regardless of their shape and size. However, grains less than 30 μm were neglected, because they are too small to survive all analyses (U-Pb, O and Lu-Hf isotopic analyses) and to provide a robust data set. At least 100 zircon grains from each sample were carefully mounted on a double-sided adhesive tape (Fig. 2.2b) with a fine-tipped needle, except those samples which have a very small fraction of zircon grains in the non-magnetic remains after mineral separation, such as samples from the IODP sites 113-692B and 119-740A. Optical photomicrographs with reflected and transmitted light were used to map and select least-fractured and inclusion-free zircons for U-Pb analysis.

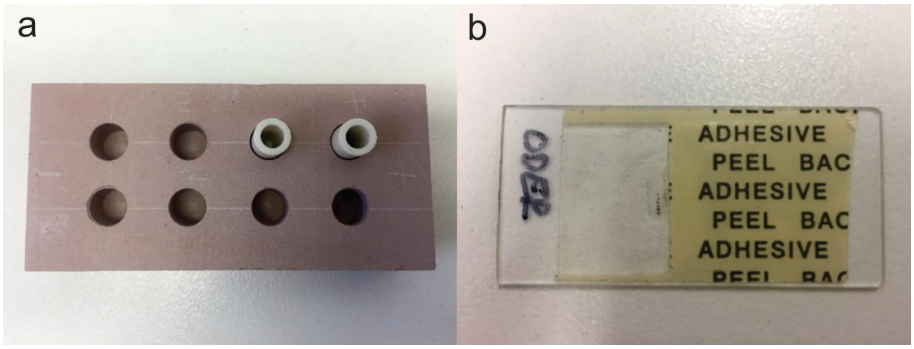

Fig. 2.2 a). Picture of aluminium oxide ceramic crucible cups located in high-temperature resistant brick; b). Picture of randomised zircons mounted on double-sided adhesive tape attaching on a thin section.

The age of each zircon grain was determined by U-Pb isotope geochronology using a 193 nm ArF Excimer LA-ICP-MS. Zircon U-Pb data were acquired by Agilent 8800 ICP-MS at Queensland University of Technology (QUT) and Agilent 7500 ICP-MS at the Research School of Earth Sciences (RSES), Australian National University (ANU). The pulsed UV laser generated by premix ArF gas was focused on zircon to produce a plume of ablated material which was swept into the plasma. The plasma made from argon gas ionized the ablated materials. These ions then were extracted into the quadrupole mass analyser as a mass filter and were filtered according to their mass-to-charge ratios. The filtered ion signals were measured by the electron multiplier detector.

Radiogenic isotopes of $^{206, 207, 208}$Pb and radioactive elements of ^{232}Th and ^{238}U with elements of ^{29}Si, ^{31}P, ^{49}Ti, ^{51}V, ^{89}Y, ^{91}Zr, ^{93}Nb, ^{139}La, ^{140}Ce, ^{141}Pr, ^{146}Nd, ^{147}Sm, ^{153}Eu, ^{163}Dy, ^{172}Yb, ^{175}Lu, ^{177}Hf and ^{181}Ta were measured concurrently. The acquisition time for the isotopes used for dating was at least three times longer than for the other elements in each session (i.e., 20191107; Table 2.3). The rim-piercing method of Campbell et al. (2005) was adopted for the U-Pb dating and simultaneous trace element analyses. A 28-µm-diameter laser beam ablated into the unpolished zircon at the repetition rate of 5 Hz, through the rim of grain towards its centre, to produce continuous ca. 13 µm depth profiles of isotopic ratios from rim to core for each analyzed grain. The data of each spot were acquired for a period of 75 s consisting of 20 s pre-ablation, 40 s laser ablation, and 15 s post-ablation. The pre-ablation time allows ICPMS to measure the background, and the post-ablation time is for sweeping the remains of each grain in the instrument to avoid contaminating the next analysis. The primary references (zircon 91500 and Temora 2 for U-Pb ages; NIST 610 glass for trace elements) were analyzed after every 10

unknown zircon grains, with secondary standards (zircon R33 or Plešovice, and NIST 612 glass) after 20 unknowns, to calibrate the isotopic ratios and concentration of selected elements. 91500 was used for calibrating the $^{207}Pb/^{206}Pb$ ratio and Temora 2 for $^{207}Pb/^{235}U$ and $^{206}Pb/^{238}U$ ratios, with R33 as a secondary reference to evaluate the accuracy and precision of zircon U-Pb ages. Concentrations of elements were calibrated against NIST 610 glass as the primary standard and NIST 612 glass as the secondary standard. The U-Pb isotopic and elemental data were processed in a software package, Iolite, which is developed for the reduction of data acquired by LA-ICP-MS (Paton et al., 2011). The mass scan for each analysis was cropped to periods maintaining steady isotopic ratio signals in Iolite. And the measured U-Pb isotopic ratios were calibrated after subtracting the background and correcting the downhole fractionation based on the measurement of the primary reference. Silicon was used as the internal standard element for internally normalized trace element abundance calculation and is assumed to be 15.32 wt. % based on the chemical composition of zircon ($ZrSiO_4$).

A robust of U-Pb age is essential for calculating a meaningful Hf model age for zircons (see detail in Chapter 3). Therefore, the following criteria were adopted for determining zircon U-Pb ages: (i) A U-Pb age was calculated if at least 15 mass sweeps have the steady signal. (ii) Zircons with P > 2000 ppm, Ti > 80 ppm or La > 10 ppm usually contain inclusions of apatite or rutile, and were rejected; (iii) Uncorrected $^{207}Pb/^{206}Pb$ ages was used for old zircons (>950 Ma), within 95% of concordance including 2SE (Standard Error) (uncorrected $^{206}Pb/^{238}U$ age vs uncorrected $^{207}Pb/^{206}Pb$ age); (iv) A ^{207}Pb common Pb-correction was applied only for young grains (<950 Ma) if the correction brought the data closer to Concordia. The amount of common Pb was determined by the ^{207}Pb correction method following the calculation of Vermeesch (2018) and the common Pb composition used the two-stage crustal evolution model from Stacey and Kramers (1975). If the fraction of common Pb is over 0.02, the common Pb corrected age is discarded, and the concordance is based on calculation from the uncorrected ages. The $^{206}Pb/^{238}U$ ages, within 95% of concordance ($^{206}Pb/^{238}U$ age vs $^{207}Pb/^{235}U$ age) including 2SE, were used for young grains. Whether a common Pb uncorrected age or a common Pb corrected age was chosen depends on whether the common Pb correction brought the analysis closer to Concordia. In addition, to test the effectiveness of the ^{207}Pb method, the ^{208}Pb method is also used for comparison, which used the calculation

from Compston et al. (1984) with the Pb isotopic composition from Cumming and Richards (1975). Both methods produced similar best age results within 2SE for young grains (<950 Ma) (i.e., Table 2.4). The U-Pb age reported in this study was based on the ^{207}Pb correction. Although age-zoned zircons were not analyzed for Hf or O isotopes, U-Pb dates were calculated for the rim and core of grain (marked in the Table 4.1) if both meet the criteria described above.

2.3.2 Oxygen isotopic analysis

Reference standards for O analysis (e.g., Mud Tank, R33, Plešovice and Temora 2) were transferred onto the same tape where the dated zircons were mounted. Both dated zircons and reference standards were then set in a 25 mm conventional electron microprobe-style epoxy mount. The reverse side of dated zircons, where the adhesive tape was attached, was polished in one-third to half to expose the midsection and ideally to make the mount's surface as flat as possible. All mounts were microscopically photographed and imaged using cathodoluminescence (CL) spectroscopy to identify any internal texture, such as the presence of an inherited core or over-growth rim, grain cracks and mineral inclusions. Before O analysis, the mounts were carefully cleaned to remove any contaminants from the mount's surface that may disrupt gold coating and affect O analysis, then were coated with ~25 nm thick gold. The grains for O and Lu-Hf isotopes analyses were strictly selected by inclusion and age zonation free, validly steady mass sweeps, trace elements limitations, high concordance. O isotopic compositions of selected zircon grains were measured via SHRIMP (Sensitive High Resolution Ion Microprobe) II at RSES. SHRIMP allows the high energy primary ions to sputter a small amount of material from the zircon surface, and ionized atoms and molecules can be extracted as secondary ions for analysis.

Analytical conditions and measurement procedures were similar to those described by Iizuka et al. (2013) and Ickert et al. (2008). A 3.5 nA, 15 keV $^{133}Cs^{+}$ primary ion beam was focused into a ~25 µm diameter spot on the zircon surface to generate O^{-} secondary ions. To neutralize charge for insulating samples the electron gun equipped delivered ~1 µA of electrons to the sample surface with a 45° incident angle in the typical energy setting of 1.1–1.3 keV. The secondary ions were extracted through the source slit and filtered by the secondary mass analyser, which consists of an Electrostatic Analyser,

Quadrupole Matching Lens and Magnet. A mass resolution of ~2,500 at 1% peak height was adopted to separate potential isobaric interferences from $^{16}OH_2^-$, $^{16}OD^-$ and $^{17}OH^-$ on $^{18}O^-$. The secondary $^{18}O^-$ and $^{16}O^-$ ions were collected by dual Faraday cups and measured simultaneously with 10^{11} and 10^{10} Ω resistors. Electron induced secondary ion emission (EISIE) defined by Ickert et al. (2008), which is resulted from electron-stimulated desorption (ESD) (Madey, 1986), was measured to calibrate the isotopic ratios if the EISIE effect is significant. Backgrounds of ^{18}O and ^{16}O are measured at the start and end of each spot. Single O data acquisition consists of 1 set of 6 scans, each with 20 s integration times, leading to a total count time of ~120 s and complete analysis within approximately 6 minutes. Mud Tank (or R33) as primary reference was analyzed after every 3 or 5 unknowns, with Temora 2 (or Plešovice) as a secondary reference after 10 unknowns, to monitor the analytical accuracy and precision during each analytical session. The raw data were processed by the POXI MC Labview application, a data-reduction program of RSES. This application allows Instrumental Mass Fractionation (IMF) and relative gain to be corrected by normalizing all background-corrected data to the measured primary reference zircon with independently known isotopic compositions. All corrected $^{18}O/^{16}O$ ratios of samples are presented as delta notation, expressed as permil deviations from Vienna standard mean ocean water (VSMOW) with $^{18}O/^{16}O$ of 0.0020052 (Baertschi, 1976):

$$\delta^{18}O_{\text{ VSMOW\_sample}} = \left[\frac{(^{18}O/^{16}O)_{\text{ corrected}}}{(^{18}O/^{16}O)_{\text{ VSMOW}}} - 1\right] \times 1000\ (‰)$$

Analytical uncertainty of a single spot analysis, at 95% confidence level, combines the reproducibility of the primary zircon reference (2σ, after the instrumental drift correction) with the within-spot precision (2SE) during a measurement session, which was added in quadrature.

2.3.3 Lu-Hf isotopic analysis

After O isotope analyses, Lu-Hf isotopic compositions of the selected zircon grains were analyzed by using the Laser Ablation system coupled with a Thermo Finigan Neptune Multicollector (MC) ICPMS at State Key Laboratory of Isotope Geochemistry, Guangzhou Institute of Geochemistry, Chinese Academy of Sciences (GIG-CAS), for Session 201707, and at RSES, ANU for the rest of sessions. The laser ablation sites for Lu-

Hf isotopic analysis were selected within a similar internal structure and centred as close as possible to the original spot for O isotopic analysis to correlate O isotopic data with Hf isotopic compositions.

For the session conducted at GIG-CAS, a Neptune Plus MC-ICP-MS (Thermo Scientific) coupled with a RESOlution M-50 193 nm laser ablation system (Resonetics) is used for Lu-Hf isotopic analysis. The Plešovice zircons were analyzed as the primary reference after every 10 unknown grains, and 91500, R33 and Mud Tank were measured as secondary after every 20 analyses to monitor the data quality. To improve the sensitivity of the instrument an X skimmer cone was used in the interface region. All isotope signals were detected with Faraday cups under static mode. The laser parameters were set as the following: beam diameter, 45μm; repetition rate, 6 Hz; energy density, ca. ~4 J/cm^2. Helium was chosen as the carrier gas (800 ml/min). A "squid" device on the gas line to the MC-ICPMS gives a smooth signal. Each analysis consisted of 300 cycles with an integration time of 0.135 s per cycle. The first 10 s was used to detect the gas blank with the laser beam off, followed by 30 s laser ablation for sample signals acquisition with the laser beam on. The data of each analysis were processed once the analytical cycles were completed with choosing the period with a platform with steady sample signals, by using coupled Matlab program for isotopic data reduction from Zhang et al. (2015). The parameters used for calibration is similar to the description below.

For sessions conducted at RSES, ANU, the data were acquired using a HelEx ArF excimer (λ = 193 nm) Laser Ablation system coupled with a Thermo Finigan Neptune multiple collector (MC-ICP-MS). 91500 zircons were analyzed as the primary reference after every 10 unknown grains, and R33, Temora 2 and Mud Tank were measured as secondary after every 20 analyses to supervise the data quality. A spot size of 35-45 μm (depending on the size of sample grains) and a laser repetition rate of 5 Hz were adopted with 15 s for baseline measurement, 60 s for the ablation time and 20 s for post-ablation for flushing the ablated remains. Helium gas was used for flushing the ablated material and ca. 4 ml/min N_2 was mixed into the Argon sample carrier gas to augment the signal intensity (Iizuka and Hirata, 2005). $^{171, 173}$Yb, ^{175}Lu, ^{174}Hf, ^{176}(Hf+Lu+Yb), ^{177}Hf, ^{178}Hf, ^{179}Hf and ^{181}Ta isotopes were measured simultaneously in a static-collection mode on 9 Faraday cups with 10^{11} Ω resistors. $^{171, 173}$Yb and ^{175}Lu were measured to correct the

isobaric interferences of ^{176}Lu and ^{176}Yb on the intensity of ^{176}Hf before the mass bias correction for $^{176}Hf/^{177}Hf$. $^{173}Yb/^{171}Yb$ and $^{179}Hf/^{177}Hf$ were used to directly to calculate the mass bias factor β_{Yb} and β_{Hf} using an exponential law, and β_{Lu} is assumed to be equal to β_{Hf} (Iizuka et al., 2005; Fisher et al., 2014b). For correcting mass discrimination effects, the true value of $^{173}Yb/^{171}Yb = 1.132685$ and $^{179}Hf/^{177}Hf = 0.7325$ from Chu et al. (2002) and Patchett and Tatsumoto (1981) separately were adopted. For the interference correction, the true value of $^{176}Yb/^{173}Yb = 0.79618$ (Thirlwall and Anczkiewicz, 2004) and $^{176}Lu/^{175}Lu = 0.02656$ (Blichert-Toft et al., 1997) were employed. The corrected ^{176}Hf were calculated with the following equation:

$$^{176}Hf_{\ corrected} = {}^{176}(Hf + Yb + Lu)_{measure} - {}^{175}Lu_{measure} \times \left(^{176}Lu/^{175}Lu\right)_{true} \times \left(^{176}M_{Lu}/^{175}M_{Lu}\right)^{\beta_{Lu}} - {}^{173}Yb_{measure} \times \left(^{176}Yb/^{173}Yb\right)_{true} \times \left(^{176}M_{Yb}/^{173}M_{Yb}\right)^{\beta_{Yb}}$$

The true $^{176}Hf/^{177}Hf$ was then corrected for mass bias:

$$\left(^{176}Hf/^{177}Hf\right)_{true} = \left(^{176}Hf_{corrected}/^{177}Hf_{measure}\right) \times \left(^{176}M_{Hf}/^{177}M_{Hf}\right)^{\beta_{Hf}}$$

The data reduction was done by using the Hf isotope Data Reduction Scheme of Iolite (Paton et al., 2011). Each analysis uncertainty was calculated by its internal standard error (2SE) associated with the reproducibility of the primary zircon reference 91500 (2SD), which was added in quadrature. The initial $^{176}Hf/^{177}Hf$ of zircon at its crystallization time were calculated and reported rather than the present-day $^{176}Hf/^{177}Hf$ of zircons, using the ^{176}Lu decay constant of 1.867×10^{-11} yr^{-1} (Söderlund et al., 2004).

There is a typical systematic bias of the MC-ICP-MS at RSES based on a detailed assessment of $^{176}Hf/^{177}Hf$ analyses between the measured values and the accepted solution values of each reference determined by Woodhead and Hergt (2005) over a decade at ANU (Wang et al., 2009). Accordingly, the measured values of the mean $^{176}Hf/^{177}Hf$ ratio of the references were normalized to the solution values. The average offset between the measured mean $^{176}Hf/^{177}Hf$ ratios and the solution values of the references in each session (Table 4.7 and 5.6) then were applied to calibrate the $^{176}Hf/^{177}Hf$ ratio of unknown zircons. The average offsets in this study are less than 1 $\varepsilon Hf_{(0)}$ unit (=0.000028; CHUR value is from Bouvier et al. (2008)) with the mean offset of 0.000016 and the median of 0.000015. This offset is not related to an inaccurate Yb

interference correction as demonstrated by analyses of reference zircons, which have widely different Yb concentrations, from 4 sessions in 2020 (Fig. 2.3).

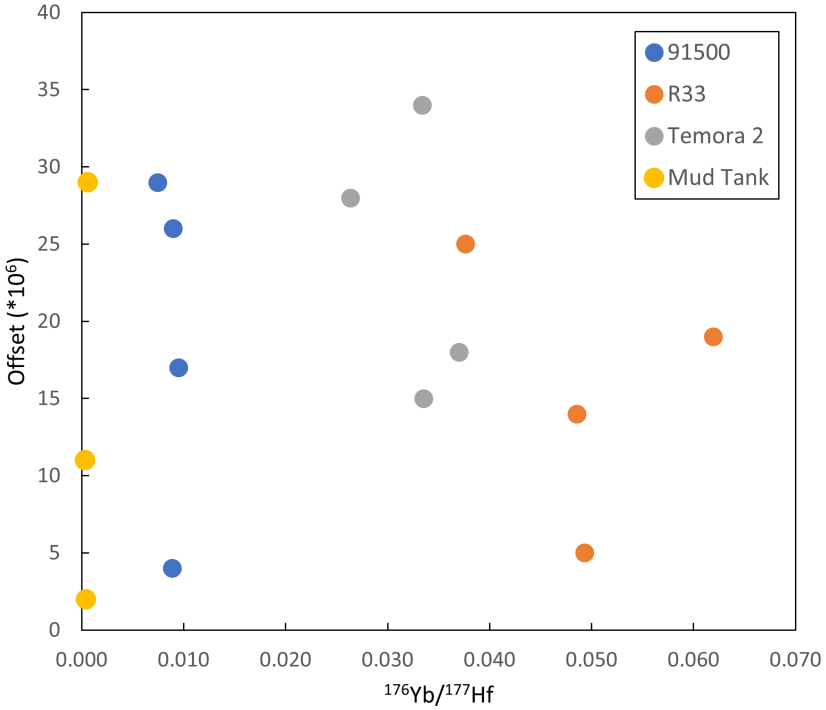

Fig. 2.3 Scatter plot of the average offset between the measured values and the solution values of different reference zircons analyzed in 2020 (4 sessions), based on Table 4.7.

Chapter 3

Reliability of Zircon Hf Model Ages

3.1 Introduction

The isotope ^{176}Lu is unstable and spontaneously decays by β-emission to stable ^{176}Hf with a half-life of approximately 37 Gyr (McNair, 1961). With rapid advances of techniques, from TIMS (Thermal Ionization Mass Spectrometry) to MC-ICP-MS, for precisely measuring of Lu-Hf isotopes, their applications are accelerating in earth sciences. The ^{176}Lu-^{176}Hf radioactive decay system has been widely used to track the history of crust-mantle differentiation and thus constrain global growth models of the continental crust (e.g., Kemp et al., 2006; Dhuime et al., 2012; Iizuka et al., 2017). The once uniform initial Lu/Hf ratio for Earth, approximate the chondritic value, has progressively altered over time by episodes of partial melting of the mantle that generates magmas to form the crust and have depleted Hf isotopic composition in the residual mantle. The enriched crust was, correspondingly, generated. Consequently, the evolution of Hf isotopic composition of the mantle reservoir and the enriched crust diverge from that of primitive mantle over time. As a crucial carrier of uranium, thorium, and the rare earth elements (REE) at ppm level, and hafnium at the percent level (>10,000 ppm), zircon can be precisely dated by the U-Pb geochronology and effectively records the initial Hf isotopic composition at the time of crystallization because of its low Lu/Hf. Thus, the Hf isotopic composition of zircons can be utilized as a geochemical tracer for the origin of their parental magmas.

Zircon Hf model age aims to determine the average time at which the source material(s), which melted to form the magma from which the analyzed zircon crystallized, separated from the mantle. And they are commonly considered to be the approximate time of addition of juvenile, mantle-derived material to the continents. Consequently, model ages provide an important parameter for constraining the growth and evolution of the continental crust. The calculation of zircon Hf model ages follows the same way as Nd model ages from whole rocks (McCulloch and Wasserburg, 1978), but with one essential difference. In brief, Sm–Nd model ages of whole-rock samples use the present-day $^{143}Nd/^{144}Nd$ compositions to extrapolate backwards using the measured $^{147}Sm/^{144}Nd$ in the rock as the slope until this evolution intersects a reference curve for a terrestrial reservoir. The time corresponding to that intersection is referred to as their model ages. Zircon Hf model age calculations, unlike model ages from whole rocks (McCulloch and Wasserburg, 1978), require a two-step model because the zircons

have lower Lu/Hf than the source rocks from which they were generated (e.g. Vervoort and Kemp, 2016). Therefore, the first step is to calculate the initial Hf isotope ratio at the time of zircon crystallization. The second is to estimate a $^{176}Lu/^{177}Hf$ ratio of the crustal reservoir that melted to form the zircon's parent magma. This $^{176}Lu/^{177}Hf$ ratio is then used as the slope to project the zircon's initial $^{176}Hf/^{177}Hf$ back the reference mantle's $^{176}Hf/^{177}Hf$ growth curve (depleted mantle: DM or arc mantle: AM) to obtain the model age $T_{DM|AM}$ (e.g., Payne et al., 2016). These calculations are as following equations:

$$\frac{^{176}Hf}{^{177}Hf}_{(Zrn,\,t)} = \frac{^{176}Hf}{^{177}Hf}_{(Zrn,\,0)} - \left[\frac{^{176}Lu}{^{177}Hf}_{(Zrn,\,0)} \times \left(e^{\lambda t} - 1\right)\right] \qquad (1)$$

$$T_{DM|AM} = t + \frac{1}{\lambda} \cdot ln\left[\frac{\frac{^{176}Hf}{^{177}Hf}_{(Zrn,\,t)} - \frac{^{176}Hf}{^{177}Hf}_{(DM|AM,\,t)}}{\frac{^{176}Lu}{^{177}Hf}_{(crust)} - \frac{^{176}Lu}{^{177}Hf}_{(DM|AM,\,t)}} + 1\right] \qquad (2)$$

Where Zrn is for zircon, λ is the decay constant for ^{176}Lu, t is the zircon crystallization age, and crust displays the crustal reservoir.

However, it must be noted that model ages are not exact, quantifiable ages in the strict geochronological meaning. Instead, they are used as a derivative parameter providing approximate time for crustal evolution with several key assumptions: 1) zircon U-Pb date used for calculation is robust; 2) the Lu/Hf ratio of the source rock in which zircon formed has to be estimated due to the missing information of the host rock for detrital zircons; 3) the Hf isotopic composition of the reference mantle, which new crust was derived from, is assumed to follow a linear evolution extrapolated from its modern-day's value back to the CHUR value at ca. 4.5 Ga. Each of these variables has an uncertainty that must be taken into account and minimized to obtain the best possible model age.

This chapter discusses the major uncertainties regarding the calculation of zircon Hf model age. In particular, this research proposes an integrated method by combining U-Pb, O and Lu-Hf isotopes systematics to address the potential problems associated with model ages and to obtain meaningful model ages.

3.2 Uncertainties of Hf model age

3.2.1 U-Pb dates of detrital zircons

Apart from the quantifiable analytical uncertainty of zircon U-Pb date, the principal sources of its error in zircon U-Pb dating are discordance and age zoning. Zircons that have undergone Pb loss tend to be discordant and give young apparent ages. This results in the inaccurate initial $^{176}Hf/^{177}Hf$ ratio thus erroneous Hf model age. However, discordance is not a major factor in zircons collected from modern rivers, drainage areas or sand dunes, because most metamict zircons, which are most susceptible to Pb loss, are destroyed by natural abrasion during transport. And this source of error was minimized by restricting the zircons analyzed for Hf and O isotopes to those with U-Pb ages that comply a series of criteria which include the filter of the 95 % high concordance (within 2σ standard errors) as described in Chapter 2.3.1. More than 78% of the analyzed zircons met these concordance criteria. $^{207}Pb/^{206}Pb$ ages were used for zircons older than 0.95 Ga, and $^{206}Pb/^{238}U$ ages for younger grains (<0.95 Ga). A ^{207}Pb common Pb-correction was applied for younger grains if the correction brought the date closer to Concordia. The correction, where applied, was small (Table 3).

It is noteworthy that recognizing small amounts of ancient Pb loss is vexing, especially in old detrital zircon grains, as the reset U-Pb isotopic system may appear concordant or slightly discordant within analytical uncertainty. Unrecognized ancient Pb loss from an old grain produces a $^{207}Pb/^{206}Pb$ date less than the true magmatic age, resulting in an incorrect older Hf model age. This is particularly an issue for zircon from high-grade metamorphic terranes. Combined with another two filters of time-resolved U-Pb signal and selected trace element concentration below, this issue can be alleviated. The error introduced by a few such grains will be minimal when using a large data set for modelling the growth curve, as in most of the old grains from the database it is unlikely that ancient Pb loss has gone undetected.

Zoned zircons yield the issue that the U-Pb age and Hf isotope analyses of zircon are decoupled if discrete domains with different crystallization ages and Hf isotope compositions in the zircon are analyzed. This will produce geologically meaningless Hf model ages unless the zones can be resolved and analyzed separately. The rim piecing method used in this study (Campbell et al., 2005), in which unpolished zircons are

mounted on tape and ablated from rim to core, is ideal for identifying zoned grains. Zoned zircons were not analyzed for Hf or O isotopes, but U-Pb dating dates were calculated, where a steady signal of greater than 15 mass sweeps was identified. Inclusions in zircon were also avoided by identifying their existence from a combination of CL and microscope images, inspecting concentration curves for spikes, and the concentrations of trace elements. Zircons with P > 2000 ppm, Ti > 80 ppm or La > 10 ppm usually contain inclusions of apatite or rutile and were ruled out for further isotopic analyses.

The criteria for selecting zircons analyzed for O and Hf isotopes and for determining U-Pb age potentially filter the dated zircons to those that have coupled U-Pb, O and Hf isotopic composition and yield a robust age for their Hf model age calculation.

3.2.2 $^{176}Lu/^{177}Hf$ ratio of the crustal reservoir

The $^{176}Lu/^{177}Hf$ ratios of source magma, from which zircon crystallized, is essential for calculating two-stage Hf model ages. It is required to extrapolate this $^{176}Lu/^{177}Hf$ ratio, as the slope, at the time of zircon crystallization back to the mantle reference curve. As a first estimation, the commonly adopted $^{176}Lu/^{177}Hf$ value is that of average bulk continental crust either 0.015 used by Griffin et al. (2002) or 0.012 recommended by Rudnick and Gao (2003). However, when zircons crystallize from magmas derived from variable components, for example from mantle-derived or sedimentary material, misuse of the $^{176}Lu/^{177}Hf$ ratios can cause inaccurate model ages of up to several hundred million years, depending on the difference of the initial Hf composition between zircon and the mantle reference (e.g., Fig. 3b fromVervoort and Kemp, 2016).

Because large fractionations of $\delta^{18}O$ had been observed in the different granitoid source regions in the Earth's surface (Valley et al., 2005). Oxygen isotopes were introduced and analyzed as a filter to reduce uncertainty in the choice of $^{176}Lu/^{177}Hf$ used in the Hf model age calculation. $\delta^{18}O$ in zircon can potentially indicate the continental region where zircon source rocks were generated. For example, sedimentary rocks, if they formed with a high fraction of shale, have $\delta^{18}O$ > 10 ‰ and consequently, their zircons have elevated $\delta^{18}O$ values, whereas zircons generated from a magma originally derived from primitive mantle have the mantle-like $\delta^{18}O$ value of 5.3 ± 0.6 ‰ (2σ) (Valley

et al., 2005). Following Wang et al. (2011) and Iizuka et al. (2013), two end-members were assumed: zircons with mantle-like $\delta^{18}O$ (< 5.9 ‰) are suggested to have crystallized from a melt generated by melting mafic crust with $^{176}Lu/^{177}Hf$ = 0.021 (Kemp et al., 2006) and zircons with $\delta^{18}O$ > 10.0 ‰ to have crystallized from a melt dominantly derived from the upper continental crust (mainly sedimentary material) having $^{176}Lu/^{177}Hf$ = 0.0083 (Rudnick and Gao, 2003). Any $\delta^{18}O$ in between, the $^{176}Lu/^{177}Hf$ ratio is calculated by a linear interpolation formula by adopting these two members:

$$^{176}\mathrm{Lu}/^{177}\mathrm{Hf} = 0.0393 - 0.0031 \times \delta^{18}\mathrm{O} \qquad (3)$$

3.2.3 Mantle reference curve

One of the largest uncertainties in model age calculations is the $^{176}Hf/^{177}Hf$ evolution curve for the mantle reservoir from which the continental crust grew. The Hf composition of the mantle commonly used to calculate Hf model ages is that of Griffin et al. (2000) (present-day $^{176}Hf/^{177}Hf$ = 0.28325, $^{176}Lu/^{177}Hf$ = 0.0384, ε_{Hf} = +16.4), which assumes that the continental crust was derived from the depleted upper mantle, as represented by MORB. The linear evolution curve for depleted mantle (DM) was extrapolated from its present-day value back to ca. 4.5 Ga when the Hf composition of undifferentiated Earth is similar to the chondritic value (CHUR). However, it has been suggested that Hf model ages calculated from these values are inappropriate for estimating the timing of continental crust generation for two reasons. First, the average upper mantle value, based on $^{176}Hf/^{177}Hf$ compilation of the Griffin et al. (2000), is distorted by a high fraction of North Atlantic MORB with an unusually high $^{176}Hf/^{177}Hf$ (Iizuka et al., 2013), which results in artificially old model ages when used in model age calculations. A global database of detrital zircons from world major rivers compiled by Iizuka et al. (2017) shows only a very small fraction of zircons can be plotted within or near this evolution curve and regarded as juvenile grains. Second, Rudnick (1995) used mass balance to show that at least 80% of the continental crust was formed at subduction zones along destructive plate margins. Consequently, the arc mantle tends to be more representative than the MORB mantle of the source reservoir for the continental crust (Dhuime et al., 2011).

Two estimates have been made for the global mean value of $^{176}Hf/^{177}Hf$ in island arc volcanic rocks. Iizuka et al. (2013) compiled 382 Neogene island arc basalts and obtained a mean of 0.283160 (ε_{Hf} = +13.3), compared with the ε_{Hf} of +13.2 ± 1.1 obtained by Dhuime et al. (2011). Both values are similar to the mean MORB value of +13.9 compiled by Chauvel et al. (2008). The last compilation suggests that the distinction between the MORB and arc mantles is not as important as suggested by Dhuime et al. (2011) and Iizuka et al. (2013). In this study, the values of Iizuka et al. (2013) for the modern upper mantle were used because they include rigorously calculated uncertainties at the 95 % confidence level, which give an upper limit of 0.283271 (ε_{Hf} = +17.2) and the lower limit of 0.282913 (ε_{Hf} = +4.5). The large uncertainty in the Hf composition of the modern-day arc mantle matches a comparable range in Nd isotopic composition of Neogene island arc volcanic rocks compiled by Hao et al. (2022), with εNd varying between -0.2 and +9.2, and averaging +6.1.

A linear extrapolation of the average Hf isotopic composition of the modern-day arc mantle reservoir, back to ca. 4.5 Ga, has been used to calculate Hf model ages. Similarly, the upper and lower values (95% conf.) of arc mantle have been extrapolated back to 4.5 Ga to calculate uncertainties in the model ages arising from uncertainties in the arc mantle growth curve. This is a simple linear assumption for the arc mantle evolution through the time. Note that the Hadean and Early Archean evolution of the mantle could be different, if an extensive crust was formed during the Hadean or early Archean but rapidly recycled back into the mantle or no differentiation process during the first 200 Myr of Earth's history. The arc mantle evolution is widely accordant with Hf isotopes of juvenile rocks with ages up to 3.4 Ga as compiled by Vervoort and Blichert-Toft (1999) (Iizuka et al., 2013). Because the upper and lower curves converge with age at 4.5 Ga, the uncertainty of model age, arising from this source, is smaller for older grains (i.e., Archean) than for young grains. Furthermore, old grains are less likely to be derived from mixed sources, each with a distinct Hf isotopic composition, and where there are differences, smaller time differences in the early Earth time make them less significant. Calculated Hf model ages within 95% confidence level are used to produce the cumulative growth curves of the Antarctic and Australian continents in this research (See Chapters 4 and 5).

Nebel et al. (2014) have found a notable exception to the linear $^{176}Hf/^{177}Hf$ evolution curve for the mantle reservoir. They recognized that some 3.5 to 2.9 Ga komatiites from the Pilbara, Western Australia, have $^{176}Hf/^{177}Hf$ values that lie well above the linear curve. In this study, the model ages for grains that have $\varepsilon Hf_{(t)}$ that lie above the Hf mantle curve are assumed to have model ages equal to their U-Pb crystallization ages.

3.3 A conundrum of magma mixing

Although uncertainty in the evolution curve for $^{176}Hf/^{177}Hf$ in arc mantle introduces considerable uncertainty into the model age calculated for individual zircons, these errors are largely random, and therefore, tend to cancel out when used to construct continental growth curves from large data sets. A less traceable problem arises when zircons crystallize from magmas produced by melting mixed continental sources or mantle melts that have been contaminated by continental crust. Zircon Hf model age calculations assume the magma source, either the mantle or continental crust, to be homogeneous. Mixed sources give mixed apparent ages that can be misleading. Magma mixing in igneous rocks can sometimes be identified from outcrop relationships, petrology, and/or geochemistry, whereas detrital zircons, which crystallized from mixed magmas, are more difficult to identify. In this study, if any zircon with a complex texture, such as an inherited core, metamorphic rim, or multiple age zoning, was rejected for Lu-Hf and O isotopic analyses. However, this approach does not exclude zircons that have crystallized in chemical equilibrium with a well-mixed magma. This is not a problem for calculating continental growth curves if the components have comparable Hf contents because the model age will be appropriate for the average of the components. It becomes a problem if one of the components has a Hf content that is appreciably higher than the others, because this component will contribute disproportionately to the model age.

An example of the influence of mixing magmas on model ages is the study of Hao et al. (2019) on the ore-bearing porphyries and regional diorites from the Escondida igneous suites in Chile. The trace elements and Sr, Nd, Pb, Hf and O isotopic characteristics of this suite suggest they were derived from a mantle-derived magmatic source with only minor crustal contamination. However, the calculated zircon Hf and

whole-rock Nd model ages both show an unexpectedly old age of ca. 800 Ma, over 750 Myr older than the crystallization age of ca. 40-35 Ma of the rocks in which the zircons were found. These model ages fail to represent the timing of the mantle melting event that gave rise to the bulk of the magmas. This failure may, in part, be attributed to using the wrong evolution for Hf in the arc mantle. If the Hf curve defined by the lower curve (most unradiogenic) is used instead of the average curve, the model age falls to a more reasonable ca. 240 Ma for zircon Hf model ages. Use of the lower curve can be justified on the basis that the Escondida magma was derived from the mantle above a subduction zone where the Pacific plate, including sediments, subducted under the west coast of Chile. Melting of these sediments would have added unradiogenic Hf and Nd to the source of the Escondida magma. However, even if the lower 95% confidence curve is used to calculate the model age there is still an age difference of 200 Myr. This residual can be attributed to the Escondida magma being contaminated by the unradiogenic continental crust. For example, the average Hf content of primitive intra-oceanic arc magma is 1.12 ppm, compared with 3.7 ppm for the average continental crust (Fig. 3.1). If a magma, originating from the average arc mantle, is contaminated by 10% average continental crust during its ascent, 23% of the Hf in the hybrid magma will come from the contaminant, which will distort the calculated model age to older values. This is the most likely explanation for the 200 Myr residual error in the Escondida model age. In large data sets, errors arising from uncertainty of the arc mantle evolution curve for Hf isotopes will largely cancel out, but those associated with contamination of continental crust in the primary magmas will not if the contaminate has a much higher Hf content than the primary magma.

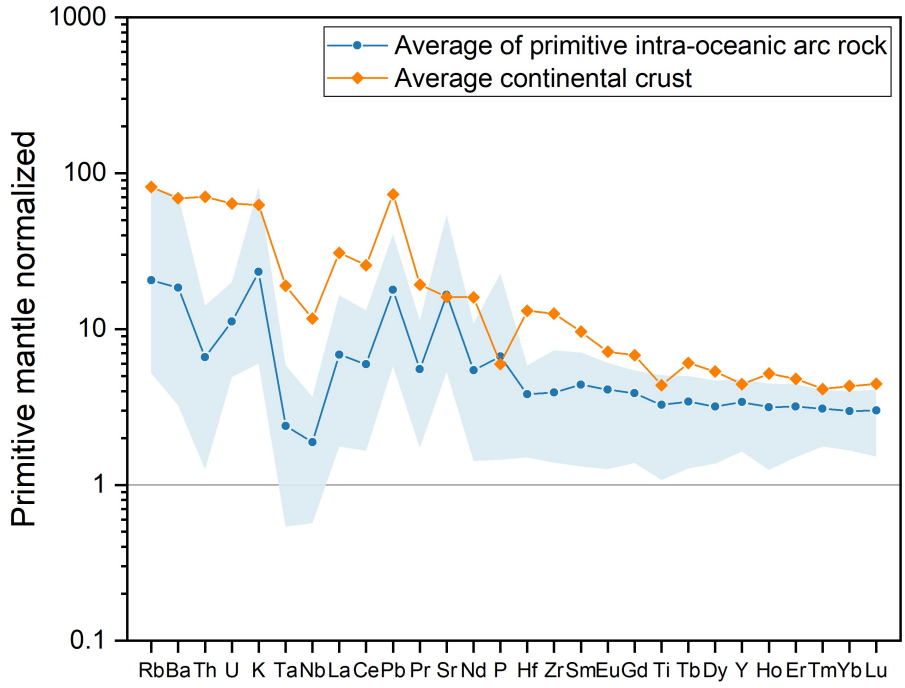

Fig. 3.1 Primitive mantle normalized trace element patterns of the average of primitive intra-oceanic arc rocks (Schmidt and Jagoutz, 2017) and the continental crust (Rudnick and Gao, 2014). Blue area marks the range of primitive intra-oceanic arc rocks.

Despite the limitations of zircon Hf model ages, several encouraging lines of evidence suggest that appropriately weighted detrital zircon Hf model ages, when applied to large data sets, give reliable estimates of crustal growth. First, zircons with O isotopic values that lie close to the mantle value are assumed to have formed by direct melting of the mantle, or mafic crust, or a combination of both. Because the range of their O isotopic compositions is minimal, and the $^{176}Lu/^{177}Hf$ of the source is well constrained, these zircons should give the most reliable model ages. In Chapter 5, the model ages calculated from zircons with $\delta^{18}O$ between 4.5‰ and 6.5‰ and from all grains in the Australian database were compared (Fig. 5.6 in Chapter 5). Differences between the major Hf model age peaks, and cumulative growth curves, are minimal. Second, Iizuka et al. (2017) compared Hf model ages for zircons from the world's major river with Os model ages for mantle xenolith from kimberlites, for which hybrid model ages are not a problem. The major peaks for both methods occur during the Paleo- to Mesoarchean and Paleo- to Mesoproterozoic periods, which they interpret as giving the major periods of the growth of the preserved continental crust. Third, the oldest model ages obtained for Greater Russia, Africa, and Australia, are ca. 4.1 Ga with ca. 3.7 Ga for Antarctica, Contiguous USA (Fig. S5.3 in Chapter 5) and zircon older than 3.8 Ga are very rare, in agreement with the observed growth of the continental crust, based on outcrops.

There are no surprises, such as model ages older than the age of the Earth. Even young, unradiogenic zircons, which projected back to the arc mantle $^{176}Hf/^{177}Hf$ growth curve, give geologically reasonable ages. Finally, detrital zircon Hf model age continental crust growth curves agree with the Nd growth curve, where comparisons have been made for the Australian continent (Fig. 5.7a in Chapter 5).

3.4 Summary

In summary, although uncertainty in the model age calculated for individual zircon is considerable, their errors tend to cancel out when used to construct continental growth curves from large data sets. With better constraining uncertainties for model age calculation using the methodology in this study, Hf model ages from a large database of zircons can be used as an average estimation of the timing of major continental crustal formation thus to reconstruct the growth curve of the preserved continental crust.

Chapter 4

Under the Antarctic Ice

Part of this chapter has been prepared for publication: **Chen, B**., Campbell, Ian H., Arculus, Richard J. What lies under the Antarctic ice?

Abstract

Ice covers over 99.5% of the surface of Antarctica and, consequently, little is known about the underlying geology. An obvious strategy is to analyze the detritus carried by glaciers from the continent onto the surrounding continental shelf. This chapter reports U-Pb dates, analyses of selected trace elements, O and Hf isotopes in detrital zircons collected from scientific ocean drilling sites (International Ocean Discovery Program) that potentially sampled 85% of the Antarctic continent. There are three surprises. First, existing dates from rare outcrops give the impression that Antarctica is an old continent, whereas this study shows the reverse. Less than 3% of the dated detrital zircons have Archean U-Pb ages, and significant continental growth started one billion years later than that on other well-studied continents. Second, although the Pan-African orogeny (650-450 Ma), associated with the amalgamation of Gondwana, was previously known, its full nature and significance were not. The Antarctic data show that it was by far the most important tectonic event that has affected Antarctica. Detritus shed from its mountains dominated the Antarctic sedimentation and produced a giant turbidite fan that extended across Antarctica into south-eastern Australia. These sediments trapped primitive magmas that were generated from underlying subduction zones, forming magma chambers that melted their sedimentary roof rocks/sediments. The result was sediment-dominated sources for the granites that characterize the 650-450 Ma magmatism in Antarctica. Finally, although Antarctica is relatively young, two of the analyzed detrital zircons have cores with concordant Hadean ages.

4.1 Introduction

Antarctica, the coldest, remotest continent in the southern hemisphere, is the fifth-largest continent, with an area twice that of Australia. It is the central piece in the Gondwana jigsaw, connecting Australia, India and Africa. Its geology can provide new insights into the relationship between Antarctica and its neighbours and elucidate its role in the amalgamation of the Gondwana supercontinent. Little is known about that geology, however, because the Antarctic surface is largely obscured by thick ice sheets that cover over 99.5% of the continent. In recent decades, the integration of geophysical and geological investigations, together with tectonic reconstructions from well-studied once-conjugate continents (i.e., Australia), has led to a better understanding of

Antarctica's geological evolution (e.g., Nogi et al., 2013; Scheinert et al., 2016; Artemieva and Thybo, 2020). What is known comes from rare outcrops or nunataks around the margins of the continent, such as those found on the Antarctic Peninsula, in Prince Charles and Ellsworth Mountains, and from the up to 4,000 m high and 100–300 km wide Transantarctic Mountains that divide East from West Antarctica. Previous studies have suggested that Antarctica is composed of two discrete, diverse, and contrasting geological provinces, each of which has a different tectonic evolution (Fig. 4.1).

Fig. 4.1 Outline of Antarctica. Yellow marks the area covered by the thick ice sheet.

East Antarctica, the main landmass of Antarctica, is the older part of the continent. It is thought to be composed of a metamorphic and igneous platform that is the basis of the continental shield. Few exposures of Archean rocks have been found, except from the 3.9–2.5 Ga Napier Complex in Enderby Land, the ca. 3.65 Ga Oygarden Group in Kemp Land, the 3.4–3.1 Ga Ruker Terrane in the Southern Prince Charles Mountains and the > 3.27 Ga and ca. 2.82–2.80 Ga Mather Terrane in Prydz Bay (Harley and Kelly, 2007). Proterozoic terranes in East Antarctica, dominated by Meso– to Neoproterozoic tectonism (1.40–0.91 Ga), include four domains: the Maud (Dronning Maud Land), Rayner (Enderby, Kemp and MacRobertson Lands), Rauer (Princess Elizabeth and Queen Mary Lands) and Wilkes (Wilkes Land coast) Provinces (Fig. 1 from Pierce et al., 2014).

Several phases of regional metamorphism and magmatism have been recognized in these terranes, especially during the assembly of Rodinia (ca. 1.10–0.90 Ga) (Fitzsimons, 2000b). During the Paleozoic, various rocks, such as sandstones, limestones, and terrestrial sediments, were deposited in these terranes. Intense 650–450 Ma Pan-African magmatism and low- to high-grade metamorphism associated with deformation, melting and plutonism in East Antarctica were due to the assembly of the Gondwana supercontinent. The study by Pierce et al. (2014) of detrital zircon, biotite and hornblende collected from ocean drill holes and piston cores around the eastern half of Antarctica shows a remarkable age peak for all minerals at ca. 650–400 Ma, emphasizing the importance of the Pan-African tectonic event in East Antarctica. The Ross Orogeny (550–450 Ma), attributed to the subduction of paleo-Pacific oceanic lithosphere, involved uplift, folding and metamorphism of sediments, associated with and followed by widespread granitoid intrusives, especially in the central Transantarctic Mountains.

In contrast to East Antarctica, West Antarctica is much younger and dominated by an active continental margin from ca. 500 Ma, marked by multiple magmatic and tectonic events. It consists of three geological divisions: 1) the Weddell Sea, 2) the West Antarctica Rift System (WARS) and Marie Byrd Land (MBL), and 3) the Antarctica Peninsula and Thurston Island (Fig. 1 from Jordan et al., 2020). Long-lived subduction along the entire margin of West Antarctica commenced in the Ordovician (488–444 Ma) and continued to the Permo-Triassic (ca. 250 Ma) (e.g., Siddoway and Fanning, 2009; Riley et al., 2012; Yakymchuk et al., 2015). The Antarctic Peninsula has a record of almost continuous arc magmatic events since the Ordovician, especially with significant volcanism and plutonism during the Permian to Triassic, Jurassic and Cretaceous (Jordan et al., 2020). In MBL, a mid-Cretaceous magmatic event occurred synchronously along the margin, attributed to arc magmatism along with extensive subduction (Brown et al., 2016; Riley et al., 2018). However, the tectonic setting of different divisions began to diverge after the Triassic. The cessation of subduction along the margin of MBL from ca. 100 Ma (Mortimer et al., 2019) led to crustal thinning and exhumation of lower crustal rocks and resulted in extensive magmatism across MBL and the WARS. Since the late Cretaceous, the MBL and WARS developed as a passive margin, later reactivated by continental rifting at ca. 43–26 Ma (Davey et al., 2016) and upwelling of hot mantle associated with widespread mafic volcanism (LeMasurier, 2013). In contrast, subduction

along the Antarctic Peninsula ceased by ca. 20 Ma, leading to localized and limited magmatism in that part of West Antarctica. From the Cretaceous, sedimentary and intra-arc volcanic successions were well preserved in the northern Antarctic Peninsula, particularly the South Shetland Islands and James Ross Island (e.g. Hathway and Lomas, 1998). Unlike the main part of West Antarctica, the Ellsworth-Whitmore Mountains province is marked by intra-plate granites and possibly was translated along the edge of East Antarctica (Jordan et al., 2017).

All these inferences are based on limited samples from exposures around the margin of Antarctica or in the Transantarctic Mountains. In order to decipher the geology of ice-covered Antarctica, I measured the U-Pb, O and Lu-Hf isotopic compositions of detrital zircons separated from the sediments sampled by the International Ocean Discovery Program (IODP) around the perimeter of Antarctica (Fig. 4.2). The sediments from the continental shelf were mainly derived by glacial erosion of ice streams fed by tributaries draining the deep interior of the continent (Bamber et al., 2000). As a result, these sediments could reasonably reflect the compositions of the source regions. Differing with previous studies, which locally focused on the eastern half of Antarctica or the Antarctic Peninsula of West Antarctica, the present research aims to elucidate the major tectonic events that have affected Antarctica from the sedimentary records and the growth of the preserved Antarctic continental crust on a continental scale, with a comparison with similar studies of other continents, based on the integration of U-Pb, O and Lu-Hf isotope systematics from detrital zircons.

4.2 Results

U-Pb dates and element concentrations of 1712 detrital zircons from 12 sites were measured for this study. 488 of these grains, which are free of U-Pb zoning and inclusions, were analyzed for O isotopes and 446 for Lu-Hf isotopes. To minimize sampling bias, age and trace element data from the literature are also included to better represent the whole continent. 1837 detrital zircons with U-Pb dates from Pierce et al. (2014) and 372 grains with U-Pb dates and trace element data from Paulsen et al. (2017a); (2017b) were added to the Antarctic zircon database. The latter dataset included trace element data (i.e., REE and P concentrations), but for only two closely

spaced sites (sites 13 and 14). The total sampling area covers 85% of Antarctica. Sample locations and details are shown in Fig. 4.2 and Table 2.1.

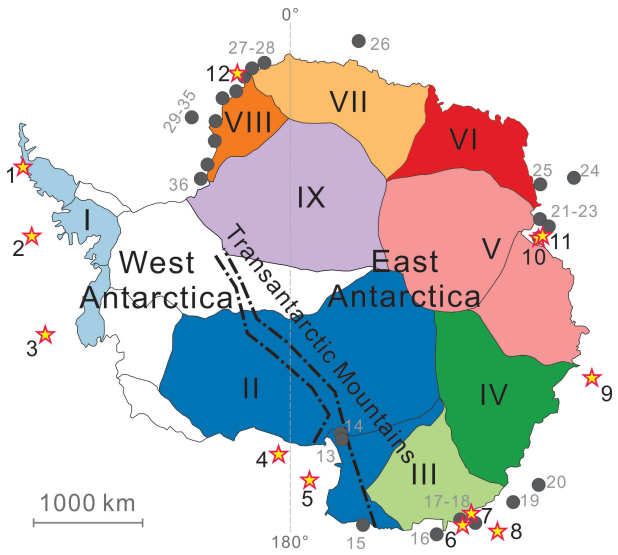

Fig. 4.2 Sample locations of scientific ocean drilling and piston core sites. Stars show the samples analyzed in this study whereas the grey dots show the sites for the reference data. The sample details are given in Table 2.1. 9 sampling divisions are based on the area of ice flow of the Antarctic ice sheet (Rignot et al., 2011).

4.2.1 U-Pb dates

The U-Pb isotope and trace element data of analyzed randomly picked detrital zircons from the Antarctic continent, and of reference zircons, are presented in Tables 4.1 and 4.2. As mentioned in Section 1.1, several factors can introduce sampling bias into the detrital zircon record. In the case of Antarctica, one more factor to be noted is glacial erosion. Because river samples are unavailable from the Antarctic continent, detrital zircons separated from continental shelf sediments, mainly eroded by glaciers, were used for investigating the Antarctic continent itself.

According to the study of ice flow in the Antarctic ice sheet by Rignot et al. (2011), if a low ice velocity of 1 m/yr near the ice divides is used, the glacier can cross 2000 km in 2 Myr, eroding the continental surface and effectively transporting eroded materials from the interior of the continent to its margins. The different rates of glacial erosion from different ice flow areas will generate biased sediment records, by extracting larger amounts of detrital zircon, for example, from the areas with higher erosion rates. Although glacial erosion rates can be modelled from glacier sliding velocities and climate (such as air temperature and precipitation) (e.g., Cook et al., 2020), much remains

undiscovered about the Antarctic bedrock topography and climate, impeding decreasing this potential bias in this study. More information about the Antarctic bedrock and topography is required to understand the relationship between the detrital zircon record and glacial erosion.

In this study, the Antarctic continent was divided into 9 ice flow areas based on the distribution of the ice movement velocity vectors from the remote sensing study of Rignot et al. (2011). The weighting of each sample is according to the size of the ice flow area from which the sample was most likely derived, for partially decreasing the sampling bias. The weight for Site 1, for example, is associated with Area I. Fig. 4.3a is a weighted histogram of U-Pb age populations for the 3921 detrital zircons from this study and the literature. Four major peaks can be identified: 1.60–1.40 Ga, 1.25–1.00 Ga, 650–450 Ma and 300–100 Ma. Less than 3% of the dated detrital zircons from Antarctica are older than 2.0 Ga. Detrital zircons aged 650–450 Ma, mostly derived from Areas II, V and IX, dominate the U-Pb spectrum, with 33% of the total population falling within this narrow age range. Another prominent group of zircons aged 300–100 Ma was mainly derived from Areas I and II. This study adopted weighting to minimize the sampling bias and its advantage is manifest by the comparison between non-weighted and weighted U-Pb age distribution (Fig. S4.1). For zircons from Area I, for example, their proportions are overestimated in the non-weighted histogram whereas, after weighting, the sampling bias of this group is minimized thus their weighted proportions of U-Pb ages are a proper representation on a continental scale. Because the feature of age peak at ca. 100 Ma in young zircons mainly from Area I (the Antarctic Peninsula), which is small (only 4% of the covered sampling area), is regional or local, failing to reflect the whole of Antarctica. And if the overestimated proportion of this age peak is used for further weighting in the calculation of Hf model ages distribution, an unrealistic growth curve of Antarctica based on the cumulative results from model age proportions will appear.

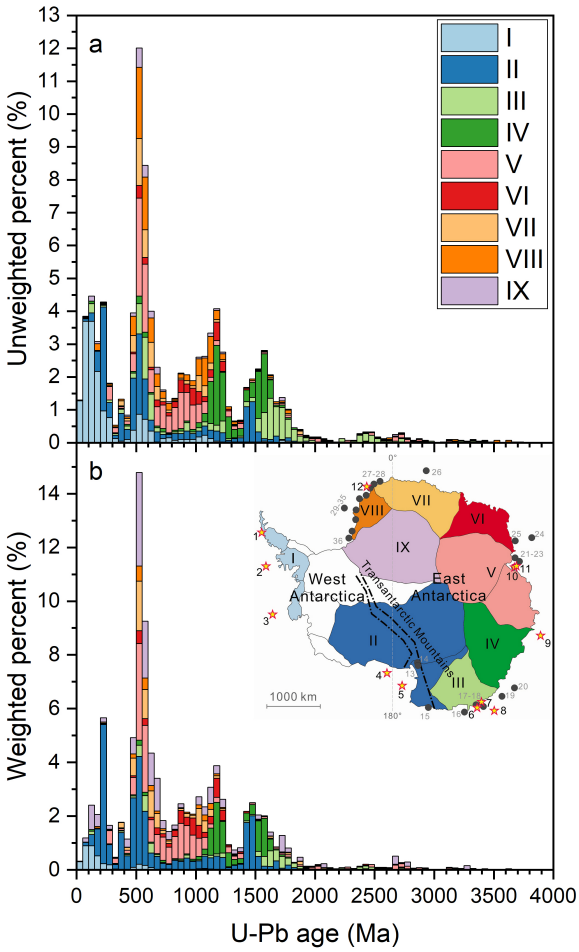

Fig. S4.1 U-Pb age histogram of detrital zircons from Antarctica. a) Histogram (50 Ma bins) of U-Pb dates for 3921 detrital zircons (1712 grains from this study, 1837 from Pierce et al. (2014) and 372 from Paulsen et al. (2017a); (2017b). b) Weighted histogram (50 Ma bins) using the same database in a. The weightings are according to the size of 9 areas as shown in Fig. 4.2.

Although less than 2.5% of the detrital zircons in this Antarctic database are Archean, an unexpected result from zircons analyzed in this study is the discovery of two grains with core domains that give concordant Hadean $^{207}Pb/^{206}Pb$ dates of 4250 ± 75 (2SE, standard error) (Grain 41) and 4274 ± 49 Ma (Grain 149) from IODP site 318-U1358A (Fig. 4.4 and Table 4.3). The uncertainties from ion counting statistics based on the study by Wielandt and Bizzarro (2011) are also calculated (Table 4.3).

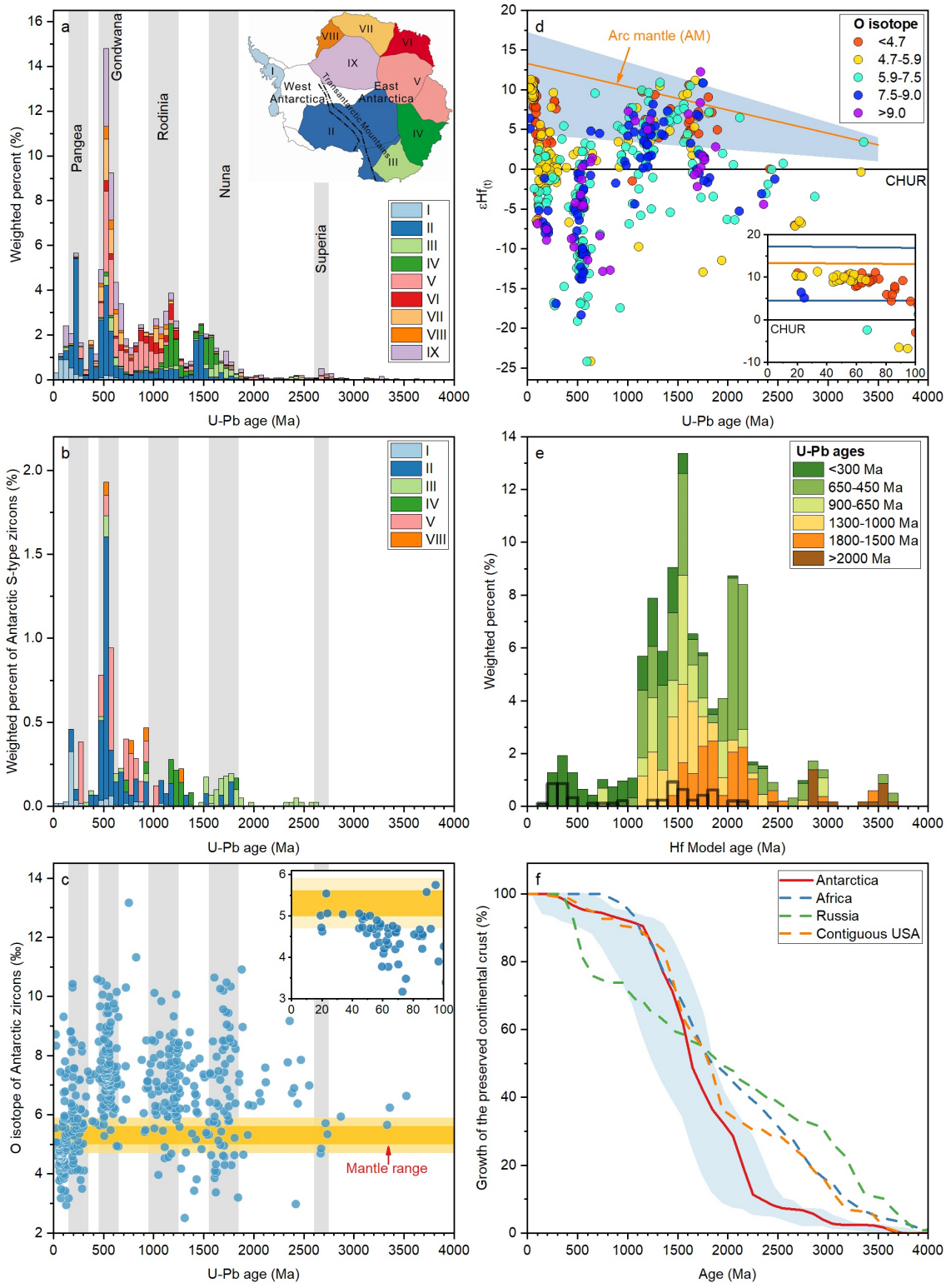

Fig. 4.3 Geochemical results from Antarctic detrital zircons. a) Weighted histogram (50 Ma bins) of U-Pb dates for 3921 detrital zircons (1712 grains from this study, 1837 from Pierce et al. (2014) and 372 from Paulsen et al. (2017a); (2017b), weighted by the size of 9 areas as shown in Fig. 4.2. Grey columns show the timing of supercontinent assembly; b) Weighted histogram of Antarctic zircons from S-type granites for the 1712 Antarctic zircons analyzed in this study, and 372 zircons from Paulsen et al. (2017a); (2017b), which include the required element concentrations (e.g., P and REE). S-type zircons were identified using the criteria (P: >15 malor; (REE +Y)/P: 0.77–1.23) of Zhu et al. (2020); c) Plot of $\delta^{18}O$ values against U-Pb ages with insert figure highlighting zircons of 100–0 Ma. The mantle range (5.3 ± 0.6, 2σ) (Valley et al., 1998) is shown in

yellow with 1σ in amber; d) $\varepsilon Hf_{(t)}$ values of the Antarctic detrital zircons colour-coded by their O isotopic composition (N=446), with insert figure highlighting zircons of 100–0 Ma. The blue area shows the evolution of the arc mantle (AM) at the 95% confidence level back to ca. 3.5 Ga with the orange line showing the evolution for the average Hf isotopic composition of AM from the study of Iizuka et al. (2013); e) Histogram of zircon average Hf model ages weighted by the proportion of each age group as shown in a. The dark histogram shows the proportions from juvenile zircon grains as defined in the text; f) Zircon Hf model ages growth curve of Antarctica based on the cumulative distribution of weighted Hf model age results in e, with the 95% confidence level shown in blue by using Hf arc mantle range in d. Curves for the other continents were recalculated using the method employed in this study. The data for Africa, Russia and the Contiguous USA are from Wang et al. (2009); Wang et al. (2011); Iizuka et al. (2013), respectively.

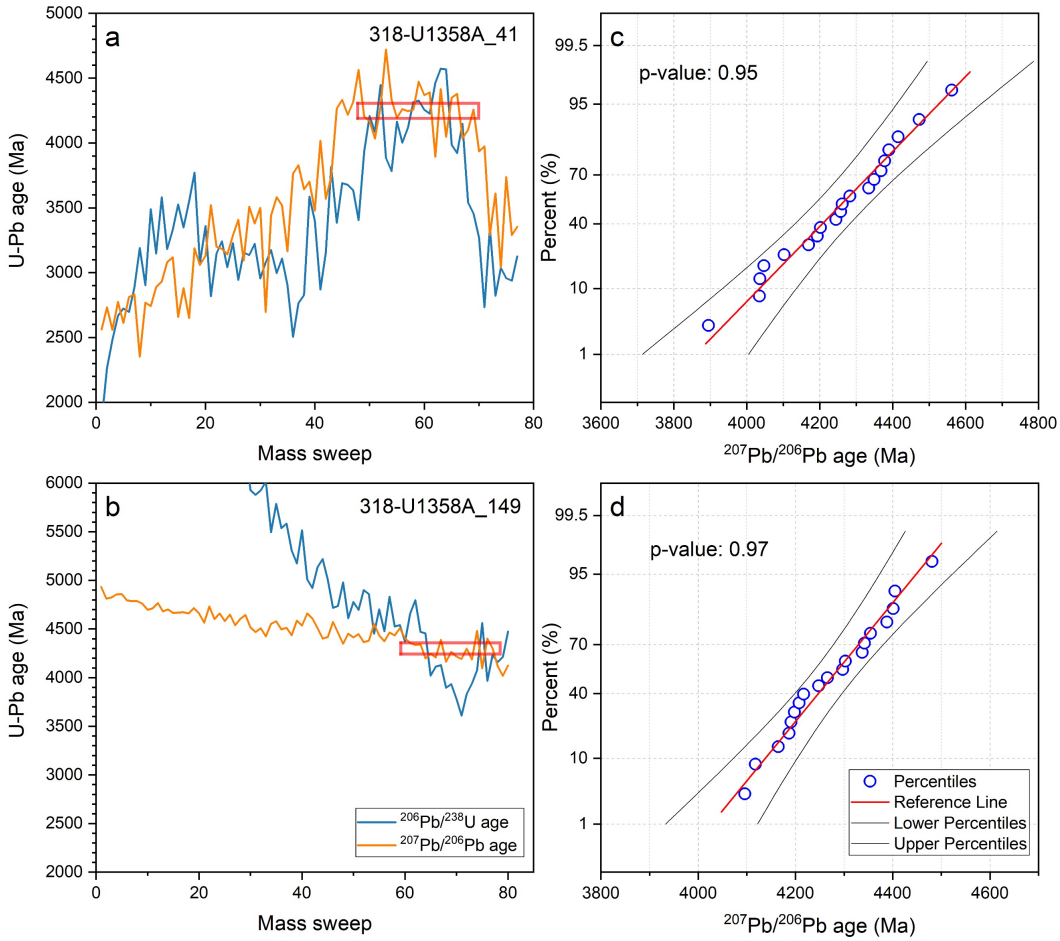

Fig. 4.4 U-Pb dating information for Grain 41 and Grain 149 from IODP site 318-U1358A. Dating results for the whole of the ablation period, and normality test for the selected mass sweeps for Grain 41 in a and c, and Grain 149 in b and d. The decrease in $^{207}Pb/^{206}Pb$ vs $^{206}Pb/^{238}U$ dates of Grain 149 suggests the presence of unsupported radiogenic Pb (Williams et al., 1984). The red rectangle shows the selected mass sweep for both grains used to calculate $^{207}Pb/^{206}Pb$ dates and for the concordance test ($^{207}Pb/^{206}Pb$ vs $^{206}Pb/^{238}U$ dates). The normality test is at a 95% confidence level.

4.2.2 Oxygen and Lu-Hf isotopes

The O isotope composition of 488 dated zircons and reference zircons are presented in Tables 4.4 and 4.5. Lu-Hf isotope data for 466 grains and their model ages

(see the calculation details in Chapter 3) are listed in Table 4.6, with reference zircon data listed in Table 4.7.

Fig. 4.3c shows the $\delta^{18}O$ values versus U-Pb ages, together with the $\delta^{18}O$ range of 5.3 ± 0.6‰ (2σ; Valley et al., 1998; 2005) for mantle zircons. Fig. 4.3d summarizes the Lu-Hf isotope systematics, plotted as $\varepsilon Hf_{(t)}$ against U-Pb ages and colour-coded by their O isotopic compositions. The present-day chondritic values from Bouvier et al. (2008) were used to calculate $\varepsilon Hf_{(t)}$. The range in the $\varepsilon Hf_{(t)}$ of the arc mantle from Iizuka et al. (2013), which has a mean of +13.3 (+3.9/-8.7ε, 95% confidence level) at present-day, is also plotted and extrapolated back to $\varepsilon Hf_{(3.5\ Ga)}$, given that the arc mantle evolution during the Early Earth's history is still unclear. In addition, Fig. 4.3 e and f illustrate the model age results and the cumulative growth curve of the Antarctic continental crust compared with the growth curves of other continents (African, North American and Russian) by adopting the same calculation method in this study.

Five distinctive time intervals can be identified from the O and Lu-Hf isotopic compositions of the dated zircons, each with contrasting Hf and O isotopic characteristics (Fig. 4.5 and Table 4.8): 1.80–1.50 Ga, 1.25–1.00 Ga, 650–450 Ma, 300–100 Ma and 100–0 Ma. The mean $\delta^{18}O$ values of zircons from the five intervals are 6.8 ± 0.5‰ (1.80–1.50 Ga), 7.0 ± 0.3‰ (1.25–1.00 Ga), 7.6 ± 0.3‰ (650–450 Ma), 5.8 ± 0.3‰ (300–100 Ma), and 4.8 ± 0.3‰ (100–0 Ma). Noticeably, the trends for mean $\delta^{18}O$ and $\varepsilon Hf_{(t)}$ through time display a clear negative relationship. The $\varepsilon Hf_{(t)}$ values of zircons between 650 and 450 Ma show the lowest mean $\varepsilon Hf_{(t)}$ value of -7.0 ± 1.2, whereas zircons younger than 100 Ma have the highest mean value of +8.3 ± 1.0.

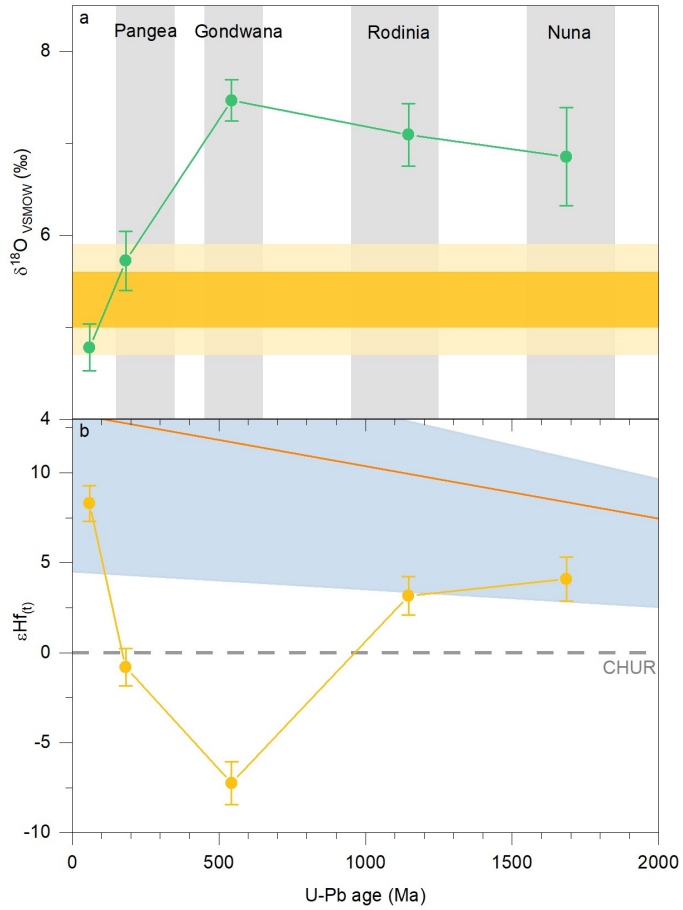

Fig. 4.5 Mean values of $\delta^{18}O$ and $\varepsilon Hf_{(t)}$ for five time intervals, with the error bar showing 2SE (standard error). Grey areas show the timing of supercontinent assembly, and the mantle range (5.3 ± 0.6, 2σ) is presented as yellow area with 1σ in amber area in a. AM evolution is also plotted (same with that in Fig. 4.3d) with the grey dash line marking CHUR (chondritic uniform reservoir) in b.

4.3 Discussion

4.3.1 Provenance of detrital zircons

There are four major peaks in the weighted U-Pb zircon age distribution: 1.60–1.40 Ga, 1.25–1.00 Ga, 650–450 Ma and 300–100 Ma (Fig. 4.3a). The peaks at 1.25–1.00 Ga, 650–450 Ma and 300–100 Ma correlate with the peaks at 1.1 Ga, 550 Ma and 260 Ma in the global detrital zircon age database (Campbell and Allen, 2008) and coincide in time with the amalgamation of the Rodinia, Gondwana and Pangea supercontinents respectively. However, older global peaks at ca. 2.70 and 1.80 Ga, which correlate with the amalgamation of Superior and Nuna, are absent. The only significant age peak older than 1.30 Ga is the one at ca. 1.60–1.40 Ga, which is slightly younger than the Nuna peak in the global database. Events of this age have been recorded in felsic volcanic rocks and intrusions from Bunger Hills in Wilkes Land, East Antarctica, at ca. 1.70–1.50 Ga (Tingey,

1991), and in felsic orthogneiss from Adélie Land and King George V Land, which has ages between 1.70 and 1.45 Ga (Stüwe and Oliver, 1989).

There have been several studies of Archean nunataks (Harley and Kelly, 2007; Kusiak et al., 2013; Hiess and Bennett, 2016; Guitreau et al., 2019) that give the impression that Archean terranes are an important feature of Antarctica. My results show otherwise. Less than 3% of the dated detrital zircons from Antarctica are older than 2.0 Ga, compared with 6% from North America, 7% from Europe, 10% from Africa, 14% from South America, 17% from Australia, and 20% from Asia (including China, Russia and India) in a global detrital zircon compilation (Zhu et al., 2020). Therefore, Antarctica is a young continent with no significant granite-forming orogenic event older than 2.0 Ga.

However, there is a surprise as shown in U-Pb age results. Two Hadean orphans were detected in the dated zircons. The core domains of Grain 41 and Grain 149 from the site IODP 318-U1358A (Site 6) yielded Hadean U-Pb ages, both over 95% concordance. Grain 149 shows “reverse discordance” (Fig. 4.4b). The phenomenon of reverse discordance was documented in zircons from the Napier Complex by Black and James (1983), Williams et al. (1984) and Hiess and Bennett (2016). In the detailed SHRIMP U-Pb zircon study by Williams et al. (1984), they confirmed that the presence of excess unsupported radiogenic Pb is the reason for the reverse discordance. Kusiak et al. (2015) suggested that metallic Pb nanospheres representing melt inclusions generated during ultra-high temperature metamorphism can result in this phenomenon. Despite the heterogeneity of U-Pb, Pb-Pb isotopic compositions in Grain 149, its core domain yielded a highly concordant $^{207}Pb/^{206}Pb$ age. Although the dated domains are small, the CL images show that the analyzed areas are inclusion free with P < 2000 ppm, Ti < 80 ppm, La < 10 ppm and have moderate Th/U (0.49 and 0.69). The calculated ages were based on 20 and 19 mass sweeps for Grains 41 and 149 respectively (Fig. 4.4 a and b). O isotopes were also analyzed for the two zircon cores, which yielded $\delta^{18}O$ values of 5.1‰ for Grain 41 and 5.3‰ for 149 respectively, which are within the normal ranges for Archean and Hadean zircons (Valley et al., 2005). Their calculated $^{207}Pb/^{206}Pb$ ages from mass sweeps for both grains passed the normality test (at 95% confidence level; Fig. 4.4 b and d) and the 1RSD uncertainties of their mean $^{207}Pb/^{206}Pb$ ages are slightly

higher than the uncertainties of random error calculated from ion counting statistics based on the counts of ^{207}Pb and ^{206}Pb (Table 4.3). Consequently, they provide plausible evidence for a remnant felsic crust of Hadean age within the Antarctic continent, although the area covered by this crust must be small, because grains with Hadean cores are very rare. However, no rocks older than 4.2 Ga have previously been reported from Antarctica. Previous studies show that the oldest rocks in Antarctica are found in the Archean Napier Complex where granulite-facies rocks give U-Pb zircon ages between 4.1 Ga and 3.9 Ga (Harley and Black, 1997; Guitreau et al., 2019; Król et al., 2020). However, the Napier Complex in Enderby Land is more than 3,700 km away from site 318-U1358A (Site 6 in Fig. 4.2) and the glaciers that feed Site 6 do not sample the Napier Complex. It is therefore an unlikely source of the putative Hadean zircons.

The 650–450 Ma Pan-African peak dominates the U-Pb age spectrum, with 33% of the zircon population falling within this narrow age range (Fig. 4.3a). Similar dominant age peaks were found in the detrital biotite and hornblende $^{40}Ar/^{39}Ar$ age spectra from Antarctica (e.g., Roy et al., 2007; Pierce et al., 2014). Pan-African peaks are also prominent features in the Australian, Indian and African zircon age spectra (Squire et al., 2006) and they correspond to the timing of Gondwana assembly. During this time, East Antarctica is suggested to have collided with other landmasses (Africa, India, Australia) to form Gondwana. The assembly of Gondwana during 650–450 Ma, associated with intense deformation, melting and the emplacement of syn- to late- tectonic intrusives, is recognized in four potentially distinct crustal fragments in Antarctica (Fig. 3.2-1 from Harley and Kelly, 2007): 1) Dronning Maud Land (East African-Antarctic Orogen: Jacobs et al. (1998)), 2) Lützow-Holm Bay (Lützow-Holm Belt), 3) Prydz Bay and Southern Prince Charles Mountains (Prydz Belt) and 4) Denman Glacier region (Pinjarra Belt) (Fitzsimons, 2000a, 2003). The coeval Ross Orogeny (ca. 590–490 Ma), characterized by voluminous granitoid magmatism, is manifest in a few areas in the Transantarctic Mountains at the current levels of exposure (Goodge et al., 2012). The distribution of this narrow age group of 650–450 Ma in Fig. 4.3a is consistent with the locations of the studied area affected by the Pan-African magmatism and the Ross Orogeny. More importantly, 22% of this age group is derived from Area IX, where the geology is inaccessible, suggesting that the effect of Pan-African magmatism on Area IX (Fig. 4.3a) might have been underestimated by previous studies due to limited exposure in that area.

In contrast with previous studies of detrital zircons from Antarctica (e.g., Phillips et al., 2006; Elliot et al., 2015; Castillo et al., 2017; Paulsen et al., 2017a), this study has revealed, even after weighting (Fig. S4.1), a prominent group of detrital zircons at 300–100 Ma. Those zircons are interpreted to be derived from felsic volcanism and igneous intrusions along the margin of West Antarctica and the central Transantarctic Mountains. Igneous rocks of this age have been documented by previous studies (e.g., Pankhurst et al., 2000; Artemieva and Thybo, 2020; Jordan et al., 2020) and interpreted to be the product of arc magmatism. The 300–100 Ma peak was not recorded in the previous detrital zircon study of Pierce et al. (2014) because that study was confined to East Antarctica.

4.3.2 Hf and O isotopic systematics

4.3.2.1 Juvenile zircon grains

The Hf and O isotopic characteristics of the zircons can be used to constrain the age of the source of the magma from which they crystallized. As a first approximation, zircons with $^{176}Hf/^{177}Hf$ ratios that lie within the arc mantle array (AMA, 95% conf.) can be assumed to have crystallized from mantle-derived magmas. This definition of zircon from juvenile crust will overestimate the percentage from that source because, for example, zircons, especially young zircons, crystallizing from a melt that initially lay within the upper half of the AMA, but became contaminated by continental crust, could still lie within the lower part of the mantle array. Using oxygen isotopes as an additional constraint, however, can minimize the number of zircons that will be misclassified. O isotopes in magmatic rocks are highly sensitive to the incorporation of supracrustal material that has been subjected to low-temperature processes, especially the production of clays by weathering, or to fluid-rock alteration. Valley (2003) has shown that magmatic zircons can preserve their igneous $\delta^{18}O$ values through subsequent high-grade metamorphism, hydrothermal alteration, magmatic assimilation or anatexis. In this study, zircons with a $^{176}Hf/^{177}Hf$ ratio that lies within the AMA, and have $\delta^{18}O$ values that fall within analytical uncertainty of the mantle value of 5.3 ± 0.6‰ (2σ) from Valley et al. (1998) are classified as juvenile grains. Zircons with these characteristics are assumed to have crystallized from juvenile magmas, whereas those with $^{176}Hf/^{177}Hf$ ratios below the AMA and/or $\delta^{18}O$ values above 5.9‰ are interpreted to have crystallized from partially melted continental crust or mantle-derived melts that were

contaminated by continental crust and/or sediments. Despite its limitations, this filter does distinguish zircons that crystallized from melts of a predominantly mantle origin from those containing a significant, or dominant, crustal component. The Hf and O isotopic compositions of zircons, in combination, therefore, provide valuable insight into the tectonic setting at the time of zircon crystallization.

4.3.2.2 Insights into the tectonic setting of Antarctica

Fig. 4.3 c and d show O isotopes and $\varepsilon Hf_{(t)}$ values of the analyzed zircons plotted against U-Pb ages. Zircons with U-Pb ages corresponding to the time of the four supercontinent forming events were recognized in Antarctica: Nuna (1.85–1.50 Ga), Rodinia (1.25–1.00 Ga), Gondwana (650–450 Ma) and Pangea (300–100 Ma). They have contrasting Hf and O isotopic characteristics (Fig. 4.5 and Table 4.8).

Although O and Hf isotopic compositions were measured on only 20 grains older than 2.0 Ga, 70% of those have $\delta^{18}O$ values over 5.9‰ and only 2 grains plotted within the AMA for Hf composition. None of these old Antarctic zircons is from juvenile crust. Most of the grains were produced from the partial melting of reworked older continental crust, with minor contamination by sediments. Their average incubation time (difference between their model age and crystallization age) of 500 Myr supports this interpretation (Fig. 4.6). This study cannot take account of the contribution to the continental crust from juvenile basaltic rocks that do not crystallize zircon, for example, continental tholeiitic and basaltic arc magmas. The conclusion that no Antarctic zircon older than 2.0 Ga is from juvenile felsic crust may change once older detrital zircon grains with juvenile signatures are recognized.

Although 56% of the Nuna-aged zircons have $^{176}Hf/^{177}Hf$ ratios that fall within the AMA, 64% have $\delta^{18}O$ values higher than the mantle range. Consequently, only 14% meet the criteria for juvenile zircons. Similarly, although 65% of the Rodinia-aged zircons fall within the AMA, 88% have $\delta^{18}O$ values above the mantle range so that only 5% are classified as juvenile. Overall, 83% of the Nuna- and Rodinia-aged grains have $^{176}Hf/^{177}Hf$ ratios higher than the chondritic value, but 75% have elevated $\delta^{18}O$ values higher than the mantle value. The Nuna- and Rodinia-aged zircons are therefore interpreted to have crystallized from mantle-derived magmas that have undergone generally small, but

variable amounts of sedimentary contamination, with the average contamination being greater for the Rodinia than the Nuna datasets.

In sharp contrast, only 1% of zircons of Gondwana age lie within the AMA, and none of those has mantle-like $\delta^{18}O$ values. Therefore, none of the juvenile zircons in the Antarctic dataset formed during the Gondwanan era. Furthermore, their average $\varepsilon Hf_{(t)}$ values are significantly lower than those of other periods (Fig. 4.5b), so that many of their model ages are correspondingly older and their average incubation times are appreciably longer than those of zircons that formed during the amalgamation of Nuna or Rodinia (Fig. 4.6).

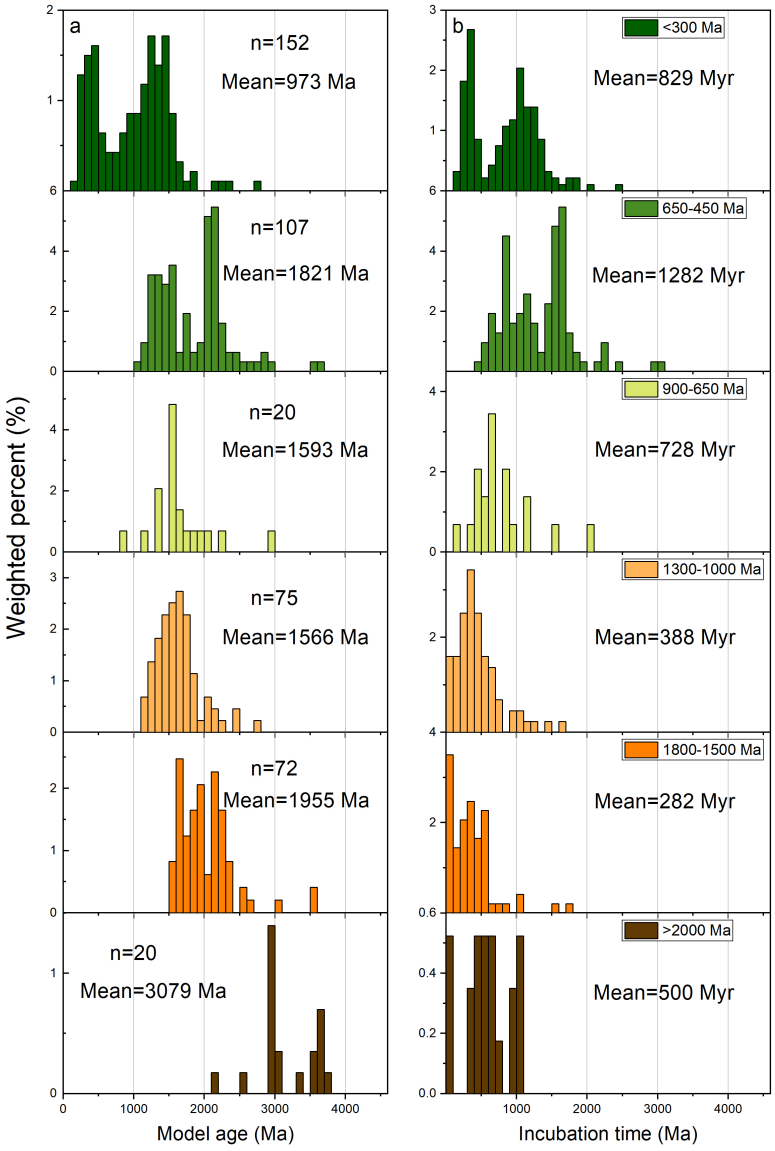

Fig. 4.6 Hf model ages and incubation times for the Antarctic detrital zircons analyzed in this study. a) Weighted histograms of Hf model ages for six age groups. b) Weighted

histograms of incubation time for six age groups. The weighting follows the proportions of each age group as shown in Fig. 4.3a.

Based on a near 1:1 correlation between (REE + Y) and P in zircon from S-type granitic magmas (Burnham and Berry, 2017) that formed by melting sources dominated by sedimentary rocks, total (REE + Y) and P in zircon grains can be used to identify those that come from S-type igneous rocks. Fig. 4.3b shows the weighted histogram of zircon dates from S-type granites, using the filter of Zhu et al. (2020). It shows that S-type zircons of the Gondwanan age dominate the spectrum in the Antarctic zircon database. Gondwana amalgamation was recognized by Zhu et al. (2020) as the most important period of S-type zircon production in the dataset of detrital zircons from Earth's major rivers, which sampled all continents except Antarctica. Similar conclusions have been reached based on O isotopes in the zircons from the study by Spencer et al. (2014). By adding the Antarctic dataset to the compilation of Zhu et al. (2020), the updated global database from this study shows that almost one-third of the 600–450 Ma S-type zircons are from Antarctica (see Chapter 6 for details), which makes S-type granite production even more important during the amalgamation of Gondwana than recognized by either earlier studies.

S-type granites are suggested to be produced by melting of rocks within a former giant turbidite fan (Zhu et al., 2020). The Antarctic data are consistent with this interpretation. Squire et al. (2006) suggested that the collision between East and West Gondwana was pincer-like, starting with the collision between the Arabian-Nubian Shield and North Africa at ca. 650–590 Ma, followed by the collision between India and Africa at ca. 580–550 Ma and finally East Antarctica colliding with Africa at ca. 525–490 Ma. The resulting >8,000 x 1,000 km Transgondwanan Supermountains eroded to form two giant turbidite fans one down each side of the supermountains chain. During the early stages of supermountain formation, much of the detritus shed from the eroding mountains was transported into the closing ocean basin between East and West Gondwana (Squire et al., 2006), where it was continuously added to and reworked by the pincer movement of the closing basin. The result on the eastern side was a giant turbidite fan, which extended across East Antarctica into south-eastern Australia (see Chapter 6 for details). The volume of turbidites in south-eastern Australia alone is estimated to be equal to that of the modern Bengal Fan, twenty times larger than any

other modern river fan. This study suggests that the turbidites in the eastern giant fan were too buoyant to be subducted into the mantle and they became wedged between the closing continents to form an extensive turbidite sequence similar to, but much larger than, the one preserved in south-eastern Australia. The low density of this thick sedimentary sequence prevented mantle-derived magmas, originating from the subduction zones associated with the closure of the Mozambique ocean basin (Emmel et al., 2008; Collins et al., 2021) and Ross Orogeny (Foden et al., 2006), from reaching the surface. These magmas ponded at or near the base of the sedimentary sequence to produce large magma chambers that provided the heat and melted their low melting point, sedimentary roof rocks. This resulted in the magmas, from which the Antarctic Gondwana-era zircons crystallized, becoming highly contaminated by heterogeneous sedimentary materials with variable ages. It explains their highly variable Hf model ages, high O isotope values and the complete absence of pristine mantle-derived magmas. S-type granites were produced where the bottom of the thickened turbidite sequence reached the temperature required for spontaneous partial melting, without requiring significant additional heat input from mantle-derived magmas.

Most of the zircons younger than 300 Ma were derived from West Antarctica. Magmatism in West Antarctica during this period was dominated by arc-related, Paleo-Pacific volcanism, which also manifests itself in Zealandia and Patagonia. Magmatic flare-ups of similar age are recognized in all three regions, suggesting that they are due to plate reorganization rather than local tectonic processes (Jordan et al., 2020). The isotopic characteristics of the 300–100 Ma zircons are consistent with their being derived predominantly from convergent continental subduction zones. They have $\varepsilon Hf_{(t)}$ values that cluster around the chondritic value, with only 11% lying within the AMA and have a mean $\delta^{18}O$ value of 5.72 ± 0.32‰ (2SE), which lies within the mantle range (Fig. 4.5a). The majority of zircons that formed during the Pangean era are therefore interpreted to have crystallized from mantle-derived melts that formed above a subduction zone and have been variably contaminated by older igneous crust, except for the 35% that have $\delta^{18}O$ above the mantle zircon range. That 35% is suggested to have incorporated variable amounts of sedimentary materials. Permian detrital zircons from metasandstones (Castillo et al., 2016) and metaturbidites of the Duque de York Complex (Sepulveda et al., 2010), both in Patagonia, South America, show that Permian

subduction-related arc magmatism extended along the Pangean margin of the Antarctica Peninsula into South America. The Patagonian zircons have similar $\varepsilon Hf_{(t)}$ values to those from the Permian Antarctic Peninsula, but higher $\delta^{18}O$ values, averaging about 7‰ (Castillo et al., 2016). These higher $\delta^{18}O$ values show that the Patagonian section of the arc incorporated more sediments into its magmas than the section in the Antarctic Peninsula did.

The zircons with ages between 100 and 0 Ma have distinctive isotopic characteristics. 95% have $\varepsilon Hf_{(t)}$ values falling within the AMA, but unlike zircons from other periods, only 5% have $\delta^{18}O$ values above 5.9‰. 35% can be classified as zircons derived from juvenile crust, and most of those are from the Antarctic Peninsula, where there are voluminous subduction-related basaltic to silicic volcanic and volcaniclastic rocks of Late Cretaceous to Early Paleogene age. An unusual attribute of the 100–0 Ma zircons is that, although they have an average $\delta^{18}O$ value of 4.78 ± 0.26‰, within the mantle zircon range, more than half have $\delta^{18}O$ values below the lower limit of 4.7‰ expected for zircons crystallizing from mantle-derived melts. Some values extend as low as 3.17‰ (insert figure in Fig. 4.3c). Low $\delta^{18}O$ zircons crystallize from low $\delta^{18}O$ magmas, which are produced when magma assimilates rocks that have been hydrothermally altered by low $\delta^{18}O$ meteoric water. This can only happen, with the required intensity, in shallow magma chambers where abundant meteoric water is available in the magma chamber wall rocks. Low $\delta^{18}O$ zircons from Yellowstone (Bindeman and Valley, 2001), Timber Mountain (Bindeman and Valley, 2003) and Iceland (Carley et al., 2017) are examples. They are interpreted to form in association with plume volcanism (Yellowstone and Iceland) or extensional settings (Timberland) (Bindeman and Valley, 2003). The West Antarctic rift system and Marie Byrd Land were sites of extreme rifting at ca. 100 Ma (Jordan et al., 2020) and a progressive shutdown of subduction along the Antarctic Peninsula margin during the Late Cretaceous to the Neogene led to further rifting (Fretzdorff et al., 2004). Consequently, the likely tectonic setting for the 100–40 Ma period, when most of the low $\delta^{18}O$ zircons formed, is an oceanic or continental back-arc rift. Sub-AMA $\varepsilon Hf_{(t)}$ values prior to 40 Ma suggest that the arc was initially continental, but became oceanic at ca. 40–35 Ma, causing the $\delta^{18}O$ values of the zircons to shift from sub-mantle to mantle values and the $\varepsilon Hf_{(t)}$ values to move into the AMA (insert figures in Fig. 4.3 c and d). The timing of this change corresponds to the opening of the Drake

Passage between Antarctica and South America at ca. 34 Ma (Eagles et al., 2006). This led to a back-arc extension on the Scotia Plate, and subduction and ocean island arc volcanism on the southern side of the Drake Plate, which is close to the easternmost tip of the Antarctic Peninsula and a likely source of the zircons with mantle $\delta^{18}O$ values.

4.3.3 Implications for the growth of the Antarctic continental crust

Hafnium model ages provide estimates of the time when the source of the magma from which the zircon crystallized separated from the mantle. Despite the limitations discussed in Chapter 3, major periods of continental crustal growth can still be retrieved from Hf model age distributions. To minimize sampling bias, the distribution of Hf model ages of the zircons were further weighted based on the proportion of the U-Pb age group with which the zircons were associated. Weighted model ages in Fig. 4.3e confirm the earlier observation based on the zircon U-Pb ages that Antarctica is a young continent. The main period of crustal growth in the Antarctic continent did not start until 2.2 Ga. The growth peaked between 2.2 and 1.1 Ga, with minor peaks at ca. 3.7–3.4 Ga, ca. 3.0–2.7 Ga and ca. 500–200 Ma. The lack of juvenile zircon grains though the time indicates that reworked pre-existed crust played an important role in the evolution of Antarctic continental crust and that juvenile granitic crust is rare, though 45% of the crust formed during 500–200 Ma was probably juvenile (Fig. 4.3e). Evidence for crustal reworking also can be found in the crustal incubation times (Fig. 4.6b), the difference between the Hf model age and crystallization age of zircon defined by Wang et al. (2009). The average incubation time for the six age groups is consistently longer than 280 Ma, with the highest value of 1.28 Ga for the 650–450 Ma zircon age group. In general, the significance of crustal reworking increases as zircon age decreases. No obvious correlation between the major periods of crustal formation and the major periods of zircon crystallization implies the complexity of the formation of felsic magmas, which zircon crystallized from.

Fig. 4.7 also shows the weighted model age results but colour-coded by the region from which the analyzed samples were probably derived. This supports the conclusion that West Antarctica is much younger than East Antarctica, consistent with previous investigations reported in the literature. Major crustal growth of West Antarctica

occurred between 1.6 and 1.1 Ga, 600 Myr later than that of East Antarctica. In addition, East Antarctica scarcely grew after 1.1 Ga, whereas there is another boost of crustal growth during 500–200 Ma for West Antarctica, which probably evolved a tectonically active margin after 500 Ma (Jordan et al., 2020).

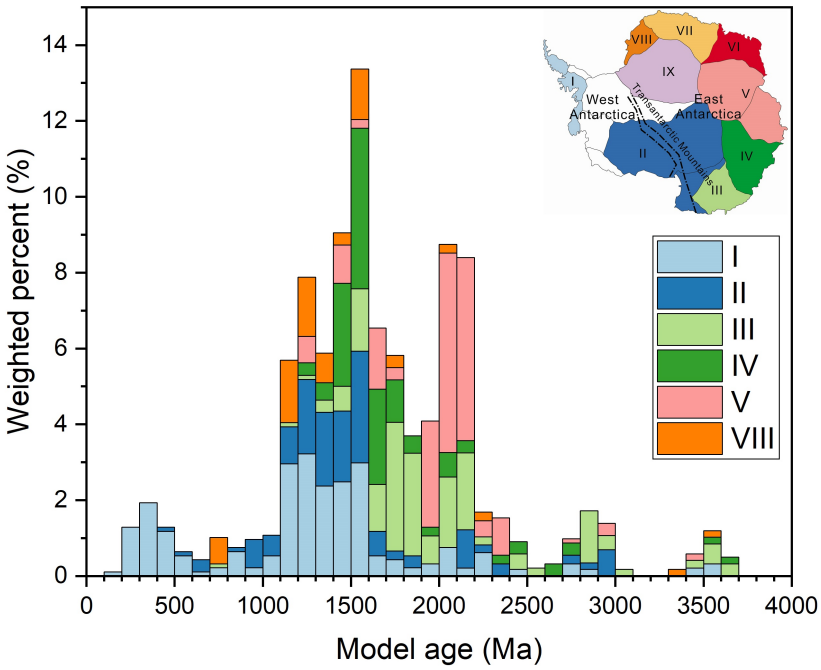

Fig. 4.7 Histogram of zircon average Hf model ages weighted by the proportion of each age group as shown in Fig. 3a and colour-coded by the area from which the samples were derived.

Fig. 4.3f shows a cumulative growth curve for the Antarctic continental crust, comparing it with similar curves for Africa, Asia (Russia) and North America (Contiguous USA). As discussed in Chapter 3, although the uncertainties associated with individual Hf model ages are considerable (e.g., Vervoort and Kemp, 2016), most of the errors are random. Consequently, conclusions drawn from a large dataset, especially when used for comparisons with other large datasets by using the same methodology, should be reliable as a good first approximation. Furthermore, the 95% confidence level of the curve for Antarctica is further constrained by using the arc mantle Hf range (95% conf.) as shown in Fig. 4.3d. The reliability of Hf model ages increases as zircon age increases because (i) the uncertainty window of the AMA narrows with age, and (ii) the time difference over which the $^{176}Hf/^{177}Hf$ must be extrapolated from the zircon crystallization age to the mantle growth curve decreases.

The results show that although Antarctica started to form at ca. 3.7 Ga, with an upper limit of ca. 3.9 Ga, which is consistent with the oldest dates recorded from the exposed rocks in the East Antarctica craton, the amount of continental crust produced during the Archean was small. Only 8% of the Antarctic continental crust had formed by the end of Archean, compared with 30% in Africa, 28% in North America (the contiguous USA), and 38% in Asia (Russia). The main period of growth occurred between 2.2 and 1.1 Ga, with 91% of the preserved crust having formed by 1.1 Ga. There was a minor peak of crustal growth between 500 Ma and 200 Ma, albeit at a slower rate than before 1.1 Ga, with nearly half of the crust generated during this period being juvenile (Fig. 4.3e).

4.4 Summary

In summary, detrital zircons were collected from scientific ocean drilling sites around Antarctica that sample 85% of the Antarctic continent and analyzed for U-Pb ages, trace element concentrations, and O and Hf isotopic compositions. There were three surprises. First, the U-Pb ages and Hf model ages show that Antarctica is a young continent, whereas the previous implied the opposite. Although Antarctica started to grow at ca. 3.9 Ga, only 8% of the Antarctic continental crust had formed by 2.5 Ga. Significant growth of Antarctica started at 2.2 Ga, nearly one billion years later than other well-studied continents. Second, the Antarctica dataset reveals that the collision between East and West Gondwana (650–450 Ma) is by far the most influential tectonic event that regulated the records of Antarctica. The Pan-African peak dominates the zircon U-Pb age spectrum in Antarctica. Enormous amounts of detritus, shed from the Transgondwana Supermountains, produced a giant turbidite fan that expanded across Antarctica into south-eastern Australia. These thick sediments prevented primitive magmas, which were generated from underlying subduction zones, from reaching the surface. Ponded magmas formed magma chambers that melted their sedimentary roofs. As a result, 650–450 Ma magmatism in Antarctica is characterized by a large contribution from granites derived from sediment-dominated sources. Lastly, the presence of two detrital zircons with cores of concordant Hadean age implies that, under the Antarctic ice, there is a tiny remnant of the Hadean crust.

Chapter 5

The Growth of Continental Australia

Abstract

Detrital zircons from fluvial deposits and sand dune fields in Australia have been analyzed for U-Pb, O and Lu-Hf isotopes to model the growth of the preserved Australian continental crust. Major peaks in the zircon U-Pb age spectra correspond closely to the times of supercontinent assembly. However, the abundance of Pan-African (650–450 Ma) and Grenvillian (1.3–1.0 Ga) zircons in Australia is likely to be an overestimate for continental Australia itself—those zircons were a large component of the enormous volumes of detritus shed from the Neoproterozoic Transgondwanan Supermountains and transported across Antarctica to Australia. The calculated incubation times (time difference between primitive crust formation and crustal melting) clearly show that crustal reworking was most significant during the assembly of Gondwana. The zircon Hf model age growth curve for Australia agrees well with the revised whole-rock Nd model age growth curve.

Using the same methodology, Hf growth curves for Antarctica, Africa, Asia, and North America have been constructed, suggesting an approximately similar crustal growth for Australia, Africa, and North America, while Antarctica and Asia differ. About 30% of Australia, Africa and North America formed by 2.5 Ga, with 85% established by 1.2 Ga. Asia grew faster, with 30% already formed by 3.0 Ga and 75% by 700 Ma. Antarctica evolved much slower than all other continents, only 8% having emerged by 2.5 Ga. Compiling the results from the five continents has made it possible to propose a growth model for the preserved continental crust on a global scale. The model demonstrates continuous growth of the continental crust, with at least 25% formed by the end of the Archean and 90% established by 0.9 Ga.

5.1 Introduction

Australia, the largest island and smallest continent, has a land area of 7.69 M km^2. It was part of Gondwana until ca. 95 Ma, when the continent began to drift away from Antarctica (Williamson et al., 1990), defining its present-day geographical position and tectonic setting. The geological history of Australia spans 4.4 billion years. Australia is home to some of the oldest rocks in the world, some dating back to more than 3.7 Ga, with the oldest-known detrital zircons (4.4–4.2 Ga) found in the Yilgarn Craton, Western

Australia. The long and relatively stable geological history of Australia, which closely links to supercontinent cycles that control the major tectonic events and shape the tectonic setting of Earth, made Australia a symbolic natural laboratory for understanding how Earth worked during its early history and how the continental crust evolved through the time.

The crustal growth of the Australian continent is generally represented as the cumulative fraction of the present crustal volume through time. McCulloch (1987) used whole-rock Nd model ages to propose a growth model for the Precambrian crust of Australia, identifying three periods of high crustal growth rates, at ca. 2.7 Ga, ca. 2.2 Ga and ca. 1.8 Ga. In recent decades, a considerable increase in new Nd isotope data from mafic to felsic igneous rocks in Australia has made it possible to calculate a new crustal growth curve on a detailed continental scale. The new curve of Champion (2013) shares overall similarities with that calculated by McCulloch (1987). Basing on two-stage Nd depleted mantle model ages, Champion (2013) confirmed the observation from the known geology that continental Australia grew predominantly from west to east, and showed that 20% of the continent had formed by 3.0 Ga, 40% by 2.5 Ga, 60% by 2.0 Ga, and ca. 75% by 1.5 Ga. Because two-thirds of the Australian land surface is covered by regolith, the contribution of igneous rocks represented by the limited samples from those areas is likely to be underestimated in the record. As discussed in Chapter 1, detrital zircons from major rivers from continents are likely to be more representative and thus particularly useful in providing some insights for studying crustal growth on a continental scale. U-Pb, O and Lu-Hf isotopic compositions of detrital zircons from Antarctica (Chapter 4), North America (Wang et al., 2009), Asia (Wang et al., 2011), and Africa (Iizuka et al., 2013) have been analyzed and integrated into the present study of the growth of the preserved continental crust.

This chapter presents the results of the integrated analyses of U-Pb, O and Lu-Hf isotopes for 646 detrital zircons from the Australian continent, uses the data to identify the major periods of crustal growth and models the growth of the preserved Australian continental crust. The reliability of the Hf growth curve for Australia is demonstrated through comparison with the Nd growth curve from igneous rocks in Australia. Combined with other datasets from Asia, Africa, and North America, using the same

methodology adopted in this research, the results make it possible to reconstruct the global growth curve of the preserved continental crust.

5.2 Regional Geology

Detrital samples were collected and analyzed from 35 sites in Australia, including 19 samples of topsoil sediment from the National Geochemical Survey of Australia (NGSA; www.ga.gov.au/ngsa), 10 sand samples from sand dunes collected by Dr Stephen D. Pell (Pell, 1994) and six sand samples from rivers. Sample locations are shown in Fig. 5.1 and listed in Table 2.2.

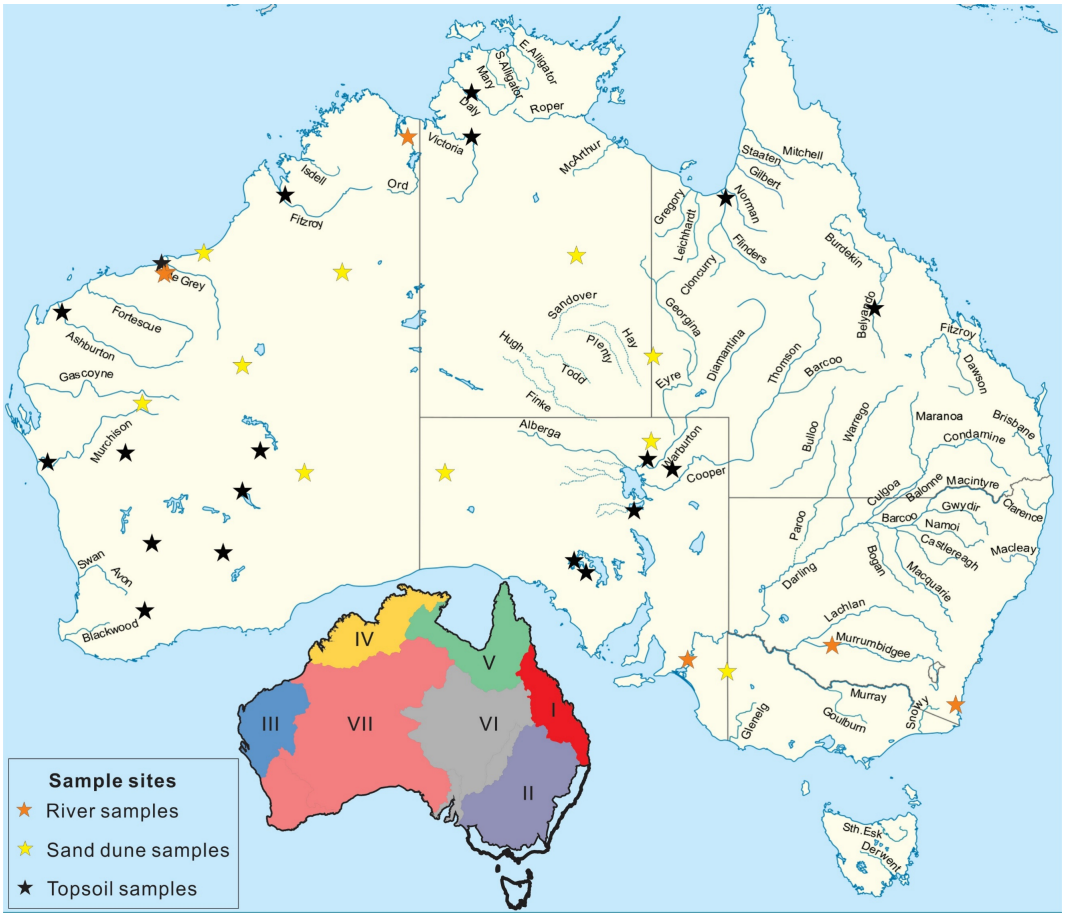

Fig. 5.1 Map of major rivers in Australia with sample locations showed as stars. Orange stars represent river sediment samples, yellow for sand dune sediment samples with black stars for topsoil samples (catchment outlet sediment samples). Seven main sampling areas are defined based on the drainage divisions and river basins according to the study of Stein et al. (2014).

Broadly speaking, the Australian continent grew from west to east, starting with two major Archean cratons, the Yilgarn and Pilbara cratons, which form the oldest part of the continent in West Australia, followed by Proterozoic rocks in the center, and

finally Phanerozoic rocks in the East. Blewett (2012) divided Australia into six major crustal elements, based on similar geological (composition) and geophysical (magnetic and gravity) characteristics: the West Australian Element (WAE), the Central Australian Element (CAE), the North Australian Element (NAE), the South Australian Element (SAE), the Tasman Element (TE) and the Pinjarra Element (PE) (Fig. 5.2).

5.2.1 Archean (>2.5 Ga)

The evolution of Australia commenced with the formation of three Archean cratons: the Yilgarn and Pilbara Cratons in Western Australia, and the Gawler craton in South Australia (Fig. 5.2). The oldest rocks in the Australian continent, dating between 3.73–3.53 Ga, are the anorthosites and orthogneisses of the Narryer Terrane in the Yilgarn Craton (e.g., Kinny et al., 1988; Wilde et al., 2001; Cassidy et al., 2002; Wyche, 2007), and the granite-greenstones of the Pilbara Craton (Van Kranendonk et al., 2002). The Pilbara Craton is dominated by ovoid-shaped granite gneiss bodies (3.53–2.83 Ga) (e.g. Bickle et al., 1983; Bickle et al., 1989; Williams and Collins, 1990), which intrude the greenstones. The granite greenstones are overlain by a stratified volcanic and sedimentary sequence, the Mount Bruce Supergroup that formed between ca. 2.78 to 2.45 Ga in the Hamersley Basin (e.g., Arndt et al., 1991; Blake et al., 2004; Trendall et al., 2004).

The Yilgarn Craton, the largest segment of Archean crust in Australia, consists of typical Archean granite-greenstone terranes that formed between ca. 3.1 and 2.6 Ga with a minor component older than 3.7 Ga (Cassidy et al., 2006). However, most of the magmatism occurred in a short, sharp peak in the period between 2.72 and 2.66 Ga, with mafic volcanism preceding the intrusion of granitic plutons (Campbell and Hill, 1988; Blewett, 2012; Ameen and Wilde, 2018).

The Archean basement of Gawler Craton comprises orthogneiss and paragneiss of the Sleaford and Mulgathing complexes with minor greenstones, which were subjected to plutonism and metamorphism during the Sleafordian orogeny between ca. 2.64 and 2.3 Ga (Daly and Fanning, 1993; Hand et al., 2007; Reid and Hand, 2012). Concurrently, in the northern part of the Northern Territory, various sediments, banded iron formation, and felsic to mafic volcanics were deposited on Neoarchean crystalline basement in the

Pine Creek Orogen at ca. 2.6-2.5 Ga (Cross et al., 2005; Hollis et al., 2009; Hollis and Wygralak, 2012). These strata were regionally deformed, metamorphosed and intruded by syn- to post-tectonic granitic rocks and mafic intrusions during the Early Proterozoic.

5.2.2 Proterozoic (2500–542 Ma)

Following the final cratonization of the Archean blocks, the Pilbara and Yilgarn cratons were amalgamated during the Capricorn Orogen between ca. 2.22 and 1.95 Ga to form the West Australian Element (Cawood and Tyler, 2004), one of the earliest components of Nuna (Huston et al., 2012). High-grade metamorphic rocks, with similar age (2.00–1.95 Ga), have been identified from the basement beneath the Pine Creek Orogen (Page, 1974, 1976; Worden et al., 2008). The amalgamation of several terranes, including the Tanami-Tennant-Mt Isa Province, the Kimberley-Pink Creek Province and the Aileron Province, led to the formation of most of the North Australian Element before 1.84 Ga (Goleby et al., 2009; Blewett, 2012; Korsch et al., 2012). Conglomerates, sandstones, siltstones, mudstones and minor felsic igneous rocks of the Speewah Group were deposited in the Kimberley Basin at ca. 1.84 Ga (Page and Sun, 1994; Sheppard et al., 2012; Tyler et al., 2012). The West and North Australian Elements amalgamated at 1.79–1.78 Ga during the Yapungku-Capricorn Orogeny (Bagas, 2004), which was initiated by north- to northeast-directed subduction. The Archean core of the Gawler Craton then collided with the southeastern margin of the North Australian Element during the Kimban-Nimrod-Strangways Orogeny between 1.74 and 1.69 Ga (Betts et al., 2008).

Contemporaneous subduction and collision resulted in the prolonged development of an extensional basin in the interior of the continent. Supracrustal sequences, which consisted initially of mafic to felsic volcanic rocks, but became increasingly sediment-rich with time, were deposited in trough-like structures starting at ca. 1.85 Ga in the South Australian Element (Cowley et al., 2003; Fanning et al., 2007; Howard et al., 2011; Szpunar et al., 2011). A series of orogenies at ca. 1.6 Ga led to the closure of a backarc basin system in the southern Proterozoic Australia, resulting in the addition of the Warumpi, Musgrave and Curnamona Provinces to the North Australian Element (Blewett, 2012). Episodic orogenesis and metamorphism were intensely overprinted the Albany-Fraser and Musgrave orogens between ca. 1.3 and 1.1 Ga (Betts and Giles, 2006;

Smithies et al., 2010; Kirkland et al., 2011). Gabbros and granites in the Albany-Fraser orogen were intensely deformed and metamorphosed between ca. 1.3 and 1.28 Ga (Betts et al., 2008). Crustal thickening and high-grade metamorphism at ca. 1.20–1.15 Ga (Camacho and Fanning, 1995) and extensive granitic magmatism at ca. 1.16–1.15 Ga (Clarke et al., 1995) overprinted the Musgrave orogen.

Extension associated with Rodinia breakup probably resulted in the development of an intracratonic basin (the Centralian Superbasin, including the Officer, Amadeus, Georgina and Yeneena basins) commencing at ca. 850 Ma (Walter et al., 1995). Deposits of shallow marine and fluviatile sandstone overlain by carbonates, evaporites and glacial deposits extend to the southeast into the Adelaide Rift System (Hansberry, 2011).

Between 650 and 525 Ma, extensive deformation (e.g. Shaw et al., 1992; Aitken et al., 2009), initiated by Gondwana amalgamation, is common especially in the West and Central Australian Elements, including the coeval King Leopold (Shaw et al., 1992) and Petermann orogenies (Aitken et al., 2009), and in the Pinjarra Element represented by the Pinjarra Orogen (Huston et al., 2012), which divides East Gondwana into Indo-Antarctic and Australo-Antarctic domains. However, the area covered by these orogens is small.

Unrelated to the West, North and South Australian elements, the Tasman Element in eastern Australia (Fig. 5.2) was built upon a passive margin that formed during the breakup of Rodinia. It evolved as the result of a series of episodic tectonic cycles (Champion et al., 2009) related to arc magmatism in a back-arc setting with contractional orogenesis (Glen, 2005).

5.2.3 Paleozoic (542–251 Ma)

The Tasman Element continuously evolved during the Middle to Late Devonian and developed a series of troughs, shelves, and volcanic arcs that were progressively cratonized eastwards with associated granite intrusion and metamorphism (Palfreyman and Adkins, 1984). Magmatism, deformation and metamorphism, associated with the 515–490 Ma Delamerian Orogeny, due to the subduction of the proto-Pacific plate, have been recognized within the Tasman Element (Foden et al., 2002; Foden et al., 2006). The Early Cambrian also marks the initiation of sedimentation along the eastern margin of

the Tasman Element. In the Late Cambrian, clastic sediments, felsic volcanic rocks, and highly evolved granites developed in Victoria, Tasmania, and southeastern Queensland.

During the accretion of the Paleozoic Tasman Element in the east, Central Australia underwent a series of intraplate deformational events, including the development of the Larapinta Seaway and the Alice Springs Orogeny (Blewett, 2012). In southern, north-central, and northern Australia, sedimentation continued from the Late Proterozoic to the Ordovician, and is represented by carbonates and interbedded clastic sediments in the Adelaide Rift System and the Amadeus, Georgina, Daly River, Wiso, Ord and Arafura basins (e.g. Walter and Veevers, 1997; Preiss, 2000), interrupted only by extensive flood volcanism in the Middle Cambrian. During the Cambrian to Ordovician, an enormous turbidite fan developed in south-eastern Australia, especially in the Lachlan Orogen (Gray and Foster, 2004). The basins in Central Australia (Arunta and Musgrave Blocks) underwent intense faulting and metamorphism during the Devonian and Carboniferous. Glacial and fluvioglacial sediments were deposited over much of Western Australia commencing in the Late Carboniferous and extending into the Permian (Mory et al., 2008).

In the east, Silurian-Devonian granitoids (ca. 425–360 Ma) now comprise over one-third of the exposed crust in the eastern Lachlan Orogen. These granitoids are divided into I and S-type based on differences in their petrology and geochemistry (Chappell and White, 1992). During the Permian and Triassic, trough and shelf sedimentation started in the Sydney, Bowen and Tasmania Basins, followed by the formation of extensive continental and deltaic coal measures (Betts et al., 2002).

The New England Fold Belt (referred as New England Orogen; Champion et al. (2016)) is characterized by two major cycles of compression-extension from the Silurian-Devonian to Triassic related to long-lived westward subduction along the eastern Australian margin, which continues today along the Tonga-Kermadec system (Glen, 2013). Extensive Carboniferous and Permian volcanism and plutonism occurred in the northern New England Fold Belt with zircon U-Pb ages ranging from 357 to 306 Ma and 280 to 265 Ma (Cawood et al., 2011; Champion et al., 2013; Jessop et al., 2020). Widespread plutonic and volcanic rocks with ages peaking between 260 and 230 Ma were exposed both in the southern and northern New England Fold Belt (e.g., Carson et

al., 2007; Murray, 2007; Walternberg et al., 2016; Jessop et al., 2020). During the Late Permian to Triassic, the eastward cratonization of the continent was completed (e.g., Betts et al., 2002).

5.2.4 Mesozoic-Cenozoic (251–0 Ma)

Initiated by the breakup of Pangaea, the opening of the Atlantic Ocean and Tethys Sea began at ca. 180 Ma and separated Gondwana (which included Australia, Antarctica, Africa, South America, and India) from Laurasia (North America and Eurasia) (Dietz and Holden, 1970; Huston et al., 2012). Sedimentary basins along the western and southern margin of Australia, including the Bremer, Great Australian Bight and Otway basins, formed mainly during Mesozoic extension that ultimately led to the separation of Australia from Gondwana (Willcox and Stagg, 1990; Veevers, 2006). A series of major Mesozoic-Cenozoic basins grouped as the Westralian Superbasin by Hocking and Preston (1998), such as the Canning and Carnarvon basins, developed as active depocenters along the northwest shelf of Australia with thick Jurassic successions reflecting the divergence of Australia from Greater India.

During the Jurassic and Cretaceous, as the Australian continent moved away from Antarctica, marine sediments were deposited in central and eastern Australia, forming the Great Australian Basin (including the Eromanga and Surat Basins), and covering much of western New South Wales and Queensland, and south-eastern Australia (Norvick and Smith, 2001). Sea-floor spreading in the Southern Ocean fully separated Australia from Antarctica at 34 Ma (e.g. Livermore et al., 2005). Cenozoic sediments were widely deposited in the Tasman and South Australian Elements, including the Lake Eyre, Eucla, Karumba and Murray basins (Huston et al., 2012). Episodic Cenozoic volcanism formed large volcanoes or volcanic complexes, mainly in the Tasman Element, and tracked the northwards movement of the Indo-Australian plate (Johnson et al., 1989) as a consequence of the upwelling of deep mantle plumes (O'Reilly and Zhang, 1995).

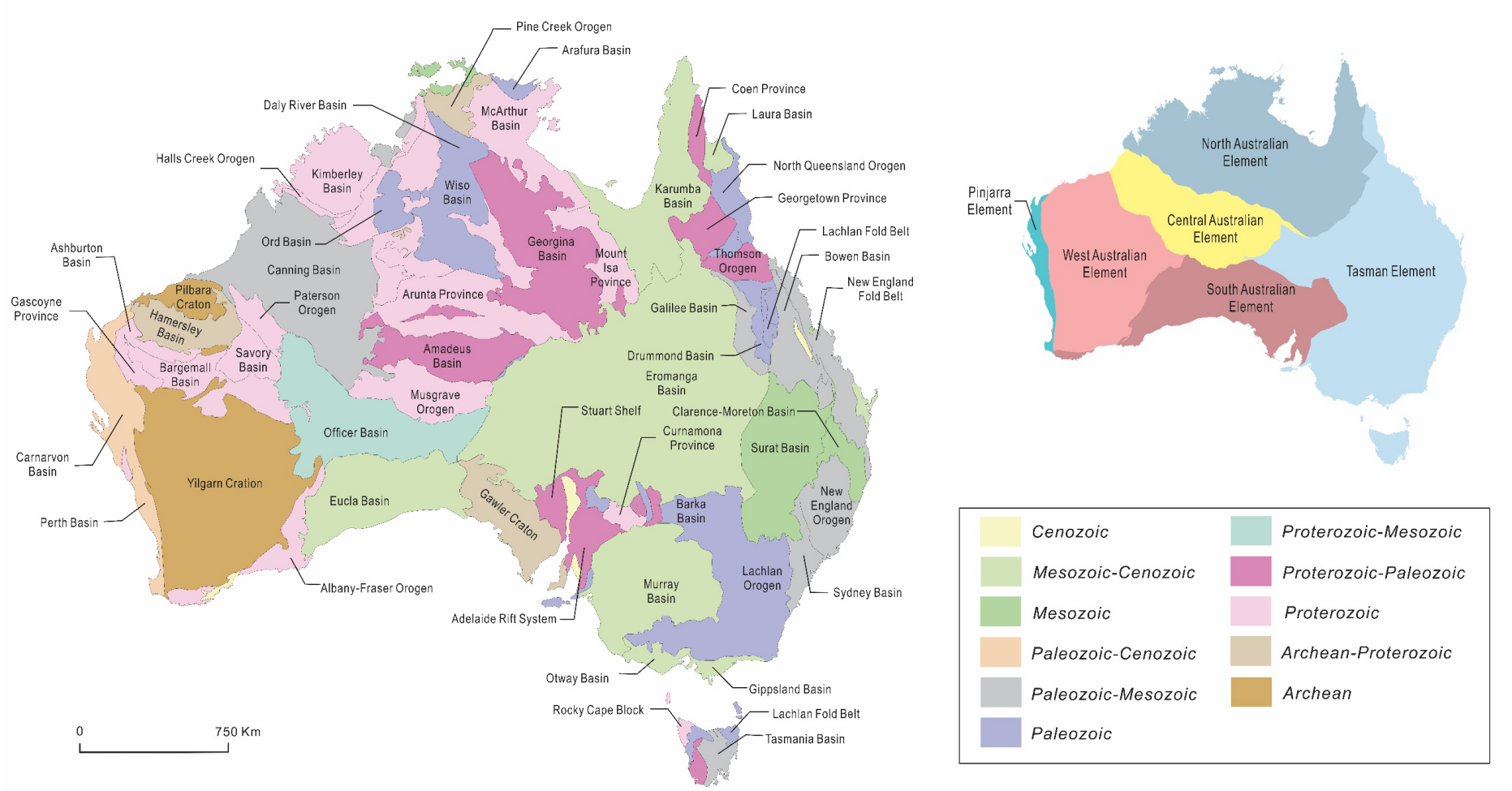

Fig. 5.2 Geological map of the Australian continent showing major cratons, inliers, and orogenic belts and Phanerozoic sedimentary basins, with six crustal elements (modified after Shaw et al., 1995).

5.3 Results

U-Pb dates and trace element concentrations of 1917 detrital zircons from 35 sites in Australia are reported in this research. 727 of these grains were analyzed for O isotopes and 646 for Lu-Hf isotopes. To minimize sampling bias, U-Pb dating data of zircons from sand dunes in the study of Pell (1994) are also included to better represent the desert covered areas (Fig. 7.1 from Pell, 1994), where limited igneous rocks/basements are exposed.

5.3.1 U-Pb dates

The U-Pb isotopic and trace element data from the randomly picked zircons from Australia and the dating results for reference zircons are given in Tables 5.1 and 5.2. Fig. 5.3a is a histogram of U-Pb dates for the 3064 detrital zircons from the 7 drainage areas, which includes 1917 grains analyzed by LA-ICP-MS in this study together with 1147 zircon SHRIMP U-Pb dates from sand dune samples previously analyzed by Pell (1994). The timing of supercontinent assembly is shown for comparison. The height of each bin is the sum of the zircon proportions from each major drainage area weighted by the surface area of the drainage division from which the samples were collected (Fig. 5.1). The weighted U-Pb age distribution indicates eight major peaks of zircon crystallization: 2.90–2.60 Ga, 1.90–1.70 Ga, 1.65–1.50 Ga, 1.30–1.05 Ga, 650–450 Ma, 450–400 Ma, 350–200 Ma and 200–50 Ma, with a minor peak at 3.50–3.20 Ga. Only three of these peaks, at 2.7 Ga, 1.9–1.6 Ga and 500–300 Ma, were found by Champion (2013) in his study of the U-Pb ages of igneous rocks in Australia. Detrital zircons from Eastern Australia, including Areas I, II, V and VI, are mainly younger than 1 Ga, whereas in the west, zircons from Area IV (Western Australia) cluster at ca. 1.9 Ga, and zircons from Area VII have U-Pb ages peaking at ca. 2.9–2.6 and 1.2–1.1 Ga (Fig. S5.1). The oldest peak of ca. 3.5–3.2 Ga is dominated by zircons derived from Area III, including the Pilbara Craton, one of the oldest terranes in Australia. This age distribution of zircons is consistent with the geological observation that Australian terranes become older westwards, contrary to Antarctica that becomes older eastwards. 13% of the detrital zircons from Australia, mainly from Western Australia, are Archean, compared with 2.5% in Antarctica.

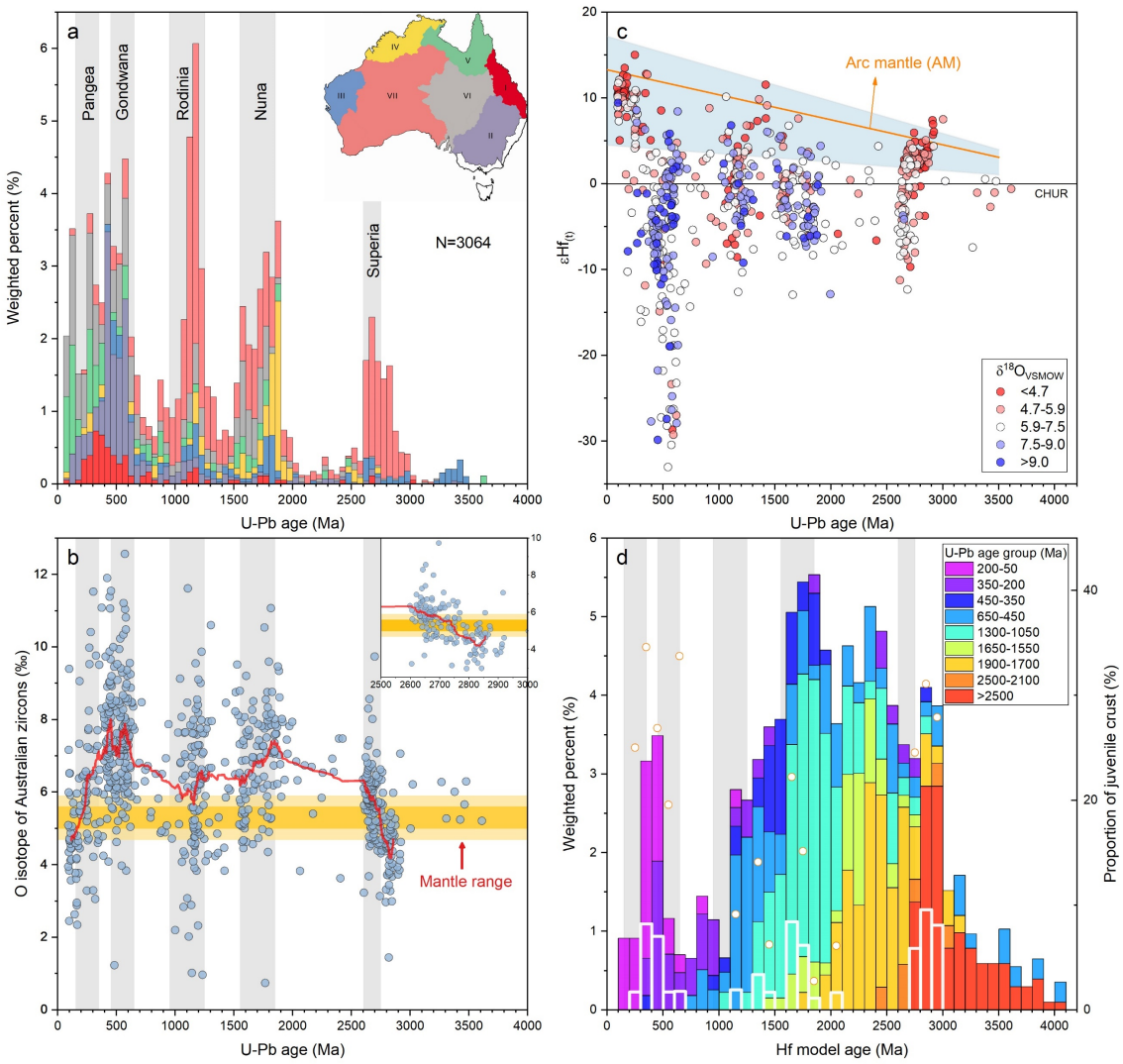

Fig. 5.3 Geochemical results from Australian detrital zircons. a) Weighted histogram (50 Ma bins) of U-Pb dates for 3064 detrital zircons. 1917 grains were analyzed by LA-ICP-MS for the present study, and 1147 SHRIMP U-Pb dates are from Pell (1994). The weighting is based on the surface areas of the seven drainage divisions shown in Fig. 5.1. Grey columns in a, b and d represent the timing of supercontinent assembly; b) Plot of $\delta^{18}O$ values against U-Pb dates (N=727), with insert figure highlighting zircons between 3.0 and 2.5 Ga. The mantle range (5.3 ± 0.6, 2σ) (Valley et al., 1998) is shown in yellow with 1σ in amber. The red curve is the 40-point moving average of $\delta^{18}O$ values; c) $\varepsilon Hf_{(t)}$ values of the Australian detrital zircons colour-coded according to their O isotopic composition (N=646). The evolution of the arc mantle (AM) at 95% confidence level is also shown, same with that in Fig. 4.3b; d) Histogram of zircon average Hf model ages (N=532) weighted by the proportion of each age group as shown in a. This data set omits 114 zircons from south-eastern Australia as explained in the text. The white histogram shows the results of average model ages calculated from juvenile zircon grains as defined in this research, with the proportion of juvenile crust in each bin shown as white dots.

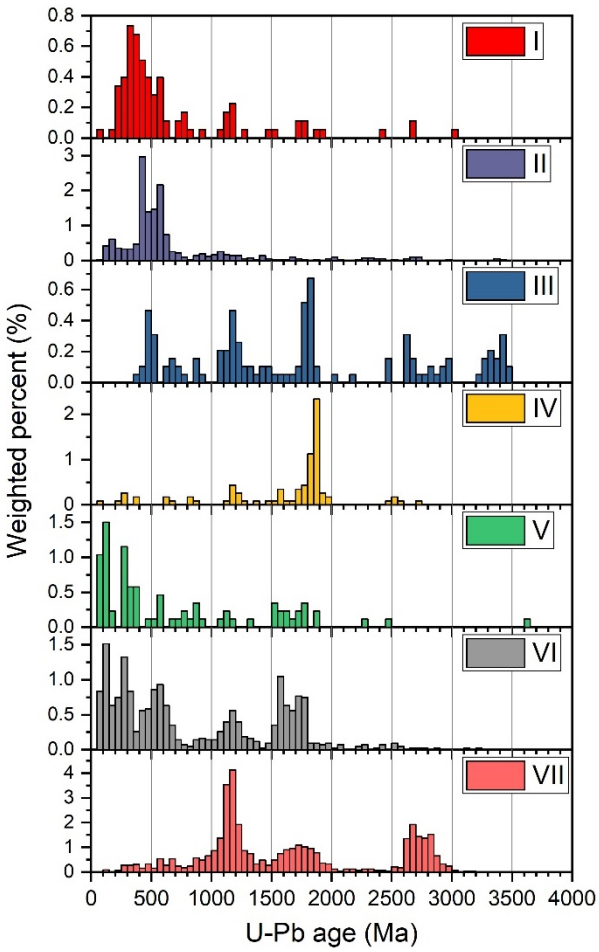

Fig. S5.1 Weighted histograms of U-Pb dates for detrital zircons in Australia, grouped by seven drainage areas given in Fig. 5.1.

5.3.2 Oxygen and Lu-Hf isotopes

The O isotopic data are presented using the $\delta^{18}O$ notation, expressed as deviations from the composition of Vienna standard mean ocean water (VSMOW, $^{18}O/^{16}O$ = 0.0020052, Baertschi (1976)) in parts per thousand. They are listed in Table 5.3, with the results from reference material given in Table 5.4. Fig. 5.3b shows the $\delta^{18}O$ values versus U-Pb dates of detrital zircons. 24.2% of the analyzed zircons have mantle-like $\delta^{18}O$ values (4.7–5.9‰). Compared with other periods, the Archean zircons (> 2.5 Ga) have a small range of $\delta^{18}O$. The Archean zircons yielded a mean $\delta^{18}O$ of 5.32 ± 0.18‰ (2SE). The mean $\delta^{18}O$ values of zircons from the other intervals are 7.16 ± 0.42‰ for 1.9–1.7 Ga, 6.46 ± 0.41‰ for 1.65–1.50 Ga, 6.11 ± 0.39‰ for 1.3–1.05 Ga, 7.49 ± 0.28‰ for 650–450 Ma, 7.75 ± 0.45 ‰ for 450–400 Ma, 6.35 ± 0.53‰ for 350-200 Ma and 4.91 ± 0.42 ‰ for 200–50 Ma (Fig. 5.4a). This suggests that the Proterozoic and Phanerozoic zircons have more varied $\delta^{18}O$ values than the Archean grains, consistent with the secular evolution of the zircon O isotope trend identified by Valley et al. (2005).

Fig. 5.3c summarizes the Lu-Hf isotope systematics, plotted as $\varepsilon Hf_{(t)}$, against U-Pb dates, and Fig. 5.3d illustrates the weighted distribution of zircon average Hf model ages. The Lu-Hf isotopic and model age results from the sample and reference zircons are presented in Tables 5.5 and 5.6. Compared with other time intervals, the $\varepsilon Hf_{(t)}$ values of zircons between 650 and 450 Ma are most varied, ranging from -37.1 to +8.6, yielding the lowest mean of -8.4 ± 1.9 (2SE) (Fig. 5.4b). In sharp contrast, zircons younger than 200 Ma show a tight cluster in $\varepsilon Hf_{(t)}$ and are closer to the average evolution curve of arc mantle, with the highest mean $\varepsilon Hf_{(t)}$ value of +8.7 ± 1.5 (2SE). Notably, the mean $\varepsilon Hf_{(t)}$ values of groups older than 1.0 Ga are close to chondritic values. The trends of average $\delta^{18}O$ and $\varepsilon Hf_{(t)}$ values of the analyzed zircons depict a negative relationship through the time in the Australian database, similar to that in the Antarctic database.

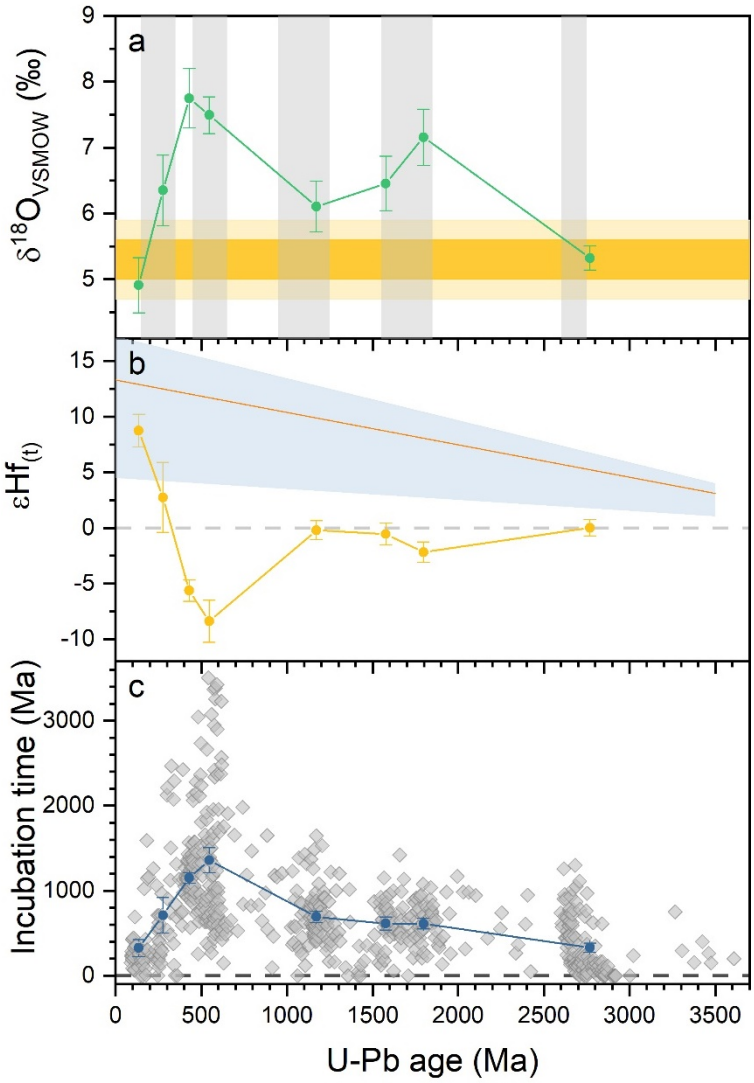

Fig. 5.4 The mean values of $\delta^{18}O$ (a), $\varepsilon Hf_{(t)}$ (b) and the incubation time (Ma) (c) for eight major age peaks in the Australian detrital zircon data set. Grey columns mark the supercontinent forming events in a, with the mantle range (5.3 ± 0.6, 2σ) shown in yellow

and 1σ in amber. The AM evolution range is given in b, same with Fig. 5.3c. The scatter plot of incubation time for individual zircon is also presented as the grey diamond in c. The error bar shows 2 standard errors of the mean $\delta^{18}O$, $\varepsilon Hf_{(t)}$ values and the incubation time (Ma).

5.4 Discussion

5.4.1 Provenances of the detrital zircon population

There is a debate as to the relative merits of using compilations of detrital zircon ages compared with dates obtained from outcropping igneous rocks (Rino et al., 2004; Hawkesworth et al., 2013; Condie et al., 2017) for determining the rate of growth of the continental crust. It has been argued that detrital zircons, from large river systems, give a better representation of major magmatic events on a continental scale (Campbell and Allen, 2008; Hawkesworth et al., 2010; Wang et al., 2011; Iizuka et al., 2013), whereas zircons from outcrops of igneous rocks identify specific regional events. Other advantages of the detrital zircon approach are that: a) natural mixing during river and wind transport minimizes sampling bias, which is more difficult to avoid when relying on outcrop sampling, and b) major rivers sample a high fraction of recycled zircons, that is zircons derived from sedimentary rocks, which in turn, sample zircons from older igneous rocks that are no longer exposed. The latter largely counters the argument that there is a general tendency of young basement rocks to be more easily sampled than old basement (Allegre and Rousseau, 1984; Cawood et al., 2003; Dhuime et al., 2011).

Many compilations of detrital zircon data include zircons from sedimentary rock of varied ages. The obvious shortcomings with such compilations are: i) that the size of the drainage area is unknown, making sample weighting unavailable, and ii) events younger than the sampled sediment are underrepresented. By including only samples from modern rivers, sand dunes and alluvial plains, these problems can be partially avoided. Instead of presenting the raw numbers of analyzed zircons, this study presents the U-Pb data weighted based on the relative size of the sampling areas divided into river basins to offset the sampling bias arising from overestimating the young generation. The effectiveness of weighting in removing the potential sampling bias from the young population is evident in the Antarctic data set. For example, the weighted proportion of ca. 100 Ma zircons from Antarctica provides a more representative record on a continental scale than the raw data without weighting (Fig. S4.1). For the Australian data

set, the comparison is also given in Fig. S5.2. The zircon peak between 600 and 400 Ma is overestimated on the continental scale in a non-weighted U-Pb age histogram (Fig. S5.2a), for example. The peak at 550 Ma is marking a usually high input of Pan-African-aged zircons into south-eastern Australia (discussed below), and the peak at 400 Ma contains a large proportion of grains from the Lachlan Fold Belt (in Area II) that exposes around 2.6% of the Australian surface landmass.

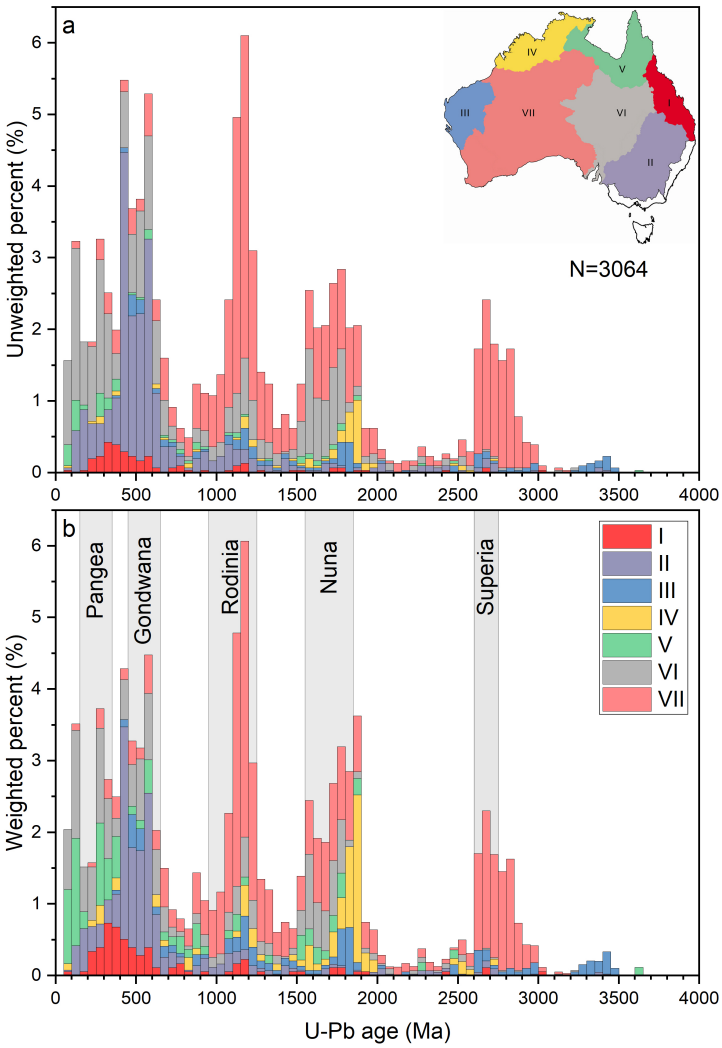

Fig. S5.2 U-Pb age histograms of detrital zircons from Australia. a) Unweighted histogram (50 Ma bins) of dates for 3064 detrital zircons; b) Weighted histogram (50 Ma bins) using the same database as in a. The weighting is according to the surface area of seven divisions of drainage areas in Fig. 5.1.

The major peaks in the Australian U-Pb ages are shown in Fig. 5.3a. They correlate well with similar peaks in the global data set for the world's major rivers (e.g., Iizuka et al., 2017; Zhu et al., 2020) and with the periods of supercontinent formation, although the latter point is disputed by some researchers (Bradley, 2011). The correlation

between detrital zircon U-Pb age peaks and the timing of supercontinent amalgamation can also be observed in other continents, such as Russia, North America and Africa (Wang et al., 2009; Wang et al., 2011; Iizuka et al., 2013).

The oldest Australian zircons, with U-Pb ages of ca. 3.45–3.25 Ga, are predominantly from the granite-greenstone terranes of the Pilbara craton, Western Australia. Granites within this age range have been reported from the Pilbara Craton by Van Kranendonk (2006). Detrital zircons with ages > 3.3 Ga are rare in other large rivers, including those of North America (Rino et al., 2004; Wang et al., 2009), Africa (Iizuka et al., 2013), North China (Yang et al., 2009) and Russia (Wang et al., 2011), suggesting that the area of continental crust older than 3.3 Ga is small. Apart from the > 3.5 Ga crust in southern West Greenland (Nutman et al., 2007), from where no detrital zircon data from river or glacial sediments are available, the only other significant area of crust older than 3.3 Ga is the 3.5–3.1 Ga granite-greenstone terrane of the Barberton area in South Africa (Moyen et al., 2007). Although it is comparable in area to the Pilbara craton, it contributed few zircons to the major African rivers.

The 2.9–2.6 Ga detrital zircons are from the West Australian Element (Area VII) and were principally derived from the Archean basement of the Yilgarn Craton. They peak at 2.7 Ga, a time of widespread granite intrusion (Hill et al., 1989; Pidgeon and Wilde, 1990). A zircon peak at 2.7 Ga has also been observed on other continents, including North and South America, Russia and Africa (e.g., Condie et al., 2009; Iizuka et al., 2017), indicating a global episode of felsic magmatism during this time, correlating with the assembly of the Superia supercontinent. The trough between 2.4 and 2.1 Ga observed in the Australian zircon pattern is also global, and can be recognized in both the detrital and igneous zircon databases (e.g., Campbell and Allen, 2008; Condie et al., 2017; Puetz et al., 2017). It is interpreted by Condie et al. (2009) as a global period of low magmatic activity.

The broad U-Pb age peak between 1.9 and 1.5 Ga, which correlates with the amalgamation of Nuna, can be subdivided into 1.9–1.7 Ga and 1.65–1.50 Ga peaks. The first period is an important one in the assembly of the proto-Australian continent and involved a series of collisional orogenies, including the later stages of the ca. 1.83–1.78 Ga Capricorn Orogeny (Cawood and Tyler, 2004) in the West Australian Element, the

1.85–1.83 Ga Halls Creek Orogeny (Huston et al., 2012) in the North Australian Element, and the 1.74–1.69 Ga Kimban-Nimrod-Strangways Orogeny (Betts et al., 2008) in the South Australian Element. These orogenic events occurred during the amalgamation of various Australian terranes and were followed, between 1.65 and 1.50 Ga, by a series of south- and north-dipping subduction systems that led to the accretion of terranes in the North, Central and South Australian Elements. These subduction events were accompanied by episodic orogenesis in different locations: i) the Isan Orogeny in the Mount Isa Province at 1.61–1.54 Ga (Geological Survey of Queensland, 2011), ii) the Liebig Orogeny in the Arunta Province at ca. 1.64 Ga (Scrimgeour et al., 2005), iii) the Chewings Orogeny in the Arunta Province at 1.60–1.58 Ga (Wade et al., 2006) in the Musgrave Province, and iv) the Olarian Orogeny in the Curnamona Province at 1.62–1.58 Ga (Gibson and Nutman, 2004).

The detrital zircons with ages between 1.25 and 1.05 Ga were derived predominantly from the West and Central Australian Elements (Area VII) and they form a remarkably prominent peak. Bearing in mind that much of the sampled area is covered by desert regolith, igneous rocks formed during this time are likely to be underrepresented by surface exposures. This was the period when the South Australian Element collided with the combined West and North Australian Elements, as part of the assembly of Rodinia, to produce the Musgrave and Albany-Fraser orogenies (Myers et al., 1996).

The principal geological event in Australia between 650 and 450 Ma was the development of the Centralian Superbasin, with extensive deformation in the West and Central Australian Elements, including the King Leopold and Petermann orogenies, which did not produce extensive granitic magmatism. Nevertheless, Fig. 5.3a shows a significant peak in detrital zircon dates ranging from 650 to 450 Ma (accounting for 13.0% of the total population), with nearly half from south-eastern Australia, coeval with the assembly of Gondwana. One possible Australian primary source for some of these zircons is the 520–490 Ma Delamerian Orogeny of south-eastern Australia in the Tasman Element, inferred to be due to the subduction of the Pacific plate (Foden et al., 2006). Compared to the zircon population between 450 and 350 Ma, which accounts for 6.7% of the total population and is attributed to the granitoids of the Lachlan Fold Belt

(≥61,000 km^2; see the discussion below), the exposed area of basement rocks between 650 and 450 Ma in Australia should be nearly twice that of Lachlan Fold Belt. However, the area covered by the Delamerian orogen is too small for it to be an important zircon source and it is too young to explain the abundant zircons older than 550 Ma. There are no known other potential sources within the well-exposed basement of south-eastern Australia that could contribute the 2nd significant peak at ca. 650–450 Ma in Fig. 5.3a. Its high abundance requires alternative sources.

Williams (2001) found that U-Pb ages of detrital zircons from the Cooma Complex of the Lachlan Fold Belt dominantly peak at 600–500 Ma and 1.2–0.9 Ga, and pointed out that the abundant Late Cambrian detrital grains were derived from a remote source likely to be the Mozambique Belt in Africa, which has a detrital zircon population with an appropriate age spectrum. An exotic source is persuasive to explain the ca. 650–450 Ma zircons that are older than 550 Ma in Australia. As discussed in Chapter 4, the rapid erosion of the Transgondwanan Supermountains produced a huge volume of sedimentary detritus that formed giant turbidite fans. The eastern turbidite fan extended across Antarctica to Australia by a 7000-km-long river system (Squire et al., 2006). This is supported by the similarity in U-Pb ages that peak at ca. 650–450 Ma and 1.25–0.95 Ga from detrital zircons both in Antarctica and south-eastern Australia (see Chapter 6 for details). The bulk of the Pan-African zircons and some zircons from the Rodinia era were derived from these turbidites. Furthermore, Pell et al. (1997b) have shown that detrital zircons from the New England Fold Belt, Lachlan Fold Belt and Adelaide Rift System show similar age peaks of 700–500 Ma and 1.2–1.0 Ga. Maidment et al. (2007; 2013) showed that the same sediment package—Pan-African-aged (650–450 Ma) and Grenvillian-aged (1.20–0.95 Ga) zircons—reached the Amadeus Basin and Georgina Basin via the Larapinta Seaway.

Zircons between 450–350 Ma correlate with the extensive granites and related volcanics in the Tasman Element, especially in the Lachlan Fold Belt, where granitoids covering 61,000 km^2 were emplaced between ca. 440 and 360 Ma. These are the classic I- and S-types granites classified by Chappell and White (1992). The Lachlan Fold Belt, which extends from Tasmania in the south to Queensland in the north, is part of the Terra Australis Orogen, a global scale orogenic system extending 18,000 km in length

along the eastern Gondwana margin (Cawood, 2005). The Lachlan Fold Belt S-type granites were most likely produced by partial melting the Australian section of this extensive sequence of thick, exotic turbidites produced by erosion of the Transgondwanan Supermountains (Zhu et al., 2020).

The peak at 350–200 Ma correlates with: i) Carboniferous granitoids and volcanics in the Georgetown Inlier, northern Queensland (Champion and Chappell, 1992); ii) Magmatism at ca. 290 Ma (Flood and Shaw, 1977) and plutonism between 300 and 250 Ma in the New England Fold Belt (Shaw and Flood, 1981); iii) Carboniferous (339–327 Ma) plutonism in the east-central Lachlan Fold Belt (Jeon and Williams, 2018), and iv) the last stage of the intra-plate Alice Springs Orogeny in central Australia spanning 340–320 Ma (Buick et al., 2008). The youngest population of 200 to 50 Ma zircon (Area V and VI), most likely sampled from the Jurassic-Cretaceous Great Australian Superbasin (Foley et al., 2021), was related to Jurassic-Cretaceous volcanism and granitoid intrusions found in the continental arc system along the eastern coast of Australia (Veevers, 2006).

The suggestion that zircon age peaks correlate with peaks in juvenile continental crust formation (e.g., Stein and Hofmann, 1994; Condie, 1998) has faced challenges from many studies that indicate that significant recycling and preserved zircons contributed to crustal production during supercontinent assembly (Condie and Aster, 2010; Iizuka et al., 2013). Hawkesworth et al. (2010) and Condie (2013) proposed that zircons in the pre-existing crust are more likely to be preserved in continental collisional settings than in subduction and extensional settings. Furthermore, based on Nd isotopes in felsic igneous rocks, Condie et al. (2017) suggested that the accretionary phase of orogens regulates the production and preservation of juvenile crust. Consequently, the supercontinent cycle, which involves all these tectonic processes, plays a significant role in regulating the growth of the continental crust and correspondingly its zircon records.

The supercontinent cycle can be divided into three main stages: a) subduction at the active margins of the assembling continents, b) collisions between continents and c) breakup. Each stage involves magmatism and/or metamorphism, resulting in different volumes of magma being generated, the largest during subduction and the smallest during breakup. Despite the high volumes of magma generated during subduction, the likelihood of those igneous rocks being preserved, as with igneous rocks formed during

breakup, is much less than that of igneous rocks generated in collision settings (Hawkesworth et al., 2013). Further, crustal reworking is enhanced in collisional orogens. Accordingly, zircon age peaks delineate an accumulated record between the magma volumes (generated and reworked) and their preservation potential. Detrital zircon age peaks can be also affected by the enhancement of crustal erosion, especially in the collision stage during supercontinent assembly since relief is a principal determining factor of crustal erosion rate (Montgomery and Brandon, 2002). As discussed above, for example, the rapid erosion of the Gondwanan Supermountains produced voluminous sediments, some of which were transported to Australia as external source material.

The age peaks of zircons that have juvenile Hf isotope signatures are likely to underestimate the amount of new continental crust generated because juvenile magmas are generally mafic to intermediate in composition and consequently contain little or no zircon. The key point is that observed detrital zircon U-Pb age peaks cannot be interpreted simply as crustal generation peaks associated with supercontinent assembly, because zircon-free mafic rocks are not represented. For that reason, two-stage Hf model ages of detrital zircons filtered using their oxygen isotopic compositions (see Chapter 3 for detail) have been used here to re-evaluate the timing of major episodes of crustal generation and constrain the growth of the preserved continental crust.

5.4.2 Juvenile and reworked crust

5.4.2.1 Juvenile crust

Following the same criteria as discussed in Chapter 4, zircons lying within the $\delta^{18}O$ range of mantle zircon and the Hf isotopic composition (95% conf.) of the arc mantle evolution are assumed to have crystallized from juvenile mantle-derived magmas, representing the generation of juvenile continental crust. Fig. 5.5 presents the weighted U-Pb age histogram of 646 grains analyzed both for O and Hf isotopes and marks the distribution of grains defined as juvenile. Only 10% of these grains can be identified as juvenile. The juvenile zircons show distinct narrow U-Pb age peaks at 2.9–2.6 Ga, 1.2 Ga and < 300 Ma, whereas the periods between 1.9 and 1.5 Ga, and 650 and 450 Ma were the periods with a low proportion of granitoid formation from primitive magmas. Iizuka et al. (2017) suggested that periods of low juvenile zircon production correlate with the

time of supercontinent assembly. The Australian data provide only partial support for this hypothesis. The assembly of Nuna and Gondwana does correlate with periods of low juvenile crust formation, but the amalgamation of the other supercontinents does not. Nor is there a correlation of the peaks between juvenile zircon production with supercontinent dispersion. In terms of the average Hf model ages from juvenile zircons, like their U-Pb ages, their Hf model age result also shows sharp peaks (Fig. 5.3d). There are small narrow peaks between 3.0 and 2.7 Ga, and 700 and 200 Ma, with a broad period between 2.1 and 1.1 Ga signifying the times when these juvenile materials separated from the mantle, adding to the continental crust. There is no consistent correlation in the Australian database between the generation of juvenile continental crust and the supercontinent cycle.

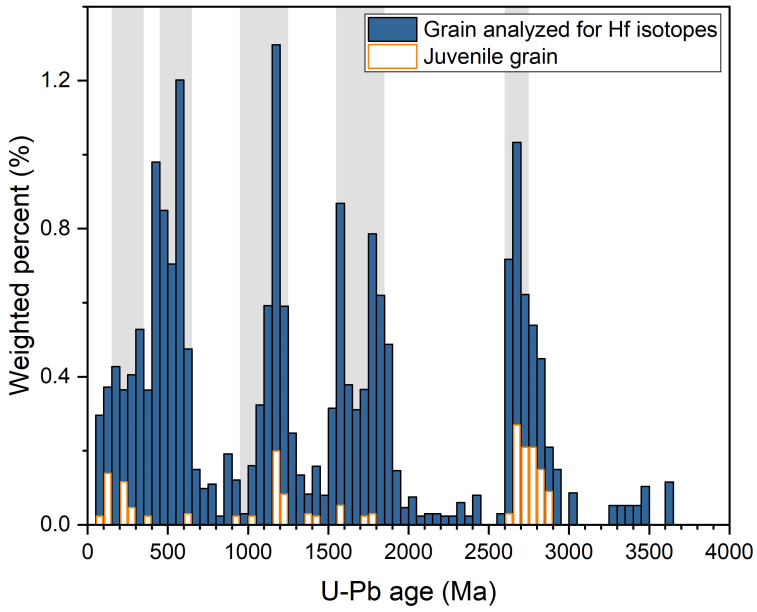

Fig. 5.5 Weighted U-Pb age histogram for zircons (N=646) analyzed for Lu-Hf isotopic composition with white columns highlighting the grains (N=64) having juvenile zircon signatures.

5.4.2.2 Reworked crust

Valley et al. (2005) recognized a secular change in zircon $\delta^{18}O$ values, which show a restricted range during the Archean ($\delta^{18}O$ normally < 7.5‰), but become increasingly varied through the Proterozoic and into Phanerozoic. Wang et al. (2009; 2011) observed an abrupt change of zircon $\delta^{18}O$ values at the Archean-Proterozoic boundary in the contiguous USA and Russia, attributing this to a systematic increase in the amount of sediment in the source region that melted to form granites following the end of the Archean. This conclusion is supported by a global study of oxygen isotopes in detrital

zircons by Spencer et al. (2014). They showed that the average $\delta^{18}O$ composition of bulk sediment remains a constant value of ca. 14.9‰ from the Archean through to the Phanerozoic and attributed the increase in $\delta^{18}O$ at the Archean-Proterozoic boundary to enhanced crustal thickening and reworking that led to an increased fraction of high $\delta^{18}O$ sediment being incorporated into the source region of post-Archean granites. Other isotopic evidence, for instance, Zn in banded iron formations (Pons et al., 2013) and Sr in seawater (Shields and Veizer, 2002), shows an abrupt change near the Archean-Proterozoic boundary, which can be attributed to a sudden increase in subaerial exposure of the continental crust on a global scale at that time (Campbell and Davies, 2017). The significant increase in atmospheric O_2 between 2.45 to 2.32 Ga, which is called the Great Oxidation Event (Holland, 2002), enhanced weathering and erosion, potentially leading to increased amounts of sediments and elevated O isotope in sediments.

O isotope data from Australia are consistent with the recognized global secular change in $\delta^{18}O$ with a few exceptions (i.e., Archean zircons with $\delta^{18}O > 7.5‰$). $\delta^{18}O$ values of detrital zircons both older than 2.5 Ga and younger than 200 Ma are less than 7.5‰. The 2.9–2.6 Ga zircons have a mean $\delta^{18}O$ value of 5.29‰ with a median value of 5.42‰, well close to the mantle value, but ranging from 2.97 to 7.43‰ if six outliners are ignored. A 40-point moving average of the data shows a systematic increase in $\delta^{18}O$ with time from 4.72‰ at 2.9 Ga up to 6.33‰ at 2.6 Ga (Fig. 5.3b). The low values at ca. 2.9 Ga are interpreted to be the product of melting hydrothermally altered basalt and the increase in $\delta^{18}O$ with time to hydrated basalt in the granite source region to be systematically replaced by a lower crust that has undergone little or no surface weathering or hydrothermal alteration. However, some of the granite magmas, especially the younger ones, must have incorporated a small sedimentary component to explain zircons with $\delta^{18}O > 5.9‰$. The 200–50 Ma zircons have a mean $\delta^{18}O$ of 4.91‰, slightly less than the mantle value. These zircons correlate with Jurassic-Cretaceous volcanism and granitoids found along the east coast of Australia. Their low $\delta^{18}O$ probably resulted from the melting of hydrothermally altered rocks, probably in a rift system in central and eastern Australia due to the westward subduction during the Jurassic and Cretaceous (Waschbusch et al., 2009).

In contrast, zircons from the other age groups (1.9–1.7 Ga, 1.65–1.55 Ga, 1.30–1.05 Ga, 650–450 Ma, 450–400 Ma, 350–200 Ma) have mean $\delta^{18}O$ values higher than the mantle range and the $\varepsilon Hf_{(t)}$ for most of these zircon grains plots below the arc mantle uncertainty triangle (Fig. 5.4a and 5.3c), indicating that the source region for the granites was older crust containing variable amounts of sedimentary rocks. Notably, the Pan-African-aged zircons, which crystallized during the assembly of Gondwana, have the highest $\delta^{18}O$ and lowest $\varepsilon Hf_{(t)}$ values, implying an unusually high sedimentary fraction in their source regions. This feature also can be seen in a global compilation of zircon O and Hf isotopic data by Roberts and Spencer (2015) and is consistent with unusually high sedimentation rates associated with erosion of the Transgondwanan Supermountains (Squire et al., 2006).

There is a negative correlation between $\delta^{18}O$ and $\varepsilon Hf_{(t)}$ that extends throughout Australian history (Fig. 5.4). Compared with the mantle range, the significantly elevated $\delta^{18}O$ values in the ca. 1.8 Ga and 550 Ma zircons correspond to the assembly of the Nuna and Gondwana supercontinents respectively, implying that the continent-continent collisions associated with these orogenic events resulted in crustal thickening, which boosted erosion and sedimentation. However, the average $\delta^{18}O$ associated with the amalgamation of Rodinia is appreciably less elevated, suggesting less erosion because the mountains were smaller (Zhu et al., 2022). The high value of $\delta^{18}O$ at ca. 450 Ma correlates with the formation of the Lachlan Fold Belt, a period of extensive granitoid magmatism, which includes a large proportion of S-type granites, formed by melting extensive turbidites in south-eastern Australia (Zhu et al., 2020 and references within).

As discussed above, the incubation time is the time difference between the Hf model age, which dates the time of separation of the primitive crust from the mantle, and the U-Pb age, which dates the melting event that produces the granitic melt from which the zircon crystallized. It is a measure of the rate at which primitive crust is reworked. There is a general increase in incubation times as zircon ages decrease, but this trend reverses at ca. 400 Ma (Fig. 5.4). Average incubation times correlate positively with $\delta^{18}O$ and negatively with $\varepsilon Hf_{(t)}$, which suggests that the period with long incubation times potentially involves more contributions from the reworked crust (normally $\varepsilon Hf_{(t)}$ < chondrites) into the crustal formation at the same time with higher chances of the

incorporation of sediment ($\delta^{18}O$ > 10‰) into the granitic source regions, rather than those with short incubation times. More than 73% of the analyzed population has an incubation time greater than 350 Myr, supporting the idea that the contributions of juvenile crust are limited in the evolution of the Australian continent. The exceptions are zircons older than 2.5 Ga and younger than 200 Ma, having mean incubation times of 330 and 326 Myr respectively. The mean incubation time of other groups is more than 600 Myr.

Notably, the period between 650 and 450 Ma has the highest mean (1359 Myr) and most varied (147–3506 Myr) incubation time (Fig. 5.4c), showing that the granites that formed during the assembly of Gondwana were produced by melting old, heterogeneous, pre-existing continental crust. The high $\delta^{18}O$ values support a high fraction of sedimentary materials in the granite source region during this time. Only one zircon grain (0.8% of the analyzed zircons) during this period has $\delta^{18}O$ < 5.9‰ and lies within the Hf isotope mantle growth uncertainty envelope and can therefore be classified as juvenile. Similar features can be seen in Antarctica (Fig. 4.5 in Chapter 4). Combined with the similarities of U-Pb age patterns of detrital zircons in Antarctica and south-eastern Australia, these observations support the hypothesis that the eastern detritus shed from the Transgondwanan Supermountains was transported across Antarctica to Australia via a > 5000 km riverine system, contributing a significant amount of exotic Pan-African-aged zircons and a small amount of Grenvillian-aged zircons to south-eastern Australia.

Another marked peak with a low mean $\varepsilon Hf_{(t)}$ value of -5.6 and consequently a long mean incubation time of 1152 Myr is ca. 400 Ma. The formation of zircon populations between 450-350 Ma is likely correlated to the cratonization of the inner Lachlan Fold Belt, which is characterized by a ca. 440 Ma volcanic arc, ca. 430–410 Ma syn-tectonic granitoids and ca. 380–370 Ma post-tectonic granitoids. Slightly more than half of the granites exposed in the Lachlan Fold Belt are S-type granites (White and Chappell, 2011) that were derived from sedimentary source rocks. The high and variable O isotopes in zircons between 450 and 350 Ma (Fig. 5.4a) mainly from Area II, south-eastern Australia, support the existence of a large proportion of S-type granites. Those S-type granites are interpreted as the product of melting the thick Cambrian-Ordovician turbidite sequence

fed by the detritus shed from the Transgondwanan Supermountains (Zhu et al., 2020). As a result, zircons in the age peak at ca. 400 Ma are likely to have inherited their elevated $\delta^{18}O$ values and variable incubation times from those sediments.

Estimating the rate of growth of the Australian continent is complicated by the distorted fraction of the exotic zircons of the Pan-African and Grenvillian populations especially from south-eastern Australia. These zircons were originally derived from the Transgondwanan Supermountains, produced by the collision between East and West Gondwana, and transported across Antarctica to south-eastern Australia by giant rivers (Squire et al., 2006). Therefore, although these zircons should be taken into account when considering continental growth on a global scale, they were not derived from the Australian crust itself and were omitted when calculating the Australian continental growth curve.

5.4.3 Growth of the preserved Australian continent

5.4.3.1 Distributions of Hf model ages

As discussed in Chapter 3, zircon Hf model ages are a reliable way to identify periods of crustal growth from a large data set. Fig. 5.3d shows a histogram of model ages successively weighted by the fraction of zircons in each of the U-Pb age peaks, which in turn, were weighted by river drainage area as previously noted. To remove the effect of the exotic zircon package (Pan-African-aged and Grenvillian-aged zircon groups) from south-eastern Australia, zircon samples from the Murray and Murrumbidgee rivers in the Murray-Darling drainage division, south-eastern Australia (in Area II in Fig. 5.1), were excluded from the Hf model age calculation for the Australian continent as shown in Fig. 5.3d.

Several conclusions can be drawn from the model age histogram. First, the principal period of continental growth was between 3.0 and 1.1 Ga. Within this period two sub-peaks coincide with periods of juvenile crust formation: 3.0–2.7 Ga and 1.8–1.6 Ga. These periods have also been documented elsewhere as important periods of crustal growth. Iizuka et al. (2017) identified 3.0–2.7 Ga as a period of global continental growth on five other continents (South America, North America, Africa, Russia and Asia) using Hf model ages of detrital zircons from river samples. Hawkesworth and Kemp (2006b) recognized the equivalent 3.1–2.9 Ga and 1.9–1.7 Ga events as two important episodes

of new crustal addition in Australia based on Hf model ages from zircons having $\delta^{18}O$ < 6.5‰. The 3.0–2.7 Ga period in Australia, which was identified in zircons from the Yilgarn Craton, followed extensive mafic and ultramafic magmatic events on that craton with a sharp peak at 2.7 Ga (Hoatson et al., 2009). Yet the highest proportion of juvenile crust is recorded at 3.0–2.7 Ga, implying that the extraction of this crust from the mantle is not exactly synchronous with the mantle plume related to that large igneous province, although the mafic and ultramafic volcanic rocks themselves do represent the addition of juvenile crust. The prominent 2.70–2.65 Ga granitic event in the Yilgarn Craton resulted from the remelting of older crust and was not a new addition of juvenile crust (Campbell and Hill, 1988). Second, there is a peak in crustal growth between 500 and 300 Ma, which coincides with a peak in juvenile crust formation. The events that dominate these largely new additions to the crust are the Permian to Triassic granites and felsic volcanic rocks of the eastern New England Fold Belt, together with the Late Paleozoic Devonian and Carboniferous volcanic arcs of the New England Fold Belt. Third, the period between 1.1 and 0.6 Ga was a period of low crustal growth in Australia. Finally, there is no obvious correlation between supercontinent assembly and zircon Hf model ages, except for the period between 1.9 and 1.6 Ga, which corresponds to the assembly of Nuna.

Because mantle zircon has a narrow range of $\delta^{18}O$ (4.7–5.9‰, 2σ), zircon with O isotopic compositions lying close to the mantle value can be interpreted to have crystallized from melts derived from the mantle, or mafic crust with no sedimentary component. Hf model ages of these zircons should reflect the timing of the crustal generation most accurately. In practice, Hf model ages from grains with $\delta^{18}O$ between 4.5 and 6.5‰ were also calculated for comparison, as shown in Fig. 5.6. Differences between the major Hf model ages peaks, and cumulative growth curves, are minimal.

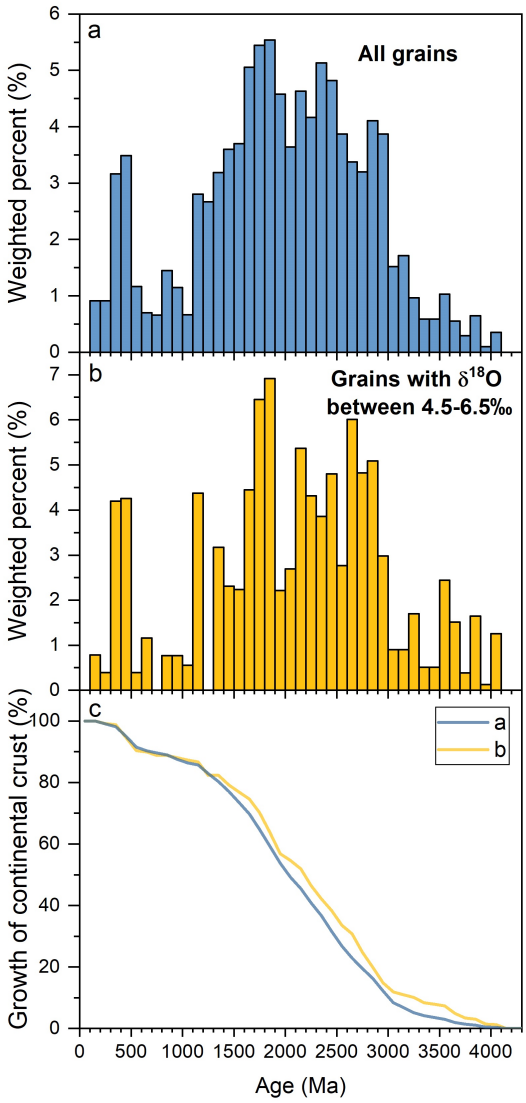

Fig. 5.6 Comparison of Hf model age results from unfiltered zircons and zircons having $\delta^{18}O$ values between 4.5 and 6.5‰. a) Weighted histogram of Hf model age results calculated from analyzed zircons in this study, except those from south-eastern Australia, same with Fig. 5.3d. b) Weighted histogram of Hf model age results calculated from zircons having O values between 4.5 and 6.5 ‰ (N=255) from the same dataset using in a. The weights are according to the proportion of each age group. c) Growth curves obtained from the results in a and b.

5.4.3.2 Comparison with other continental crust growth curves

The growth of continental crust is the sum of new juvenile continental crust minus the fraction of continental crust that returned to the mantle via subduction or delamination. Zircon Hf model ages are a measure of the preserved continental crust and take no account of the fraction of continental crust that has been returned to the mantle. The cumulative proportion of continental crust based on the Hf model ages from detrital zircons is reasonably representative of the growth curve of the preserved continental crust, although the recycled sediments might have a small proportion of materials eroded from the pre-exposed crust that has no longer been preserved.

The reliability of the Hf model age growth curve has been tested by comparing it to the Champion (2013) two-stage Nd model age growth curve for the Australian continental crust determined from analyses of Australian igneous rocks. Instead of using the Nd model ages calculated from the average depleted MORB-type mantle, as in the Champion (2013) study, the Nd isotopic composition of arc mantle from Hao et al. (2022) with an average $\varepsilon Nd_{(0)}$ of +6.1 is used, compared with the $\varepsilon Nd_{(0)}$ value of +10.0 used by Champion (2013). The uncertainties assigned to the Hf growth curve are based on the 95% confidence interval for the arc mantle evolution trend as shown in Fig. 5.3c. Fig. 5.7a shows that the two cumulative growth curves agree very well, with the largest difference being 7% between 1.7 and 1.0 Ga. The Hf growth curve suggests that crustal growth might have begun 200 Ma earlier than suggested by the Nd growth curve, although both starting points lie within uncertainty. Another point of difference is that the Hf curve identifies a period of rapid growth between 500 and 300 Ma, representing a high rate of growth for the Tasman Element in Eastern Australia, as discussed above. Both curves indicate a high rate of continental growth between 3.0 and 1.1 Ga.

Fig. 5.7a also compares the Australian continental curve with the growth curves for four other continents: Antarctica, contiguous USA, Russia, and Africa, using the same methodology. The growth curves for the contiguous USA, Australia and Africa are relatively similar. About 30% of the three continents formed by 2.5 Ga, following an extended period of rapid growth between 2.5 and 1.2 Ga, and about 85% developed by 1.2 Ga. The growth of the Russian and Antarctic continental crust followed a different path. About 30% of Russian crust had been produced by 3.0 Ga, followed by a low growth rate between 3.0 and 0.7 Ga, with only 75% of the continental crust formed by 700 Ma, compared with an average of ca. 95% for Australia, Africa, and the contiguous USA. Another important difference is that 600–400 Ma was a period of rapid crustal growth in Russia, but not in the other continents. As shown in Chapter 4, Antarctica grew nearly one billion years later than all other continents. Only 8% of Antarctica had formed by the end of the Archean, with the main period of growth occurring between 2.3 and 1.1 Ga.

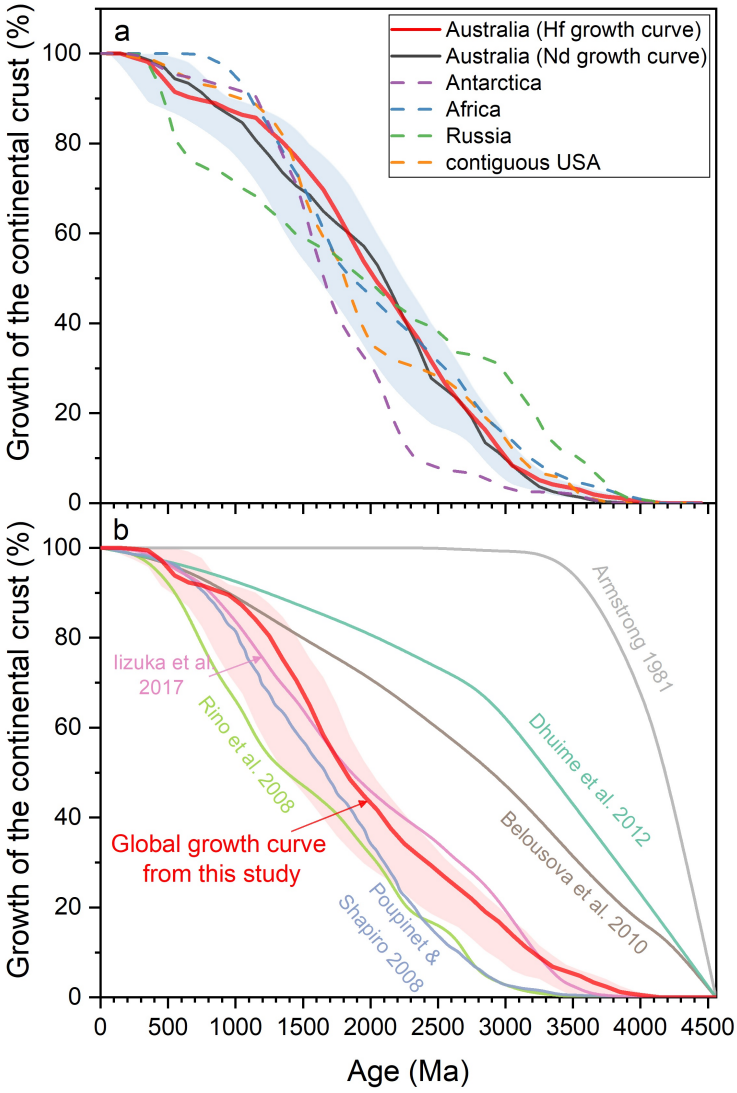

Fig. 5.7 Models for the growth of the continental crust. a) Growth curves for five continents. The black curve shows the Nd model age growth curve of Australia, based on the whole rock two-stage Nd model ages from Australian igneous rocks (data from Champion, 2013). The curves from the other four continents are calculated using the same methodology that was applied to the Australian and Antarctic zircon data. Data for the contiguous USA, Russia and Africa are from Wang et al. (2009); (2011), and Iizuka et al. (2013); b) Global growth curves of the continental crust from this study and six representative continental growth models previously proposed (Armstrong, 1981; Rino et al., 2008; Poupinet and Shapiro, 2009; Belousova et al., 2010; Dhuime et al., 2012; Iizuka et al., 2017). The global growth curve from this study is weighted according to the relative surface area of each continent: Africa (40%), Russia (22%), contiguous USA (10%, contiguous landmass), Australia (10%) and Antarctica (18%). The uncertainty (95% conf.) in the global curve from this study was calculated based on the uncertainty arising from the arc mantle Hf model age calculations for each continent.

5.4.3.3 Implications for global continental growth

Similar data sets from other continents (contiguous USA, Russia, and Africa), together with new data for Australia and Antarctica, make it possible to reconstruct a global growth curve for the continental crust as represented by these continents. To better constrain this curve, the global growth curve as shown in Fig. 5.7b in this study is

calculated from the Hf model ages results for individual continents that were further weighted by the surface area of each continent (Fig. S5.3). The uncertainty (95% conf.) of the global curve is also given based on the uncertainty arising from the arc mantle Hf model age calculations for each continent. Fig 5.7b shows the growth curve on a global scale compiled in this research and compares it with previously proposed models of continental growth.

The models for continental growth shown in Fig. 5.7b vary greatly and highlight the different views as to when continental crust began to form and how it grew to the present day. These are principally due to differences in the sample types, sampling area, size of data set, dimension of data information and assumptions for modelling. The earliest estimate from the Armstrong (1981) model, which is based on the Pb, Sr and Nd isotopic compositions of mantle-derived igneous rocks, assumes rapid early growth with the continental crust reaching its current mass by 3.5 Ga, followed by a near-steady-state condition in which continental growth is balanced by recycling of crust into the mantle. Poupinet and Shapiro (2009) obtained a seismic continental growth curve based on the relationship between the age of the lithosphere and the S wave vertical travel-time delay, which is highly dependent on how well the lithospheric age from exposed rocks is known. The remaining four growth curves used detrital zircons as a proxy. The study by Rino et al. (2008) used the U-Pb age distribution from river samples from Africa, Asia and North and South America, but without the constraints provided by Lu-Hf and O isotopes. The curves of both Belousova et al. (2010) and Dhuime et al. (2012) assume that the continental crust started to form at 4.56 Ga and suggest that more than 15% of the continental crust formed during the Hadean.

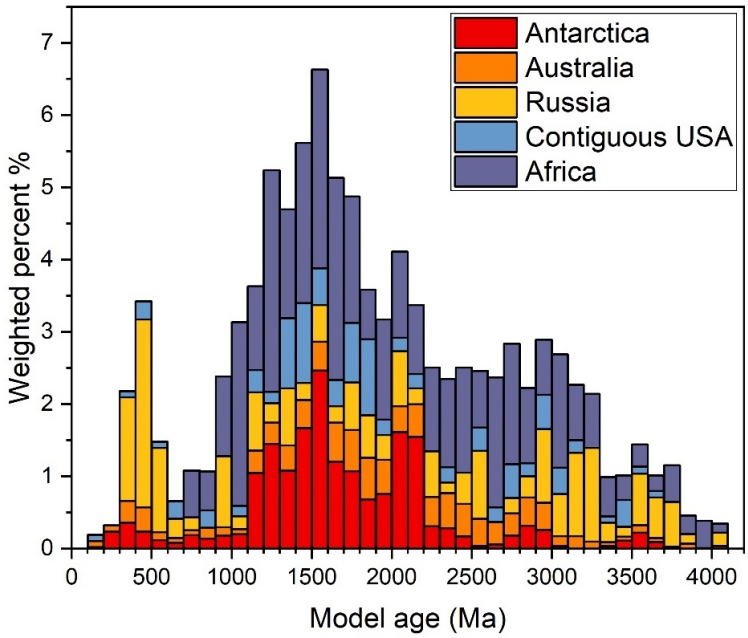

Fig. S5.3 Weighted histogram of Hf model ages from detrital zircons in each continent, by using the size of the continental land surface: Africa (40%), Russia (22%), contiguous USA (10%, contiguous landmass), Australia (10%) and Antarctica (18%). Data of the contiguous USA, Russia, and Africa are from Wang et al. (2009); (2011), and Iizuka et al. (2013).

Although there are minor differences, the new growth curve presented in this study agrees with the Iizuka et al. (2017) curve, which also used riverine sand samples. The curve derived from the present research indicates that at least 25% of the preserved continental crust was produced by 2.5 Ga, and ca. 90% by 0.9 Ga. Growth started at 4.1 Ga, was slow until 3.3 Ga, became faster until 2.2 Ga, then rapid from 2.2 Ga to 1.0 Ga, followed by a period of slow growth between 1.0 Ga and 600 Ma, with another surge between 600 and 300 Ma. Differing from the studies by Belousova et al. (2010) and Dhuime et al. (2012), the present study takes no account of the crustal reworking index for calibrating the growth curve of the continental crust. Note that the net growth curve can differ greatly from the cumulative curve of the preserved continental crust because a significant amount of continental crust was probably into the mantle through geologic history (e.g., Dhuime et al., 2018) and is difficult to quantify.

The new growth curve from the present study shows very little continental crust having formed before 4.0 Ga. This conclusion is consistent with Nd model ages of Earth's oldest sediments (Jacobsen and Dymek, 1988) and the U-Pb ages of the zircons extracted from them (Nutman, 2001), neither of which shows evidence for continental crust older than 4.0 Ga. A few detrital zircons older than 4.2 Ga have been found in

quartzites from the Narryer Gneiss Terrane in Western Australia (Wilde et al., 2001), but the fraction of Hadean-aged zircons in the global detrital zircon data set (N=24,634) compiled by Puetz et al. (2017) is less than 0.013%, suggesting that remnant felsic crust from the Hadean era is rare and of limited extent. There is no Hf isotopic signal that records the existence of anomalously unradiogenic crustal sources, or of the formation of a depleted mantle reservoir, to support the hypothesis that a significant volume of Hadean crust separated from mantle prior to 4.0 Ga (Kemp et al., 2010), although the extreme early fractionation of the mantle evident from Nd isotopes might have resulted from crustal extraction (Bennett et al., 1993). If extensive continental crust formed during Hadean, as proposed by Armstrong (1981), Belousova et al. (2010) and Dhuime et al. (2012), there should be more surviving evidence for its existence, if not as exposed continental crust or as detrital zircons, at least in zircon or sediment model ages. Apart from the extremely rare Hadean zircons, none exists. Caution is needed when interpreting the growth models from the different global data sets.

The methods employed in the present study have several advantages when reconstructing the growth of the global continental crust. First, detrital zircon data from the world's major rivers are more representative on a continental scale than igneous zircon/rock records, and are particularly useful for studying the preserved felsic crust. Second, this study compiles the data from nearly 9400 zircon grains from five different continents (Australia, Antarctica, Africa, Russia, and the contiguous USA), including the unpublished data for 1917 grains from Australia and 1712 grains from Antarctica. Third, O isotopes in zircon are introduced as a proxy to indicate the potential components of their source region, which in return influences the choice of the Lu/Hf ratio of their crustal reservoir for the calculation of model age. Fourth, different from other global compilations that report results based on the raw number of dated zircons (e.g., Rino et al., 2004; Voice et al., 2011; Dhuime et al., 2012), this study shows that a weighting method is practical, effective and essential to minimize sampling bias. Fifth, to obtain the best possible model ages and minimize their uncertainties, grains analyzed for Hf and O isotopes were carefully filtered, and more constraints were placed on the Hf model age calculation, such as a series of criteria for determining U-Pb age and the reasonable choice of mantle reference curve. Finally, the uncertainty (95% conf.) range

of the global growth curve is also given, based on uncertainties arising from the Hf isotopic composition of the arc mantle.

5.5 Summary

In summary, detrital zircons collected from fluvial and sand dune fields in Australia were analyzed for U-Pb ages, trace element concentrations, and O and Hf isotopic compositions to study the growth of the Australian continental crust. Zircon U-Pb age peaks are highly regulated by the process of the supercontinent cycle, especially during the stage of continental collision. The detrital zircon record is likely to be biased by the rapid erosion of supermountains built during supercontinent assembly. The contributions from juvenile crust are limited through the growth of the Australian continental crust, whereas crustal reworking prevailed, especially during the time of Gondwana assembly. The zircon Hf model age continental growth curve for Australia is in good agreement with the whole rock Nd model age growth curve. The Hf growth curves for Australia, Africa and the contiguous USA show relatively similar growth patterns for the continental crust, whereas the curves for Antarctica and Russia deviate. Combined with the data sets from these five continents, a more accurate global growth curve of the preserved continental crust is now proposed.

Chapter 6

The Implications for Gondwana Assembly

Abstract

The development of supercontinents has profoundly influenced the evolution of the atmosphere, biosphere, hydrosphere, and geosphere over Earth's history. The amalgamation of Gondwana resulted in extensive orogenesis worldwide. The lack of data from the ice-covered Antarctica, however, has resulted in previous studies failing to recognize the significance of Antarctica during the assembly of Gondwana. In this chapter, new data obtained in the present study highlight the critical role of Antarctica. I used two proxies in detrital zircons: i) HREE patterns for tracking mountain-building events associated with high-grade metamorphism and ii) correlation between (REE + Y) and P for identifying granitoid formation events associated with abundant S-type granites. A revised global compilation of 8995 detrital zircon U-Pb dates and element data from Asia, Europe, North America, South America, Africa, Australia and Antarctica shows that the most important period of ultra-high mountain formation and S-type zircon production coincides with the amalgamation of Gondwana.

Rapid erosion and weathering of the Transgondwanan Supermountains due to the collision between West and East Gondwana produced enormous volumes of detritus, forming the Gondwana Super Fan system. Similar detrital zircon age signatures in early Paleozoic sediments from Antarctica and south-eastern Australia show that the eastern turbidite fan extended across Antarctica to south-eastern Australia, feeding the voluminous Cambrian-Ordovician turbidites in the region and providing the source materials for S-type granites in the Lachlan Fold Belt. Zircons with low Lu and $[Lu/Dy]_N$ ratios were used for identifying the periods of high mountain formation. The results from the global database show that, on a global scale, the zircon aged between 600 and 450 Ma derived from Antarctica and south-eastern Australia together represents 34% of the zircons, 35% of the zircons with Lu < 20 ppm, and 38% of the zircons with $[Lu/Dy]_N$ < 3.5. The volume of detritus from the Antarctic section equals that of at least five Bengal Fans. This detritus was the source for the voluminous S-type magmas produced during 600–450 Ma in Antarctica. Given the vast amount of detritus produced due to the rise and subsequent erosion of such the high mountains during Gondwana assembly, delivering critical nutrients into the oceans for the subsequent evolution of complex life forms on Earth, the Antarctic section contributed nearly half of the 550–510 Ma nutrients for stimulating the Cambrian Explosion (529–514 Ma).

6.1 Introduction

The geological history of the Earth has been dominated by supercontinents, the amalgamation and dispersion of which have profoundly influenced the evolution of the atmosphere, biosphere, hydrosphere (e.g., Hoffman et al., 1998; Bradley, 2011; Müller et al., 2013; Young, 2013) and geosphere (e.g., Pisarevsky et al., 2003; Hawkesworth and Kemp, 2006a; Hawkesworth et al., 2010). Using the available Rb-Sr and K-Ar geochronological database, Worsley et al. (1982) first proposed a long-term cycle of supercontinent assembly and breakup manifest by episodic peaks in collision orogenesis and rift-related mafic dike swarms. The growing evidence from geology, tectonics and geophysics in recent decades has led to a rapidly widening interest in the supercontinent cycle and the widespread recognition of the significance of supercontinents. Several supercontinents have been proposed: i) Vaalbara (ca. 3.6-2.8 Ga; Cheney, 1996), ii) Ur (ca. 3 Ga; Rogers, 1993), iii) Kenorland (ca. 2.7-2.1 Ga; Williams et al., 1991), iv) Nuna (ca. 2.1-1.5 Ga; Hoffman, 1997) or Columbia (Zhao et al., 2004), v) Rodinia (ca. 1.2-1.0 Ga; Rino et al., 2008), vi) Gondwana (ca. 650-500 Ma; Dalziel, 2013) or Pannotia (Scotese, 2009) and vii) Pangea (ca. 320-180 Ma; Mitchell et al., 2021), although their number and configuration remain controversial (e.g., Cogné and Humler, 2008; Piper, 2015; Oriolo et al., 2017).

Gondwana, as defined by Nance and Murphy (2019), comprised mainly an assembly of the southern continents (excluding Baltica, Siberia and Laurentia) during the late Neoproterozoic. The assembly of Gondwana was marked by a series of collisional orogenies involving many continental fragments (e.g., Collins and Pisarevsky, 2005; Cawood and Buchan, 2007; Gray et al., 2008; Meert and Lieberman, 2008; Cawood et al., 2009; Meert et al., 2017). It culminated in the collision between West Gondwanan blocks (mainly Africa and South America) and East Gondwanan blocks (mainly the Arabian-Nubian Shield, India, Antarctica and Australia).

The process of Gondwana assembly was protracted, spanning the interval from ca. 650 to ca. 500 Ma (e.g., Collins and Pisarevsky, 2005; Squire et al., 2006; Veevers, 2007; Li et al., 2008; Scotese, 2009; Nance and Murphy, 2019). The amalgamation was accompanied by global-scale orogeny, commonly termed the Pan-African orogeny, arguably one of the largest in Earth history (Rino et al., 2008). The assembly of West

Gondwana started at ca. 650–620 Ma with the collision of the Amazonia-West African and Sáo Francisco-Rio de la Plata cratons (Silva et al., 2016), was followed by the collision of the Sahara Metacration with the Congo (Bouyo et al., 2013) and West African (Goodenough et al., 2014) cratons, and concluded with the collision of the Kalahari craton with the Congo (Gray et al., 2008) and Sáo Francisco-Rio de la Plata cratons (Oliveira et al., 2015) at ca. 590–530 Ma. The assembly of East Gondwana was characterized by the collision between India and East Antarctica (Meert, 2003) and the collision of India with Australia (Fritz et al., 2013) during 570–530 Ma. Gondwana assembly was completed by the closure of the Mozambique ocean basin (Emmel et al., 2008), the final suture between West and East Gondwana.

Squire et al. (2006) suggest that the collision between West and East Gondwana was pincer-like, starting with the collision between the Arabian-Nubian Shield and North Africa at ca. 650–590 Ma (Johnson, 2014), followed by the collision between India and Africa at ca. 580–550 Ma (Boger and Miller, 2004) and finally East Antarctica colliding with Africa at ca. 525–490 Ma (Meert, 2003). The ages of detrital zircons and monazites from modern African rivers peak at 700–500 Ma (Itano et al., 2016; Iizuka et al., 2017), marking increased continental arc activity (e.g., Cao et al., 2017) and granitoid magmatism as Gondwana assembled. The associated metamorphism is manifest in the record of the Pan-African ultra-high temperature granulites found in South America, Africa, India, Sri Lanka, East Antarctica and Australia (Touret et al., 2016; Brown and Johnson, 2019; Durgalakshmi et al., 2021).

Various hypotheses, based on the available geologic, geochronologic and paleomagnetic information, have been proposed for the assembly of Gondwana (e.g. Squire et al., 2006; Meert and Lieberman, 2008; Rino et al., 2008). However, due to the lack of data from Antarctica, early hypotheses place little significance on this ice-covered continent. As more data have become available, including the new data from the present study, it has become clear that Antarctica played a central role in the formation of Gondwana. Based on the new data from Antarctica and Australia, this research aims to elucidate the relationship between Antarctica and its neighbour, Australia, and to shed light on the significance of Antarctica in the amalgamation of the Gondwana supercontinent.

In this study, the HREE (heavy rare earth element) patterns in detrital zircons have been used to identify periods of high-pressure metamorphism, and the correlation between (REE + Y) and P in zircons has been utilized to distinguish zircons formed from a sediment-derived source. Assessed using these two approaches, the results from a global dataset of detrital zircons from Earth's major rivers show that the period of Gondwana assembly was the most important in Earth's history for high mountain formation and S-type zircon production. Highlighting the data from Antarctica on a global scale, this research provides insights into the nature of Gondwana assembly and reveals the crucial role of Antarctica in the Gondwanan global turbidite system, which in turn might have stimulated the Cambrian Explosion.

6.2 Methods

6.2.1. HREE pattern in zircons

Trace element partitioning between coexisting minerals can provide insights into the tectonic setting of the formation of felsic magmas, from which a zircon crystallizes. Observations from natural rocks (Rubatto, 2002), supported by experimental studies (Gilotti et al., 2004; Liu et al., 2012; Taylor et al., 2015; Zhao et al., 2016), show that zircons crystallizing in high-grade metamorphic rocks (e.g., granulite) are characterized by HREE abundances depleted relative to those in magmatic zircons because of HREE partitioning in competition with garnet. The low HREE signature and flat HREE pattern have been widely observed in metamorphic zircons in garnet-bearing eclogitic and granulitic rocks (e.g., Schaltegger et al., 1999; Hoskin and Ireland, 2000; Rubatto and Hermann, 2003; Gauthiez-Putallaz et al., 2016). Consequently, in general, high-grade metamorphic zircons tend to have low HREE concentrations and a flat HREE pattern if their host metamorphic rock is garnet-rich. Zhu et al. (2022) have argued that the zircons with low Lu and a low $[Lu/Dy]_N$ ratio were derived from erosion of the roots of ultra-high mountains where high pressure resulted in an abundance of garnet. Their study shows a strong temporal correlation between periods of ultra-high pressure metamorphism and low Lu (< 10 ppm), low $[Lu/Dy]_N$ (< 3.5) zircons in the global detrital zircon database.

In the present study, to semi-quantitatively illustrate the significance of Antarctica on a global scale during the major period of high mountain formation associated with high-pressure metamorphism, the empirical thresholds of Lu < 20 ppm (rather than < 10

ppm adopted by Zhu et al. (2022)) and $[Lu/Dy]_N < 3.5$ are adopted (Fig. 6.1). The U-Pb age distribution of zircons identified this way remains the same even if a different Lu threshold is used (Lu < 10, 15 or 20 ppm, see discussion below). One reason is that most magmatic zircons have a Lu concentration of at least 25 ppm (equivalent to 10^3 times the chondrite Lu value) (Rubatto, 2017), and most of the zircons from Antarctica have Lu higher than 20 ppm (Fig. 6.1a). Another reason is that the alternative condition for Lu provides a more similar trend that estimates the contribution from Antarctica on a global scale with that using the condition for $[Lu/Dy]_N$ in zircon, compared to those from Lu < 10 and 15 ppm zircons between 650–450 Ma (Fig. 6.6 f-h).

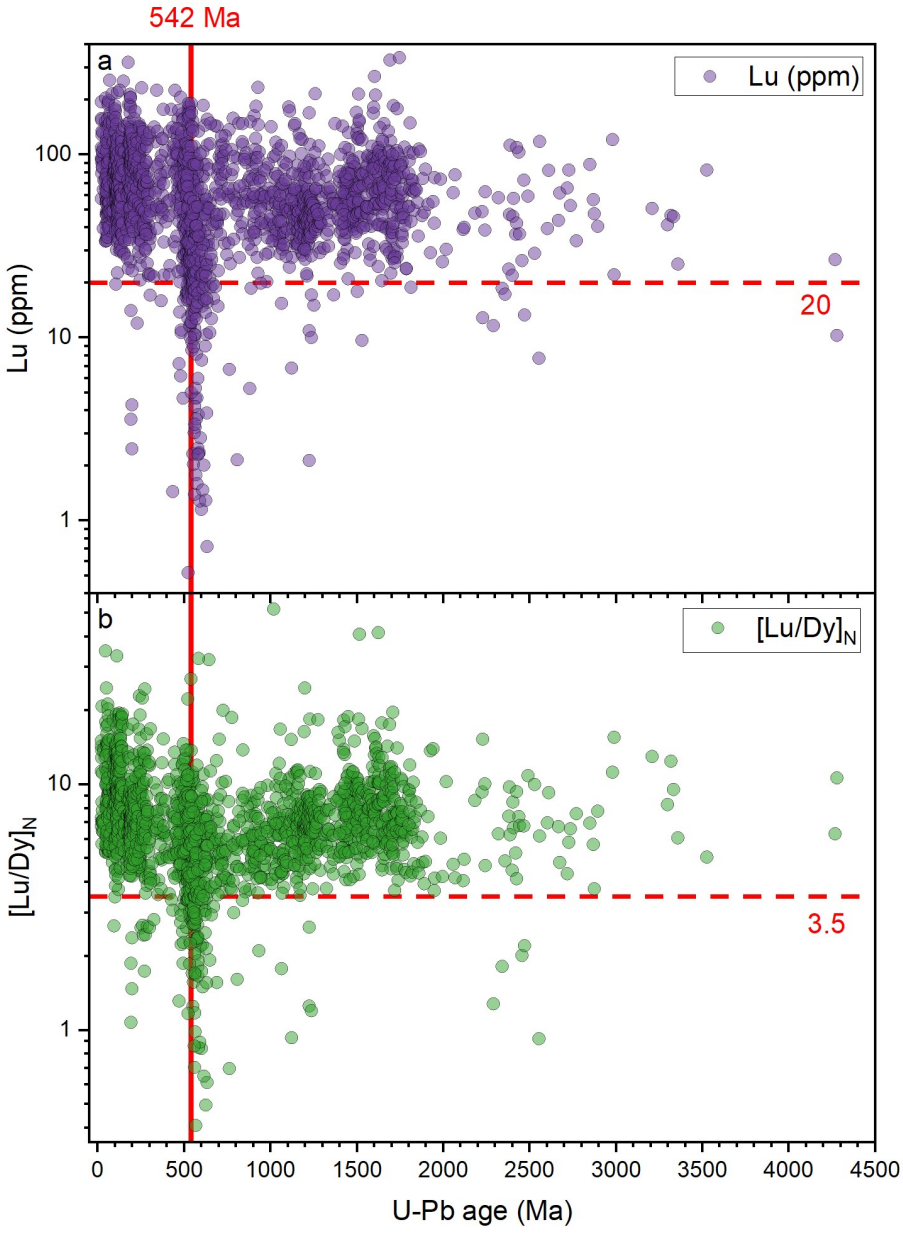

Fig. 6.1 Scatter plots of Lu (ppm) and $[Lu/Dy]_N$ versus U-Pb dates of the Antarctic detrital zircons in a and b, respectively. The Precambrian-Phanerozoic boundary (542 Ma) is

marked by the red vertical line. The thresholds of Lu = 20 ppm and $[Lu/Dy]_N$ = 3.5 are shown as red horizontal dash lines.

6.2.2. Correlation between (REE + Y) and P in zircons

Classically, granites can be simply divided into I- and S- types, derived from igneous or from sedimentary source rocks (e.g., Chappell and White, 1992). Granites from S-type magmas are generally peraluminous and contain Al-rich minerals. Recognizing the abundance of S-type granites can distinguish the major periods of granite formation with a dominant sedimentary component in their source region. The concentrations of selected indicator elements in zircons can be used to distinguish zircons crystallizing from S-type magmas. As mentioned in Chapter 4, zircons from S-type magmas can be distinguished by their (REE + Y) and P contents. Burnham and Berry (2017) recognized a strong 1:1 correlation between the molar concentrations of (REE + Y) and P in zircons crystallized from S-type granites of the Lachlan Fold Belt, whereas those from I-type granites had appreciably higher (REE + Y) than P. This is attributable to the substitution mechanism in zircon: $Zr^{4+} + Si^{4+} = (REE, Y)^{3+} + P^{5+}$ (Speer and Cooper, 1982; Hoskin and Schaltegger, 2003). This substitution is most likely to occur in S-type granites due to their commonly containing monazite, and sometimes xenotime (Sawka et al., 1986; Burnham and Berry, 2017). In addition, the concentration of P in zircons is higher and more varied in the S-type granites than in the I-types from the Lachlan Fold Belt (Burnham and Berry, 2012), a consequence of the relatively high P content of peraluminous magmas (London, 1992). Thus, the correlation between (REE + Y) and P concentrations in zircons can be utilized to identify zircons from S-type magmas. In this study, the criteria of Zhu et al. (2020), P > 15 μmol/g and 0.77 μmol/g < (REE +Y)/P < 1.23 μmol/g, are adopted to capture zircons having an S-type magmas signature (Fig. 6.2).

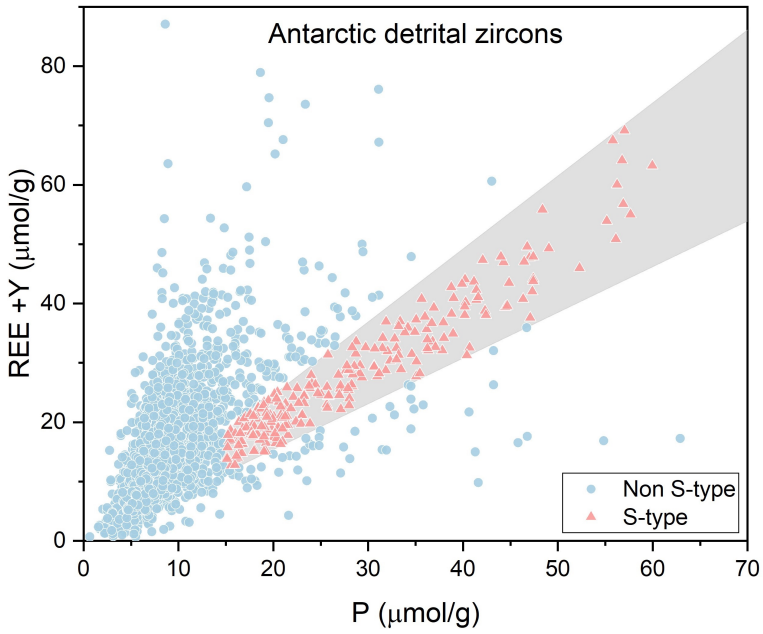

Fig. 6.2 Scatter plot of REE + Y versus P in zircons from the Antarctic detrital zircon database (N=2084). S-type zircon is filtered by the criteria of P > 15 μmol/g and 0.77 μmol/g < (REE +Y)/P < 1.23 μmol/g, as shown within the grey area.

In summary, the two different methods are adopted to distinguish zircons with two types of origins. The first is used to identify high-pressure metamorphic zircons thus capturing the major period of high mountain formation. The second aims to distinguish zircons with S-type magma signatures for estimating the major periods of formation of granites derived from S-type magmas.

6.3 Discussion

6.3.1 Antarctica and south-eastern Australia turbidite connections

As discussed in Chapter 5, the age package of the Pan-African- and Grenvillian- aged zircon populations in the Australian late Neoproterozoic to early Paleozoic sediments, especially from south-eastern Australia, are thought to be exotic (Williams, 2001). The early suggestions of a local native source (e.g., Cas et al., 1980) failed to explain the dominant peak of the Pan-African-aged zircon population (650–450 Ma) and the sub-peak of Grenvillian-aged zircons (1.20–0.95 Ga) in the turbidites, particularly from the Lachlan Fold Belt. Similar detrital zircon age packages from turbidites in both south-eastern Australia and South Africa (e.g., Foster and Gray, 2000; Gray and Foster, 2004; Veevers, 2015) raised a possible turbidite connection between these two continents, leading to a hypothesis of an African source (Williams et al., 2002; Williams and Pulford,

2008). Australia and South Africa have never been in direct contact, however, implying that there was once a channel in between. The missing piece is Antarctica.

Based on sediment geochemistry, Offler and Fergusson (2016) suggest that the turbidites deposited in the Lachlan Orogen possibly originated in part from East Antarctica. The newly available Antarctic data from the present study provide a strong link between these continents. The U-Pb age data make it possible to test the hypothesis of Squire et al. (2006) that the Lachlan turbidites, which have a volume comparable to the modern Bengal Fan (1.25×10^6 km^3; from Curray et al. 2002), were derived from Antarctica. Squire et al. (2006) suggested that rapid erosion of the Transgondwanan Supermountains formed by the collision between West and East Gondwana produced an enormous volume of detritus shed from the mountain chains, developing a Gondwana super turbidite fan system. The eastern turbidite fan, a > 5,000-km-long river system, extended across Antarctica into south-eastern Australia.

Fig. 6.3 compares the ages of the Antarctic zircons analyzed in the present study with those from the south-eastern Australian Cambrian-Ordovician turbidites. Although there are differences in the age histograms, these data sets have two prominent features in common: i) A dominant peak of Pan-African-aged (650–450 Ma) zircons in all populations. Their means are similar and lie within the uncertainty of each other; (ii) A secondary Grenvillian-aged peak between 1.20 and 0.95 Ga. In addition, the 650–450 Ma zircons have a wide range of negative to positive $\varepsilon Hf_{(t)}$ values and the Grenvillian-aged zircons have mainly positive $\varepsilon Hf_{(t)}$ values in both the Antarctic and south-eastern Australian data sets (Fig. S6.1). These observations confirm the hypothesis of Squire et al. (2006). Furthermore, the population of inherited zircons in the associated Lachlan Fold Belt S-type granites is similar to that of detrital zircon in the turbidites (Pell et al., 1997a), so the source for these granites is likely to be deep levels of the turbidite sequence (Williams, 2001). Glen et al. (2017) compared the Antarctic turbidites to Lachlan turbidites based on the range of available data: i) U-Pb age peaks, $\varepsilon Hf_{(t)}$ and inferred model age from detrital zircons, ii) Ar-Ar ages from detrital muscovite and iii) $\varepsilon Nd_{(t)}$ from the whole-rocks. Their results indicate that East Antarctica is the most significant source for the turbiditic sediments in the Lachlan Orogen. Consequently, the turbidite fan on the eastern side of the Transgondwanan Supermountains extended

across Antarctica into south-eastern Australia. The immediate source of the turbidites in south-eastern Australia was from Antarctica. It remains unclear why the minor ca. 1.5 Ga peak in the Antarctic database is absent from the south-eastern Australia age spectrum. One possibility is that the bulk of the south-eastern Australian zircon in the age ranges of 1.20–0.95 Ga and 650–450 Ma was transported from East Africa along the former Antarctic margin, not sampling ca. 1.5 Ga zircon that comes from Antarctica itself.

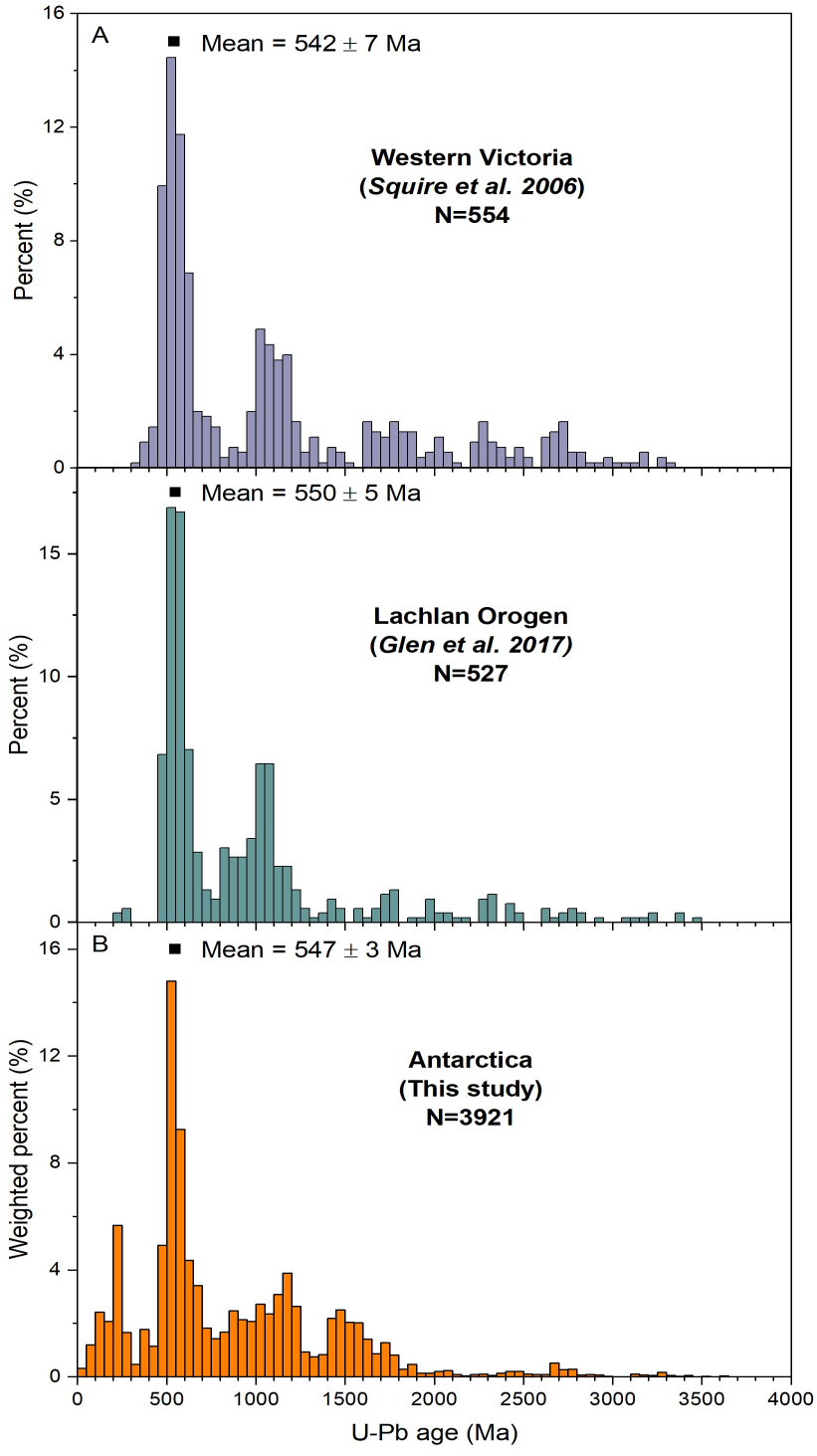

Fig. 6.3 Histograms of detrital zircon U-Pb dates from south-eastern Australia and Antarctica. a) U-Pb dates for detrital zircons from Cambrian-Early Devonian sediments in the western Victoria, southern Australia (Squire et al., 2006); b) U-Pb dates for detrital zircons from Ordovician turbidites in the Lachlan Orogen, south-eastern Australia (Glen et al., 2017); c) Weighted histogram of U-Pb dates of detrital zircons from Antarctica (from Fig. 4.3a). The means with 2SE were calculated for zircons with ages between 650 and 450 Ma.

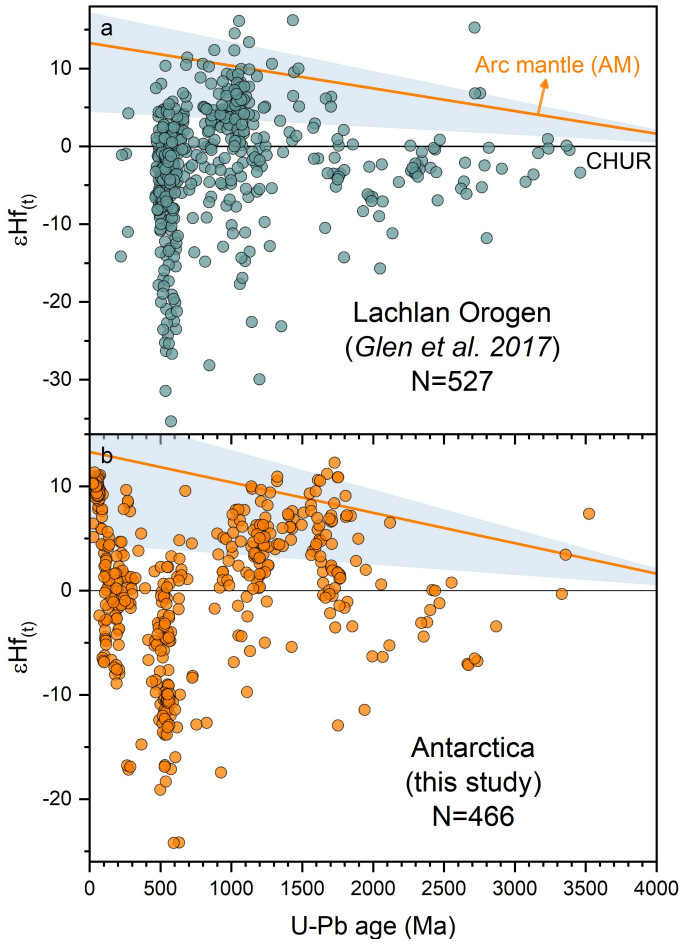

Fig. S6.1 Comparison of $\varepsilon Hf_{(t)}$ values from detrital zircons from the Lachlan Orogen and Antarctica. Data for the Lachlan Orogen are from Glen et al. (2017).

6.3.2 Implications for the collision between West and East Gondwana

A revised global database of detrital zircons (N = 8995) from the world's major rivers, sand dune fields and glacial deposits is proposed here by adding all dated zircon data from Antarctica presented in Chapter 4 of this study into the database from the study of Zhu et al. (2020), which includes river samples from Asia, Europe, North America, South America, Africa and Australia. Zircons in both studies were randomly picked for U-Pb dating. The former includes the U-Pb dates from the rims and cores of grains if both meet the criteria of age determination in Section 2.3.1. The latter database reports one date per zircon crystal, calculated by the longest period of steady signal during the

LA-ICPMS analysis. In that case, zircons with a metamorphic overgrowth of sufficient size could be included in this revised global database.

Instead of using the raw number of zircon grains, the histogram of zircon U-Pb dates is weighted according to the drainage area or inferred ice flow area (i.e., samples from Antarctica). Fig. 6.4 illustrates the differences between the unweighted and weighted histograms of U-Pb dates. There are two major advantages of the weighting method on a global scale. Firstly, it largely minimizes the sampling bias by which the young group (< 300 Ma) is likely being oversampled. The global zircon database from Lee et al. (2016) (Fig. 6.4c), for example, is distorted by a high fraction of zircons from the North American Cordilleran (250–100 Ma) because of the intensive study of that area by USA laboratories. Secondly, the estimation of the contribution from Antarctica on a global scale, which is based on the relative proportion of the Antarctic population in the revised global database within each bin, is not exaggerated and distorted due to the high input of the data set (N=2084) from Antarctica in the present study (Fig. 6.4a).

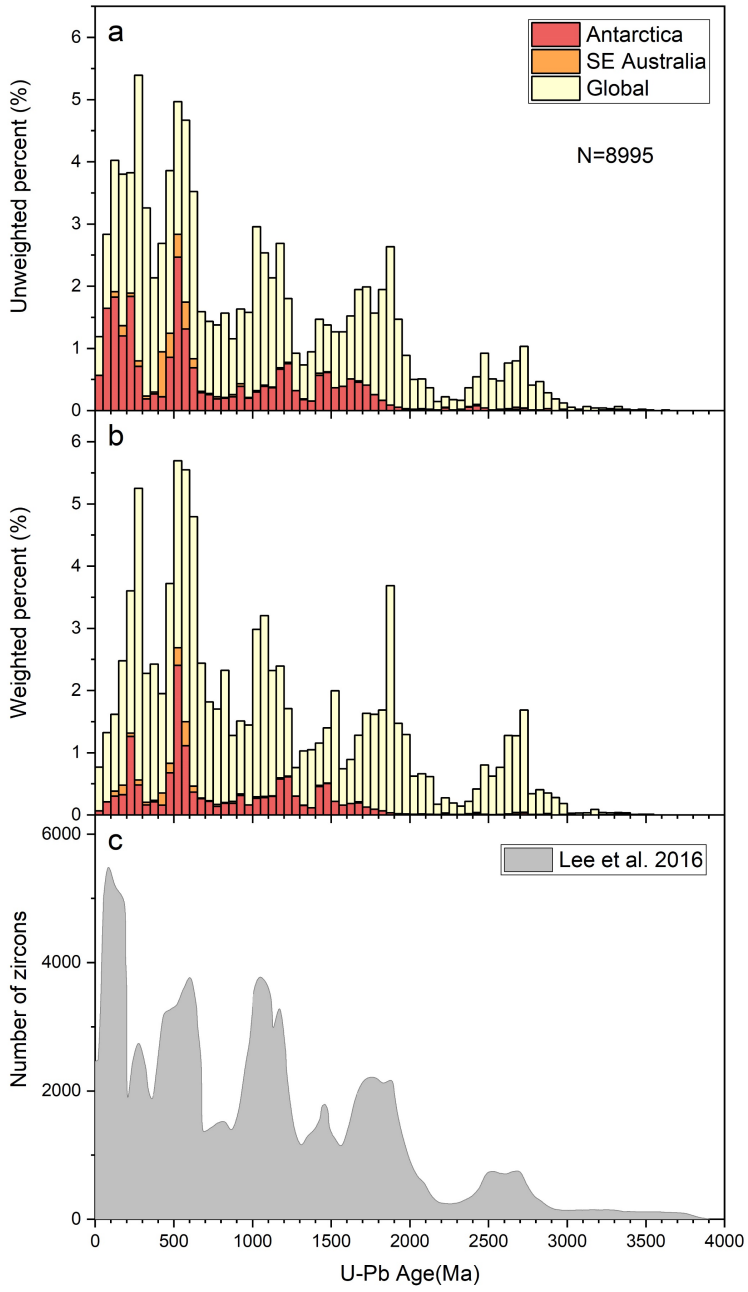

Fig. 6.4 Comparison of the unweighted and weighted histograms of U-Pb date from detrital zircons on a global scale. a) Histogram of U-Pb dates for detrital zircons from the revised global database (N=8995) from this research; b) Weighted histogram of U-Pb dates based on the database in a; c) Unweighted histogram U-Pb dates for the global compilation of detrital zircons by Lee et al. (2016).

Considering the provenance of detrital zircons in south-eastern Australia, as discussed above, the zircon population from south-eastern Australia is also highlighted in the following plots for further discussion. Fig. 6.5 a and b show the U-Pb age distributions of detrital zircons in the Antarctic database and the revised global database. The most striking feature is that the highest contribution from Antarctica to the global zircon production corresponds to the time of Gondwana assembly. Specifically, 44% of

the global zircons aged between 550 and 510 Ma are derived from Antarctica (Fig. 6.5d). These observations confirm the crucial role of Antarctica on the global stage, especially during the assembly of Gondwana.

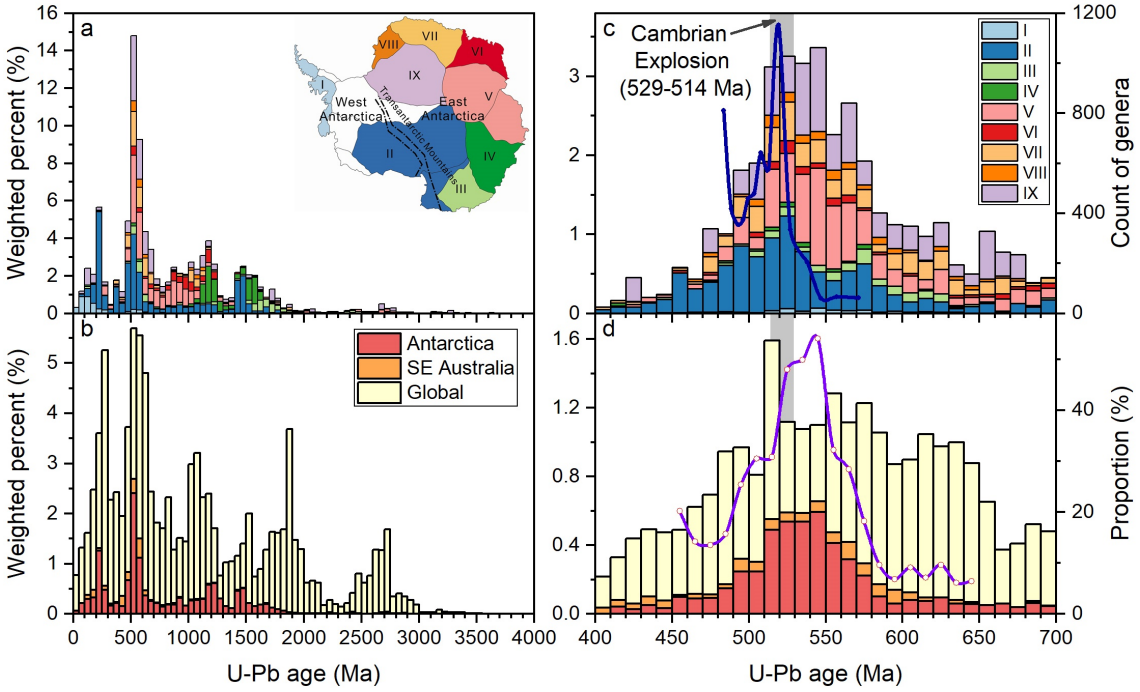

Fig. 6.5 Weighted histograms of U-Pb dates from detrital zircons for the Antarctic data set in a and c, and global data set in b and d. The time interval of 4.0–0.0 Ga is shown in a and b with the interval between 700 and 400 Ma shown in detail in c and d. The grey bar in c and d indicates the time of the Cambrian Explosion (529–514 Ma; Stage 2 and 3). The blue curve in c shows changes in the number of extant genera through time (Na and Kiessling (2015). The violet line with dots in d represents the proportion of the Antarctic zircons within the global database.

6.3.2.1. High mountains during Gondwana assembly

Low Lu and $[Lu/Dy]_N$ have been used to identify the zircons formed in the presence of garnet under high pressure. The U-Pb age peaks for these zircons correspond to periods when high mountains were forming. This correlation is evident in a temporal correlation between periods of ultra-high metamorphic pressure and low Lu (< 10 ppm), low $[Lu/Dy]_N$ (< 3.5) zircons in the global detrital zircon database from Zhu et al. (2022), which does not include the Antarctic data set. Fig. 6.6 a-d shows the weighted distribution of U-Pb dates for detrital zircons with low Lu and low $[Lu/Dy]_N$. The overwhelming majority has ages between 650 Ma and 500 Ma, which corresponds to the period of collision between West and East Gondwana.

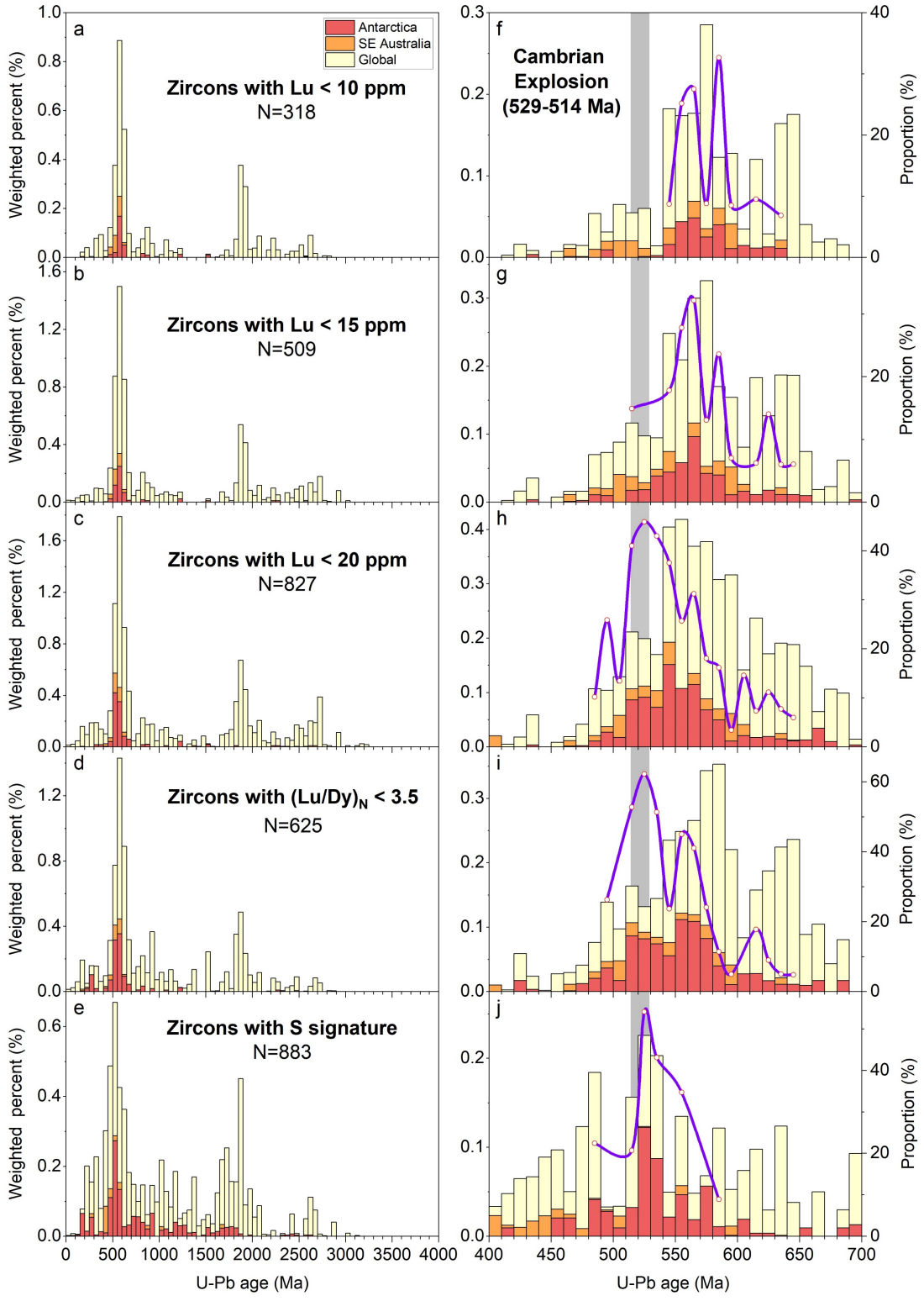

Fig. 6.6 Weighted histograms of U-Pb dates of detrital zircons filtered by using different geochemical parameters. a-e show the time window of 4.0–0.0 Ga (bin size = 50 Myr) and f-j for 700–400 Ma (bin size = 10 Myr). The relative proportions of the Antarctic zircons on a global scale are calculated if the number of such zircons from the revised global data set in each bin is over 10 (>0.1%) between 650 and 450 Ma, shown as red dots. The purple curves estimate the trend of contributions from Antarctica with the time interval of Cambrian Explosion (529–514 Ma) shown as a grey column in f-j.

To test the validity of the threshold of Lu < 20 ppm, the alternative thresholds (10 and 15 ppm) for Lu concentration were also used for comparison. All the zircon populations filtered by Lu < 10, 15 and 20 ppm show a dominant peak of 650–500 Ma with a sub-peak at ca. 1.8 Ga, while the total number of zircons with Lu < 10 ppm decreases to 318 (Fig. 6.6 a-c). Note that the distribution of zircons with Lu < 10 ppm matches best with the distribution of zircons with $[Lu/Dy]_N < 3.5$ over the full age range using 50 Myr as the bin size, compared to those with Lu < 15 or 20 ppm (Fig. 6.6 a-d). An appreciable peak at ca. 2.7 Ga can be observed in the distribution of zircons with Lu < 20, whereas it is missing using the criterion of low Lu/Dy ratio. For the smaller time window of 750–400 Ma using 10 Myr as the bin size, the peak at 600–540 Ma is common to all zircon populations filtered using different thresholds for Lu as well as by $[Lu/Dy]_N < 3.5$ (Fig. 6.6 f-i). The trends in the contribution from Antarctica in both distributions of zircons with Lu < 20 and $[Lu/Dy]_N < 3.5$ during 650–450 Ma are more closely matched, however, than those for zircons with Lu < 10 and 15 ppm. These differences produced by different empirical thresholds raise a caution while interpreting the result given only by a single filter.

Although there are minor differences in the age pattern when using Lu/Dy ratio and different Lu concentration thresholds for identifying detrital zircons with high-pressure signatures, all results show the pronounced peak at 650–500 Ma that corresponds to the collision between West and East Gondwana, suggesting that abundant garnet formed due to the high pressures resulting from that collision. As the crust thickens over ca. 30–35 km depth, garnet begins to form, and in lithologies of suitable composition can be stabilized in large quantities where the pressure exceeds 1.2 GPa (Alonso-Perez et al., 2009). Consequently, the collision between West and East Gondwana led to crustal thickening, the thickness reaching at least 60–70 km, and thus the formation of the ultra-high mountains (Zhu et al., 2022) that Squire et al. (2006) called the Transgondwanan Supermountains. It should be noted that zircon can also be found in garnet-bearing metamorphic rocks produced during high-temperature anatexis, such as metamorphic zircon rims depleted in HREE from garnet-present metapelites from Mount Stafford in Central Australia (Rubatto et al., 2006). However, the metamorphic zircon rims from the two highest-grade samples in that study have Lu contents of 54–136 ppm and $[Lu/Gd]_N$ ratios of 25-70, which fail to meet the selection criteria applied

here, ruling out the likelihood that the abundant zircon with low Lu and low $[Lu/Dy]_N$ produced during 650–450 Ma is attributable to high-temperature, not high-pressure, metamorphism.

The formation of high mountains during Gondwana assembly can also be inferred from the distribution of zircon with high Eu/Eu* (Fig. S6.2). Zircons with high Eu/Eu* mostly crystallize from magma at higher pressure (Tang et al., 2021). This is because: i) plagioclase is suppressed in the magma at high pressure (Green, 1982) and the magma is therefore not depleted in Eu; ii) as the pressure increases, the appearance of garnet, which incorporates Fe^{2+} in preference to Fe^{3+}, can elevate $Fe^{3+}/\Sigma Fe$ in magmas and therefore multivalent trace elements (i.e., Eu) will be oxidized, leading to the conversion of Eu^{2+} to Eu^{3+} (Tang et al., 2018), which is highly compatible in the zircon lattice. As a result, the increase of Eu/Eu* in zircon can indicate an increase in pressure, hence crustal thickening. Tang et al. (2021) used Eu/Eu*-in-zircon as a proxy to calculate the mean thickness of active continental crust. Based on the empirical relationship between Eu/Eu*-in-zircon and crustal thickness expressed as the following equation (where z is crustal thickness), zircons with Eu/Eu* higher than 0.30, 0.42 and 0.54 can be used for inferring crustal thicknesses over 50, 60 and 70 km respectively.

$$z = (84.2 \pm 9.2) \times \mathrm{Eu/Eu^*}_{\mathrm{zircon}} + (24.5 \pm 3.3) \qquad (4)$$

Age peaks of 650–500 Ma and ca. 1.85 Ga are present in all populations of zircons filtered by Eu/Eu*(> 0.30, 0.42 and 0.54), Lu (< 10, 15, 20 ppm) and $[Lu/Dy]_N$ (< 3.5), whereas the peaks younger than 300 Ma, such as ca. 250 Ma, are present only in the zircons with high Eu/Eu* (Fig. S6.2a-c). Despite the decoupled U-Pb age peaks observed in these zircon populations using different parameters (Eu anomaly or HREE pattern), there is one striking feature in common—abundant zircons in all populations (Fig. 6.6 a-d and Fig. S6.2 a-c) peak at 650–500 Ma, the time of the Gondwana supercontinent amalgamation. This indicates that the collision between West and East Gondwana led to the formation of ultra-high mountains (> 70 Km crustal thickness) accompanied by high-pressure metamorphism.

The high-pressure metamorphism during assembly Gondwana is also manifest in the abrupt increase in pressure at ca. 600 Ma recorded by metamorphic rocks in the

compilation of Brown and Johnson (2019). High temperature/pressure metamorphism at ca. 550 Ma is widespread in eastern Gondwana (Brown, 2006; Brown, 2007). A detailed study of U-Th-Pb dating of zircons and monazite in Antarctica, Sri Lanka, southern India and Madagascar shows a simultaneous metamorphic peak at ca. 550 Ma during the East African Orogeny (Durgalakshmi et al., 2021), establishing a direct orogenic connection between these blocks during the collision between West and East Gondwana. All these observations are consistent with there having been extensive orogenies associated with high-grade metamorphism during Gondwana assembly.

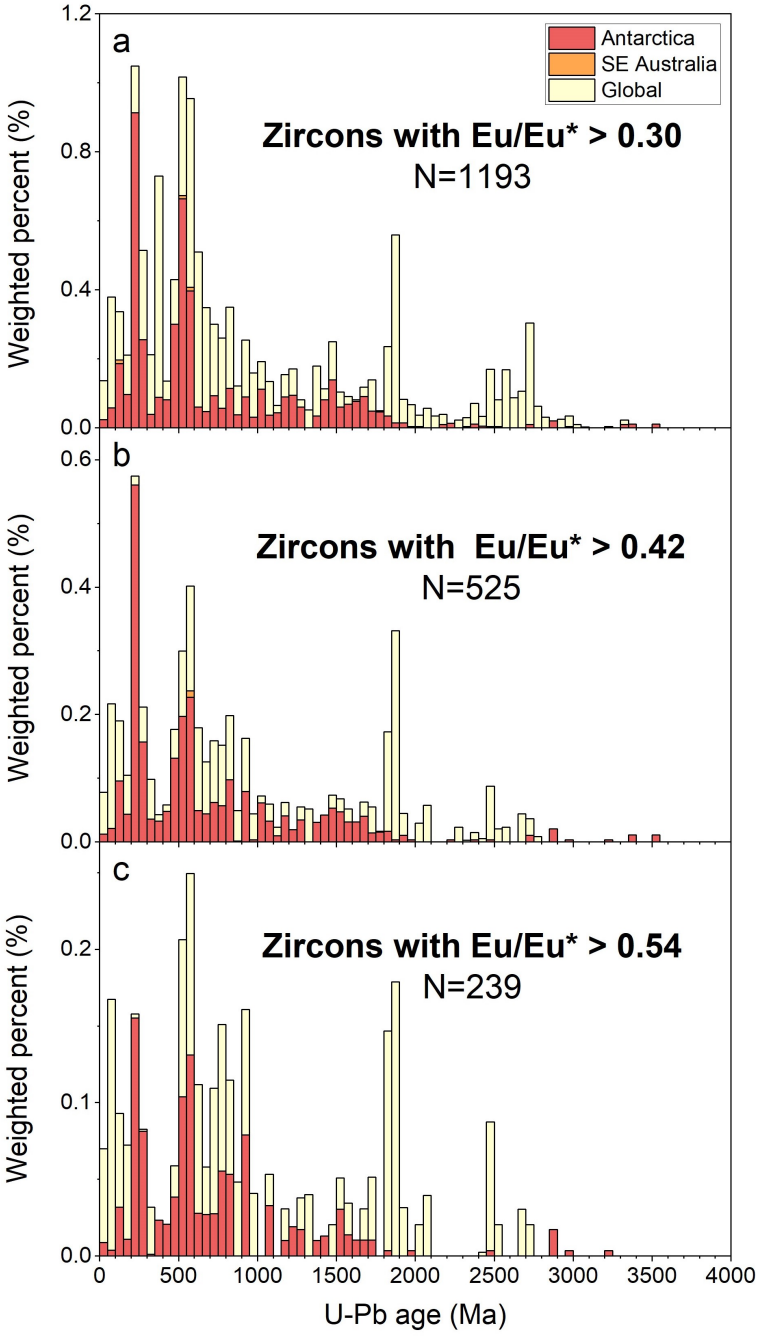

Fig. S6.2 Weighted histograms of U-Pb dates from zircons with Eu/Eu* > 0.30, > 0.42 and > 0.54 in the global database.

The most significant peak between 650 and 450 Ma in the global detrital zircon database reveals how overwhelmingly the assembly of Gondwana impacted the global record from detrital zircons (Fig. 6.5b). The amount of Gondwana-age detritus derived from Antarctica, including the south-eastern Australian turbidites but not the S-type granites, was significant. It represents 34% of the zircons, 35% of the zircons with Lu < 20 ppm, and 38 % with $[Lu/Dy]_N$ < 3.5 in the weighted global detrital zircon database (Fig. 6.5b and Fig. 6.6 c-d). More importantly, the peak production of low Lu and low Lu/Dy zircon was between 550 and 510 Ma, when 49% of the zircons, 52% of the low-Lu (<20 ppm) zircons and 53% of the low $[Lu/Dy]_N$ zircons in the weighted global database (Fig. 6.5d and Fig. 6.6 h-i).

6.3.2.2. The Gondwana Super Fan System

The high abundance of 650–450 Ma zircons with low Lu and low $[Lu/Dy]_N$, the time of the collision between West and East Gondwana during East-African Orogeny (e.g., Fritz et al., 2013) or Pan-African Orogeny (e.g., Rino et al., 2008) that formed the Gondwana Supercontinent, strongly supports the existence of Transgondwanan Supermountains. Squire et al. (2006) suggested that this mountain was > 8000 km long and > 1000 km wide. This extensive mountain was argued to be a Himalayan-scale mountains in the geological record (Jacobs and Thomas, 2004; Fritz et al., 2013; Zhu et al., 2022). When global topography is elevated, erosion and weathering are strongest because relief is a primary factor for regulating the erosion rate (Maher and Chamberlain, 2014). Higher mountains lead to greater erosion rates. As a result, rapid erosion and weathering of the Transgondwanan Supermountains produced a vast amount of detritus, developing the Gondwana Super-Fan System (Squire et al., 2006).

A high weathering rate during Gondwana assembly is also supported by the abrupt increase of $^{87}Sr/^{86}Sr$ in seawater at the time (Shields and Veizer, 2002; McArthur et al., 2012) and the increase of atmospheric oxygen (Canfield, 2005; Kump, 2008). The age package of sediments with a dominant peak of Pan-African-aged zircons and a sub-peak of Grenvillian-aged zircons is widely recognized in the late Neoproterozoic to early Paleozoic sediments of Gondwana i) the Nahuel Niyeu and El Jaguelito Formations in South America (Pankhurst et al., 2006); ii) the Table Mountain Group in Africa

(Armstrong et al., 1998); iii) the Amudei Shelomo Formation of Israel in the Arabian-Nubian Shield (Avigad et al., 2003); iv) the Tethyan margin deposits of the Himalayas (DeCelles et al., 2000); v) the Junction Formation, Balloon Melange (Jongens et al., 2003) and Greenland Group (Ireland, 1992; Ireland and Gibson, 1998) in New Zealand; vi) the Amadeus Basin in Australia (Maidment et al., 2013) and vii) Antarctica (Goodge et al., 2004 and this study). One of the distributary fans is the turbidites of the Lachlan Orogen, south-eastern Australia, which Fergusson and Coney (1992) have argued are comparable in volume to the Bengal Fan (1.25×10^6 km^3). The Pan-African-aged zircons (650–450 Ma) from south-eastern Australia represent 20% (1/5) of the Antarctic zircons, but less than 5% (1/20) of the zircons in the global detrital zircon database (Fig. 6.5b) during this period. If the Pan-African-aged zircons (650–450 Ma) from south-eastern Australia mark nearly 5% of the volume of the global detritus produced during Gondwana assembly from this database, the volume of the detritus, derived from the Transgondwanan Supermountains, is suggested to be > 25×10^6 km^3 ($1.25 \times 10^6 \times 20$), equivalent to at least 20 Bengal Fans. The amount of the detritus from Antarctica itself is equal to the size of 5 Bengal Fans.

The enormous volumes of turbidite deposited in Antarctica provided the essential source materials for the formation of S-type granites (e.g., Collins and Richards, 2008; Veevers, 2015; Zhu et al., 2020). As discussed in Chapter 4, these sediments shed from the giant mountain were transported into the closing ocean basin and were too buoyant to be subducted into the mantle. The juvenile magmas generated from underlying subduction zones failed to reach the surface. They ponded underneath, forming large magma chambers that melted their thick sedimentary roof, leading to a large amount of S-type granite being produced during the Gondwana era. Evidence for this is the zircon with S-type magmas signatures predominantly peaking at 650–450 Ma in the Antarctic database (Fig. 4.3b). The Gondwana era was also a period with the highest production of zircons with S-type signatures in the global database (Fig. 6.6e), consistent with the result of Zhu et al. (2020). The validity of the proxy based on the correlation between REE + Y and P in zircon for distinguishing S-type zircons was tested by examining Th/U ratios of S-type and non-S-type zircons. Fig. S6.3 shows that over 72% of S-type zircons, identified by the criteria above, have Th/U ratios less than 0.5 whereas non-S-type zircons tend to have higher Th/U. This is consistent with the common presence of

monazite in S-type granites that are peraluminous. Thorium is more compatible in monazite, an essential carrier of Th, than in zircon in peraluminous magmas (Stepanov et al., 2012; Breiter, 2016). Consequently, zircons from S-type magmas must compete with monazite for Th, lowering their Th/U ratios.

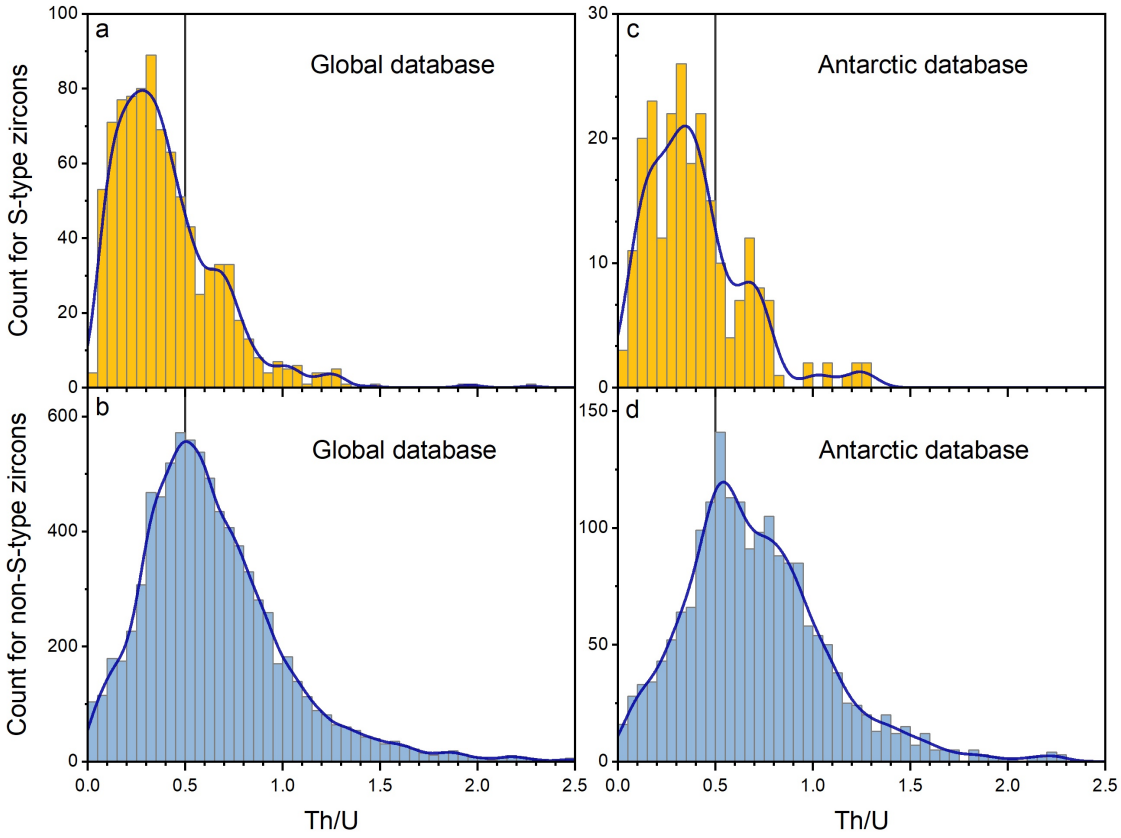

Fig. S6.3 Histograms Th/U for S-type and non-S-type zircons from the revised global database and Antarctic database, filtered by the criteria presented in Fig. 6.2.

The detritus was also transported from Antarctica to south-eastern Australia, feeding the massive Cambrian-Ordovician turbidites in that region. This made it possible that slightly more than half of the granites exposed in the Lachlan Fold Belt are S-type granites sourced from those turbidites (see in Chapter 5 for details), contributing over 25% of 450–400 Ma zircons with an S-type signature on a global scale (Fig. 6.6e). Similar scenarios are identified in Spain. Up to 11 km thick, extensive 650–470 Ma turbidites and shales in Central Iberia (Spain) are the source rocks for the 500–470 Ma Spanish S-type granites, and for the younger 330–300 Ma S-type granites formed during the late Variscan orogeny (Orejana et al., 2015). A similar association between turbidites and S-type granites is also found in Western and Central Europe, Saxo-Thuringia in Germany and the Southern Calabria-Peloritani Orogen in Italy (Zhu et al., 2020).

What is missing from the global detrital zircon compilation of Zhu et al. (2020) is the large amount of detritus contributed by the Antarctic section of the Transgondwanan Supermountains. Before the present study that was unknown. Antarctica has an area of 14 x 10^6 km^2, which is only 9% less than the combined area of Australia and the contiguous USA. 28% of the zircons and 33% of the zircons with S-type signature peaking between 600 Ma and 450 Ma on the global scale are attributed to Antarctica (Fig. 6.5b and Fig. 6.6e). The implied volume of sediment in Antarctica, derived from the Transgondwanan Supermountains, is enormous. This must be added to the volume of Cambrian-Ordovician turbidites of south-eastern Australia and the proportion of turbidites that formed the source rocks to the Lachlan Fold Belt S-type granites.

There is an offset between the age peaks of zircons with S-type signature and zircons with low Lu and a low $[Lu/Dy]_N$ ratio in both the Antarctic and global databases (Fig. 6.6 f-j). After the high mountains formed due to the continent-continent collision that formed Gondwana, the rapid erosion and weathering of the high mountains generated abundant detritus that was transported and formed a turbidite fan. That detritus was then melted or partially melted to form S-type granites in a tectonic setting (e.g., thickened crust above the subduction zone) that can provide the necessary heat. The time delay marks the period of detritus generation, transportation and melting in a desirable tectonic setting, consistent with the study of Zhu et al. (2022).

6.3.2.3. The Cambrian Explosion

The timing of the amalgamation of the Gondwana supercontinent overlaps with Neoproterozoic Oxygenation Event (NOE) (~800–500 Ma; Reinhard et al., 2017) during which (i) the oxygen content of the atmosphere rose by about an order of magnitude (Canfield, 2005); (ii) the oldest confirmed macroscopic animals (*Dickinsonia* in the Ediacaran biota) appeared (Bobrovskiy et al., 2018); and (iii) the Cambrian Explosion (529–514 Ma; Stages 2 and 3) occurred (Na and Kiessling, 2015). The last was characterized by a dramatic increase in the abundance and diversity of genera, especially metazoans with biomineralized skeletons (Fig. 6.5c). Several studies have proposed that the high erosion rate of the mountain chains associated with the amalgamation of the Gondwana supercontinent led to a massive increase in the flux of essential, continentally derived nutrients, including P, Fe, Sr, Ca and bicarbonate ions,

into the oceans, strongly enhancing the environmental conditions that were suitable for the complex animal radiation (e.g., Squire et al., 2006; Meert and Lieberman, 2008; Ganade de Araujo et al., 2014). These nutrients allowed algae and cyanobacteria to produce O_2, increasing O_2 in the atmosphere. Burial of organic carbon and pyrite led to the further rise in atmospheric O_2 peaking at ca. 500 Ma, facilitating the first appearance of complex animals, and later stimulating the Cambrian Explosion (Campbell and Squire, 2010), which is characterized by radiation and diversification of metazoan phyla (Zhuravlev and Wood, 2018). A clear consensus between high mountain erosion, nutrient supply and blooming biodiversity has not yet emerged, requiring further scrutiny. However, if the detritus from the eroded Transgondwanan Supermountains stimulated an unprecedented bloom in primitive life, which in turn provided the food for complex and diversified life forms, it should be noted that between 550 and 510 Ma, the detritus from the Antarctic section could provide nearly half of the critical nutrients required for the radiation and diversification of metazoan phyla during the Cambrian (Fig. 6.5d).

6.4 Summary

In summary, the collision between West and East Gondwana has profoundly impacted the records in the global detrital zircon database. Using two proxies (HREE patterns and the 1:1 correlation between REE +Y and P) in detrital zircons on a global scale, the period during the assembly of Gondwana has been identified as the most significant event in geological history for the formation of ultra-high mountains and the production of S-type zircons through crustal recycling. The enormous amounts of detritus from the Antarctic section of the eroded Transgondwanan Supermountains, estimated to be equivalent to the volume of five Bengal fans, were transported across Antarctica to south-eastern Australia, serving as the essential source materials for S-type zircons formed in both places. During 600–450 Ma, 28% of the total zircons, and 33% of the zircons with S-type signatures, in the global database can be attributed to Antarctica. Considering the hypothesis that the enormous volume of detritus shed from the giant mountain delivered essential nutrients into the oceans, providing a suitable environment for the subsequent evolution of complex life on Earth, nearly half of the contribution from the Antarctic section during 550–510 Ma was vital for the blooming of complex animals, the Cambrian Explosion.

Chapter 7

Conclusions and Future Work

7.1 Conclusions and future work

This thesis presents the integrated data of U-Pb, O, and Lu-Hf isotopic compositions of detrital zircons from Antarctica and Australia to investigate the growth of the preserved continental crust. Combined with the data sets from five continents (Africa, North America, Russia, Antarctica, and Australia), a new growth curve for the preserved continental crust on a global scale is proposed. The chemical and isotopic compositions of detrital zircons from Antarctica and Australia provide significant information on the amalgamation of the Gondwana supercontinent. In this chapter, I revisit the conclusions of Chapters 3–6 and then highlight the directions for future work.

In **Chapter 3**, the major uncertainties regarding the calculation of zircon Hf model age were discussed. The uncertainties are effectively minimized by the methodology adopted in this research: i) a series of criteria were used for determining U-Pb dates and selecting zircons for O-Hf isotopic analyses; ii) O isotopes in zircons were used to estimate the $^{176}Lu/^{177}Hf$ ratios of the source magmas; iii) a more appropriate mantle reference-Arc Mante, was used for the zircon Hf model age calculations. By using a large database of detrital zircons, the errors regarding the Hf model age calculated from individual zircon tended to cancel out. Therefore, the zircon Hf model ages from a large data set can be used as an estimation for the growth of the preserved continental crust.

Chapter 4 presents the integrated study of U-Pb, O and Lu-Hf isotopic compositions with trace elements from detrital zircons from the glacial deposits sampled by scientific ocean drilling sites surrounding Antarctica. U-Pb ages and Hf model ages show that Antarctica is a relatively young continent, contrary to the previous perception that Archean terranes are a significant component. By the end of the Archean, only 8% of the Antarctic continental crust had been established, although Antarctica had begun to form at ca. 3.9 Ga. The major tectonic event—the collision between West and East Gondwana—has overwhelmingly affected Antarctica. The most dominant peak of ca. 650–450 Ma zircons demonstrates that the detritus shed from the collisional orogens dominated Antarctic sedimentation and formed a giant turbidite fan. In the subduction zones, the thick detritus prevented underlying primitive magmas from reaching the surface. The magmas ponded at or near the sedimentary base and thus formed magma chambers, providing heat to melt their turbiditic roof rocks, which resulted in sediment-

derived felsic magmatism being most dominant during 600–450 Ma in Antarctica. Although Antarctica is young, the cores from two detrital zircons yielded concordant Hadean ages, signaling the presence of remnant Hadean crust in this ice-coved continent.

In **Chapter 5**, the same methodology was applied to the Australian continent to reconstruct the growth of the preserved Australian continental crust. The zircon age data suggest a potential overestimation of the abundance of Pan-African-aged (650–450 Ma) and Grenvillian-aged (1.20–0.95 Ga) zircons. This can be attributed to an exotic detrital source transported from Antarctica to Australia due to erosion of the Neoproterozoic Transgondwanan Supermountains formed by the collision of West and East Gondwana. During Gondwana assembly, the crustal reworking and associated high input from sediments were dominant in the detrital zircon records. The agreement between the growth curves for the Australian continental crust based on zircon Hf model ages and whole-rock Nd model ages confirms the reliability of the zircon Hf model age growth curve for the continental crust. Using similar data sets from other continents (Africa, North America, Russia, and Antarctica), I proposed a new model for the growth of the preserved continental crust on a global scale. The result shows that at least 25% of the global continental crust had been produced by the end of the Archean, and ca. 90% had been formed by 0.9 Ga, with no significant growth during the Hadean era.

In **Chapter 6**, the HREE patterns and correlation between (REE +Y) and P in detrital zircons were used as two proxies to identify the major periods of mountain formation associated with high-grade metamorphism and sediment-derived felsic magmatism on a global scale. The former indicates that the dominant period for high-mountain formation was during the assembly of Gondwana, which led to the Neoproterozoic Transgondwanan Supermountains forming during the protracted collision between West and East Gondwana. The consequent high erosion rate resulted in immense volumes of detritus being shed from the supermountains, developing the Gondwana Super Fan System. Similarities in U-Pb age patterns, Lu-Hf isotopic systematics of detrital zircons from Antarctica and Australia provide evidence that the eastern turbidite fan extended across Antarctica into south-eastern Australia. The volume of the detritus from the Antarctic section is estimated to be equivalent to that of 5 Bengal Fans. The detritus of the eastern turbidite fan also provided the source materials for S-type zircons

formed by magmatism and metamorphism in both Antarctica and south-eastern Australia. During 600–450 Ma, 28% of the zircons and 33% of the zircons with S-type signatures in the global database can be attributed to Antarctica. More impressively, zircons between 550 and 510 Ma from Antarctica and south-eastern Australia together represent 49% of the zircons of that age in the weighted global database. The detritus from the Antarctic section contributed nearly half of the nutrients suggested to have been vital for stimulating the Cambrian Explosion.

Zircon has been widely studied over recent decades for exploring crust-mantle evolution. This thesis shows the power of the integrated study of three isotopic systematics in detrital zircons for investigating the growth of the preserved continental crust. And combined with trace elements, the isotopic composition of zircons can reveal information on tectonic settings. In Chapter 4, two concordant Hadean-aged zircon cores light the way to track remnant Hadean crust in Antarctica. More U-Pb dating information from remaining unanalyzed detrital zircons from the same site can potentially provide insights into the evolution of the Hadean crust on Earth. In Chapter 5, more similar studies from other continents, such as South America, Europe, and China, are recommended to obtain a more accurate global growth curve of the continental crust and a better understanding of the correlation between the global growth curve and evolution of global plate tectonics through the time. Chapter 6 shows the central role of Antarctica in the Gondwana jigsaw. Although the Antarctica detrital data in the present research fill the gap of the eastern side of the Gondwana turbidite fan system, the detailed natures of the tectonic processes (e.g., East African Orogeny and Ross Orogeny) in Antarctica are still obscured by the lack of exposed rocks in the ice-covered interior. More available samples targeting the geological evolution of Antarctica during Gondwana assembly are required to facilitate this in future studies.

References

Aitken, A.R.A., Betts, P.G., Ailleres, L., 2009. The architecture, kinematics, and lithospheric processes of a compressional intraplate orogen occurring under Gondwana assembly: The Petermann orogeny, central Australia. Lithosphere 1, 343-357.
Albarède, F., 1998. The growth of continental crust. Tectonophysics 296, 1-14.
Allegre, C.J., Rousseau, D., 1984. The Growth of the Continent through Geological Time Studied by Nd Isotope Analysis of Shales. Earth and Planetary Science Letters 67, 19-34.
Allen, C.M., Campbell, I.H., 2012. Identification and elimination of a matrix-induced systematic error in LA–ICP–MS 206Pb/238U dating of zircon. Chemical Geology 332-333, 157-165.
Alonso-Perez, R., Müntener, O., Ulmer, P., 2009. Igneous garnet and amphibole fractionation in the roots of island arcs: experimental constraints on andesitic liquids. Contributions to Mineralogy and Petrology 157, 541-558.
Ameen, S.M.M., Wilde, S.A., 2018. Multiple sources for Archean granitoids in the Yalgoo area, Yilgarn Craton, Western Australia: Geochemical and isotopic evidence. Precambrian Res. 314, 76-110.
Armstrong, R., Wit, M.D., Reid, D., York, D., Zartman, R., 1998. Cape Town's Table Mountain reveals rapid Pan-African uplift of its basement rocks. Journal of African Earth Sciences 27, 10-10.
Armstrong, R.L., 1981. Radiogenic Isotopes - the Case for Crustal Recycling on a near-Steady-State No-Continental-Growth Earth. Philosophical Transactions of the Royal Society a-Mathematical Physical and Engineering Sciences 301, 443-472.
Arndt, N., Davaille, A., 2013. Episodic Earth evolution. Tectonophysics 609, 661-674.
Arndt, N.T., Nelson, D.R., Compston, W., Trendall, A.F., Thorne, A.M., 1991. The Age of the Fortescue Group, Hamersley Basin, Western-Australia, from Ion Microprobe Zircon U-Pb Results. Australian Journal of Earth Sciences 38, 261-281.
Artemieva, I.M., Thybo, H., 2020. Continent size revisited: Geophysical evidence for West Antarctica as a back-arc system. Earth-Science Reviews 202.
Avigad, D., Kolodner, K., McWilliams, M., Persing, H., Weissbrod, T., 2003. Origin of northern Gondwana Cambrian sandstone revealed by detrital zircon SHRIMP dating. Geology 31, 227-230.
Baertschi, P., 1976. Absolute18O content of standard mean ocean water. Earth and Planetary Science Letters 31, 341-344.
Bagas, L., 2004. Proterozoic evolution and tectonic setting of the northwest Paterson Orogen, Western Australia. Precambrian Res. 128, 475-496.
Bamber, J.L., Vaughan, D.G., Joughin, I., 2000. Widespread complex flow in the interior of the Antarctic ice sheet. Science 287, 1248-1250.
Barbey, P., Allé, P., Brouand, M., Albarède, F., 1995. Rare-earth patterns in zircons from the Manaslu granite and Tibetan Slab migmatites (Himalaya): insights in the origin and evolution of a crustally-derived granite magma. Chemical Geology 125, 1-17.
Belousova, E.A., Kostitsyn, Y.A., Griffin, W.L., Begg, G.C., O'Reilly, S.Y., Pearson, N.J., 2010. The growth of the continental crust: Constraints from zircon Hf-isotope data. Lithos 119, 457-466.
Bennett, V.C., Nutman, A.P., McCulloch, M.T., 1993. Nd isotopic evidence for transient, highly depleted mantle reservoirs in the early history of the Earth. Earth and Planetary Science Letters 119, 299-317.
Betts, P., Giles, D., 2006. The 1800–1100Ma tectonic evolution of Australia. Precambrian Res. 144, 92-125.
Betts, P.G., Giles, D., Lister, G.S., Frick, L.R., 2002. Evolution of the Australian lithosphere. Australian Journal of Earth Sciences 49, 661-695.

Betts, P.G., Giles, D., Schaefer, B.F., 2008. Comparing 1800-1600 Ma accretionary and basin processes in Australia and Laurentia: Possible geographic connections in Columbia. Precambrian Res. 166, 81-92.
Bickle, M., Bettenay, L., Barley, M., Chapman, H., Groves, D., Campbell, I., De Laeter, J., 1983. A 3500 Ma plutonic and volcanic calc-alkaline province in the Archaean East Pilbara Block. Contributions to Mineralogy and Petrology 84, 25-35.
Bickle, M., Bettenay, L., Chapman, H., Groves, D., McNaughton, N., Campbell, I., De Laeter, J., 1989. The age and origin of younger granitic plutons of the Shaw Batholith in the Archaean Pilbara Block, Western Australia. Contributions to Mineralogy and Petrology 101, 361-376.
Bindeman, I.N., Valley, J.W., 2001. Low-δ18O rhyolites from Yellowstone: Magmatic evolution based on analyses of zircons and individual phenocrysts. Journal of Petrology 42, 1491-1517.
Bindeman, I.N., Valley, J.W., 2003. Rapid generation of both high-and low-δ18O, large-volume silicic magmas at the Timber Mountain/Oasis Valley caldera complex, Nevada. GSA Bulletin 115, 581-595.
Black, L., James, P., 1983. Geological history of the Archaean Napier complex of Enderby Land, Antarctic earth science. International symposium. 4, pp. 11-15.
Blake, T.S., Buick, R., Brown, S.J.A., Barley, M.E., 2004. Geochronology of a Late Archaean flood basalt province in the Pilbara Craton, Australia: constraints on basin evolution, volcanic and sedimentary accumulation, and continental drift rates. Precambrian Res. 133, 143-173.
Blewett, R., 2012. Shaping a nation: A geology of Australia. Geoscience Australia and ANU E-Press.
Blichert-Toft, J., Chauvel, C., Albarède, F., 1997. Separation of Hf and Lu for high-precision isotope analysis of rock samples by magnetic sector-multiple collector ICP-MS. Contributions to Mineralogy and Petrology 127, 248-260.
Bobrovskiy, I., Hope, J.M., Ivantsov, A., Nettersheim, B.J., Hallmann, C., Brocks, J.J., 2018. Ancient steroids establish the Ediacaran fossil Dickinsonia as one of the earliest animals. Science 361, 1246-1249.
Bodet, F., Schärer, U., 2000. Evolution of the SE-Asian continent from U-Pb and Hf isotopes in single grains of zircon and baddeleyite from large rivers. Geochim. Cosmochim. Acta 64, 2067-2091.
Boger, S.D., Miller, J.M., 2004. Terminal suturing of Gondwana and the onset of the Ross–Delamerian Orogeny: the cause and effect of an Early Cambrian reconfiguration of plate motions. Earth and Planetary Science Letters 219, 35-48.
Bouvier, A., Vervoort, J.D., Patchett, P.J., 2008. The Lu-Hf and Sm-Nd isotopic composition of CHUR: Constraints from unequilibrated chondrites and implications for the bulk composition of terrestrial planets. Earth and Planetary Science Letters 273, 48-57.
Bouyo, M.H., Penaye, J., Barbey, P., Toteu, S., Wandji, P., 2013. Petrology of high-pressure granulite facies metapelites and metabasites from Tcholliré and Banyo regions: Geodynamic implication for the Central African Fold Belt (CAFB) of north-central Cameroon. Precambrian Res. 224, 412-433.
Bradley, D.C., 2011. Secular trends in the geologic record and the supercontinent cycle. Earth-Science Reviews 108, 16-33.
Breiter, K., 2016. Monazite and zircon as major carriers of Th, U, and Y in peraluminous granites: examples from the Bohemian Massif. Mineralogy and Petrology 110, 767-785.
Brown, C.R., Yakymchuk, C., Brown, M., Fanning, C.M., Korhonen, F.J., Piccoli, P.M., Siddoway, C.S., 2016. From Source to Sink: Petrogenesis of Cretaceous Anatectic Granites from the Fosdick Migmatite-Granite Complex, West Antarctica. Journal of Petrology 57, 1241-1278.

Brown, M., 2006. Duality of thermal regimes is the distinctive characteristic of plate tectonics since the Neoarchean. Geology 34, 961-964.
Brown, M., 2007. Metamorphic conditions in orogenic belts: a record of secular change. International Geology Review 49, 193-234.
Brown, M., Johnson, T., 2019. Time's arrow, time's cycle: Granulite metamorphism and geodynamics. Mineralogical Magazine 83, 323-338.
Buick, I.S., Storkey, A., Williams, I.S., 2008. Timing relationships between pegmatite emplacement, metamorphism and deformation during the intra-plate Alice Springs Orogeny, central Australia. Journal of Metamorphic Geology 26, 915-936.
Burnham, A.D., Berry, A.J., 2012. An experimental study of trace element partitioning between zircon and melt as a function of oxygen fugacity. Geochim. Cosmochim. Acta 95, 196-212.
Burnham, A.D., Berry, A.J., 2017. Formation of Hadean granites by melting of igneous crust. Nature Geoscience 10, 457-+.
Camacho, A., Fanning, C.M., 1995. Some Isotopic Constraints on the Evolution of the Granulite and Upper Amphibolite Facies Terranes in the Eastern Musgrave Block, Central Australia. Precambrian Res. 71, 155-181.
Campbell, I., Griffiths, R., 1993. The evolution of the mantle's chemical structure. Lithos 30, 389-399.
Campbell, I., Hill, R., 1988. A two-stage model for the formation of the granite-greenstone terrains of the Kalgoorlie-Norseman area, Western Australia. Earth and Planetary Science Letters 90, 11-25.
Campbell, I.H., 2003. Constraints on continental growth models from Nb/U ratios in the 3.5 Ga barberton and other Archaean basalt-komatiite suites. American Journal of Science 303, 319-351.
Campbell, I.H., Allen, C.M., 2008. Formation of supercontinents linked to increases in atmospheric oxygen. Nature Geoscience 1, 554-558.
Campbell, I.H., Davies, D.R., 2017. Raising the continental crust. Earth and Planetary Science Letters 460, 112-122.
Campbell, I.H., Reiners, P.W., Allen, C.M., Nicolescu, S., Upadhyay, R., 2005. He-Pb double dating of detrital zircons from the Ganges and Indus Rivers: Implication for quantifying sediment recycling and provenance studies. Earth and Planetary Science Letters 237, 402-432.
Campbell, I.H., Squire, R.J., 2010. The mountains that triggered the Late Neoproterozoic increase in oxygen: The Second Great Oxidation Event. Geochim. Cosmochim. Acta 74, 4187-4206.
Canfield, D.E., 2005. The early history of atmospheric oxygen: homage to Robert M. Garrels. Annu. Rev. Earth Planet. Sci. 33, 1-36.
Cao, W., Lee, C.-T.A., Lackey, J.S., 2017. Episodic nature of continental arc activity since 750 Ma: A global compilation. Earth and Planetary Science Letters 461, 85-95.
Carley, T.L., Miller, C.F., Sigmarsson, O., Coble, M.A., Fisher, C.M., Hanchar, J.M., Schmitt, A.K., Economos, R.C., 2017. Detrital zircon resolve longevity and evolution of silicic magmatism in extinct volcanic centers: A case study from the East Fjords of Iceland. Geosphere 13, 1640-1663.
Carson, C., Von Gnielinski, F.E., Bultitude, R.J., 2007. Results of the joint GSQ-GA geochronology project, New England Orogen, ROSEDALE, MOUNT PERRY and GLADSTONE 1: 100 000 Sheet Areas, March 2006-December 2006. Department of Mines and Energy.
Cas, R., Powell, C.M., Crook, K., 1980. Ordovician palaeogeography of the Lachlan Fold Belt: a modern analogue and tectonic constraints. Journal of the Geological Society of Australia 27, 19-31.

Cassidy, K., Champion, D., Krapez, B., Barley, M., Brown, S., Blewett, R., Groenewald, P., Tyler, I., 2006. A revised geological framework for the Yilgarn Craton, Western Australia. Geological Survey of Western Australia, Record 8.
Cassidy, K.F., Champion, D.C., McNaughton, N., Fletcher, I., Whitaker, A.J., Bastrakova, I.V., Budd, A.R., 2002. Characterisation and Metallogenic Significance of Archaean Granitoids of the Yilgarn Craton, Western Australia: Results of Research Carried Out as MERlWA Project No. M281 at the Key Centre for Strategic Mineral Deposits, the University of Western Australia and Australian Geological Survey Organisation. Minerals and Energy Research Institute of Western Australia.
Castillo, P., Fanning, C.M., Fernandez, R., Poblete, F., Hervé, F., 2017. Provenance and age constraints of Paleozoic siliciclastic rocks from the Ellsworth Mountains in West Antarctica, as determined by detrital zircon geochronology. GSA Bulletin 129, 1568-1584.
Castillo, P., Fanning, C.M., Herve, F., Lacassie, J.P., 2016. Characterisation and tracing of Permian magmatism in the south-western segment of the Gondwanan margin; U-Pb age, Lu-Hf and O isotopic compositions of detrital zircons from metasedimentary complexes of northern Antarctic Peninsula and western Patagonia. Gondwana Research 36, 1-13.
Cawood, P., Leitch, E., Merle, R.E., Nemchin, A., 2011. Orogenesis without collision: Stabilizing the Terra Australis accretionary orogen, eastern Australia. Bulletin 123, 2240-2255.
Cawood, P.A., 2005. Terra Australis Orogen: Rodinia breakup and development of the Pacific and Iapetus margins of Gondwana during the Neoproterozoic and Paleozoic. Earth-Science Reviews 69, 249-279.
Cawood, P.A., Buchan, C., 2007. Linking accretionary orogenesis with supercontinent assembly. Earth-Science Reviews 82, 217-256.
Cawood, P.A., Hawkesworth, C.J., Dhuime, B., 2013. The continental record and the generation of continental crust. Geological Society of America Bulletin 125, 14-32.
Cawood, P.A., Kröner, A., Collins, W.J., Kusky, T.M., Mooney, W.D., Windley, B.F., 2009. Accretionary orogens through Earth history. Geological Society, London, Special Publications 318, 1-36.
Cawood, P.A., Nemchin, A.A., Freeman, M., Sircombe, K., 2003. Linking source and sedimentary basin: Detrital zircon record of sediment flux along a modern river system and implications for provenance studies. Earth and Planetary Science Letters 210, 259-268.
Cawood, P.A., Tyler, I.M., 2004. Assembling and reactivating the Proterozoic Capricorn Orogen: lithotectonic elements, orogenies, and significance. Precambrian Res. 128, 201-218.
Champion, D., Bultitude, R., Jell, P., 2013. Kennedy igneous association. Geology of Queensland, 473-514.
Champion, D., Kositcin, N., Huston, D., Mathews, E., Brown, C., 2009. Geodynamic synthesis of the Phanerozoic of eastern Australia and implications for metallogeny. Geoscience Australia Record 18, 255.
Champion, D.C., 2013. Neodymium depleted mantle model age map of Australia: explanatory notes and user guide. Geoscience Australia.
Champion, D.C., Brown, C., Mathews, E., Huston, D.L., Kositcin, N., 2016. Geodynamic synthesis of the Phanerozoic of eastern Australia. Geoscience Australia.
Champion, D.C., Chappell, B.W., 1992. Petrogenesis of Felsic I-Type Granites - an Example from Northern Queensland. Transactions of the Royal Society of Edinburgh-Earth Sciences 83, 115-126.
Chappell, B., White, A., 1992. I-and S-type granites in the Lachlan Fold Belt. Earth and Environmental Science Transactions of the Royal Society of Edinburgh 83, 1-26.

Chauvel, C., Lewin, E., Carpentier, M., Arndt, N.T., Marini, J.C., 2008. Role of recycled oceanic basalt and sediment in generating the Hf-Nd mantle array. Nature Geoscience 1, 64-67.
Chen, B., Long, X.P., Yuan, C., Wang, Y.J., Sun, M., Xiao, W.J., Cai, K., Huang, Z.Y., 2015. Geochronology and geochemistry of Late Ordovician-Early Devonian gneissic granites in the Kumishi area, northern margin of the South Tianshan Belt: Constraints on subduction process of the South Tianshan Ocean. J. Asian Earth Sci. 113, 293-309.
Cheney, E., 1996. Sequence stratigraphy and plate tectonic significance of the Transvaal succession of southern Africa and its equivalent in Western Australia. Precambrian Res. 79, 3-24.
Cherniak, D.J., Watson, E.B., 2003. Diffusion in zircon. Rev Mineral Geochem 53, 113-143.
Chu, N.C., Taylor, R.N., Chavagnac, V., Nesbitt, R.W., Boella, R.M., Milton, J.A., German, C.R., Bayon, G., Burton, K., 2002. Hf isotope ratio analysis using multi-collector inductively coupled plasma mass spectrometry: an evaluation of isobaric interference corrections. Journal of Analytical Atomic Spectrometry 17, 1567-1574.
Clarke, G., Sun, S., White, R., 1995. Grenville-age belts and associated older terranes in Australia and Antarctica. AGSO Journal of Australian Geology and Geophysics 16, 25-40.
Cogné, J.-P., Humler, E., 2008. Global scale patterns of continental fragmentation: Wilson's cycles as a constraint for long-term sea-level changes. Earth and Planetary Science Letters 273, 251-259.
Collins, A.S., Blades, M.L., Merdith, A.S., Foden, J.D., 2021. Closure of the Proterozoic Mozambique Ocean was instigated by a late Tonian plate reorganization event. Communications Earth & Environment 2, 75.
Collins, A.S., Pisarevsky, S.A., 2005. Amalgamating eastern Gondwana: the evolution of the Circum-Indian Orogens. Earth-Science Reviews 71, 229-270.
Collins, W., Richards, S., 2008. Geodynamic significance of S-type granites in circum-Pacific orogens. Geology 36, 559-562.
Compston, W., Williams, I., Meyer, C., 1984. U‐Pb geochronology of zircons from lunar breccia 73217 using a sensitive high mass‐resolution ion microprobe. Journal of Geophysical Research: Solid Earth 89, B525-B534.
Condie, K., 2013. Preservation and recycling of crust during accretionary and collisional phases of Proterozoic orogens: A bumpy road from Nuna to Rodinia. Geosciences 3, 240-261.
Condie, K.C., 1998. Episodic continental growth and supercontinents: a mantle avalanche connection? Earth and Planetary Science Letters 163, 97-108.
Condie, K.C., Arndt, N., Davaille, A., Puetz, S.J., 2017. Zircon age peaks: Production or preservation of continental crust? Geosphere 13, 227-234.
Condie, K.C., Aster, R.C., 2010. Episodic zircon age spectra of orogenic granitoids: The supercontinent connection and continental growth. Precambrian Res. 180, 227-236.
Condie, K.C., Belousova, E., Griffin, W.L., Sircombe, K.N., 2009. Granitoid events in space and time: Constraints from igneous and detrital zircon age spectra. Gondwana Research 15, 228-242.
Cook, S.J., Swift, D.A., Kirkbride, M.P., Knight, P.G., Waller, R.I., 2020. The empirical basis for modelling glacial erosion rates. Nature Communications 11, 759.
Cooper, M., Caritat, P.d., Burton, G.d., Fidler, R., Green, G., House, E., Strickland, C., Tang, J., Wygralak, A., 2010. National Geochemical Survey of Australia: Field Data. Geoscience Australia Record 18, 93.
Cowley, W., Conor, C., Zang, W., 2003. New and revised Proterozoic stratigraphic units on northern Yorke Peninsula. MESA Journal 29, 46-58.

Cross, A., Claoué-Long, J., Scrimgeour, I., Ahmad, M., Kruse, P., 2005. Summary of results. Joint NTGS-GA geochronology project: Rum Jungle, basement to southern Georgina Basin and eastern Arunta Region 2001–2003. Northern Territory Geological Survey Record 2005–2006.
Cumming, G.L., Richards, J.R., 1975. Ore Lead Isotope Ratios in a Continuously Changing Earth. Earth and Planetary Science Letters 28, 155-171.
Curray, J.R., Emmel, F.J., Moore, D.G., 2002. The Bengal Fan: morphology, geometry, stratigraphy, history and processes. Marine and Petroleum Geology 19, 1191-1223.
Daly, S., Fanning, C., 1993. Archaean. The Geology of South Australia 1, 32-49.
Dalziel, I.W., 2013. Antarctica and supercontinental evolution: clues and puzzles. Earth and Environmental Science Transactions of the Royal Society of Edinburgh 104, 3-16.
Davey, F.J., Granot, R., Cande, S.C., Stock, J.M., Selvans, M., Ferraccioli, F., 2016. Synchronous oceanic spreading and continental rifting in West Antarctica. Geophysical Research Letters 43, 6162-6169.
De Caritat, P., Cooper, M., 2011. National Geochemical Survey of Australia: The Geochemical Atlas of Australia. Geoscience Australia Record 2011/20 (2 Volumes), 557 pp.
De Caritat, P., Cooper, M., 2016. A continental-scale geochemical atlas for resource exploration and environmental management: the National Geochemical Survey of Australia. Geochemistry: Exploration, Environment, Analysis 16, 3-13.
DeCelles, P., Gehrels, G., Quade, J., LaReau, B., Spurlin, M., 2000. Tectonic implications of U-Pb zircon ages of the Himalayan orogenic belt in Nepal. Science 288, 497-499.
Delattre, S., Utsunomiya, S., Ewing, R.C., Boeglin, J.-L., Braun, J.-J., Balan, E., Calas, G., 2007. Dissolution of radiation-damaged zircon in lateritic soils. American Mineralogist 92, 1978-1989.
Dhuime, B., Hawkesworth, C., Cawood, P., 2011. Geochemistry. When continents formed. Science 331, 154-155.
Dhuime, B., Hawkesworth, C.J., Cawood, P.A., Storey, C.D., 2012. A change in the geodynamics of continental growth 3 billion years ago. Science 335, 1334-1336.
Dhuime, B., Hawkesworth, C.J., Delavault, H., Cawood, P.A., 2018. Rates of generation and destruction of the continental crust: implications for continental growth. Philos Trans A Math Phys Eng Sci 376, 20170403.
Dietz, R.S., Holden, J.C., 1970. Reconstruction of Pangaea, Breakup and Dispersion of Continents--Permian to Present. Transactions-American Geophysical Union 51, 429-&.
Durgalakshmi, D., Sajeev, K., Williams, I.S., Reddy, D.H., Satish-Kumar, M., Jöns, N., Malaviarachchi, S.P., Samuel, V.O., George, P., 2021. The timing, duration and conditions of UHT metamorphism in remnants of the former eastern Gondwana. Journal of Petrology.
Eagles, G., Livermore, R., Morris, P., 2006. Small basins in the Scotia Sea: The Eocene Drake Passage gateway. Earth and Planetary Science Letters 242, 343-353.
Elliot, D.H., Fanning, C.M., Hulett, S.R.W., 2015. Age provinces in the Antarctic craton: Evidence from detrital zircons in Permian strata from the Beardmore Glacier region, Antarctica. Gondwana Research 28, 152-164.
Emmel, B., Jöns, N., Kröner, A., Jacobs, J., Wartho, J.A., Schenk, V., Razakamanana, T., Austegard, A., 2008. From Closure of the Mozambique Ocean to Gondwana Breakup: New Evidence from Geochronological Data of the Vohibory Terrane, Southwest Madagascar. The Journal of Geology 116, 21-38.
Fanning, C.M., Reid, A., Teale, G., 2007. A geochronological framework for the Gawler Craton, South Australia. Mineral Resources Group, Division of Minerals and Energy Resources, Primary ….
Fergusson, C.L., Coney, P.J., 1992. Implications of a Bengal Fan Type Deposit in the Paleozoic Lachlan Fold Belt of Southeastern Australia. Geology 20, 1047-1049.

Fisher, C.M., Vervoort, J.D., DuFrane, S.A., 2014a. Accurate Hf isotope determinations of complex zircons using the “laser ablation split stream” method. Geochemistry, Geophysics, Geosystems 15, 121-139.
Fisher, C.M., Vervoort, J.D., Hanchar, J.M., 2014b. Guidelines for reporting zircon Hf isotopic data by LA-MC-ICPMS and potential pitfalls in the interpretation of these data. Chemical Geology 363, 125-133.
Fitzsimons, I., 2000a. A review of tectonic events in the East Antarctic Shield and their implications for Gondwana and earlier supercontinents. Journal of African Earth Sciences 31, 3-23.
Fitzsimons, I., 2003. Proterozoic basement provinces of southern and southwestern Australia, and their correlation with Antarctica. Geological Society, London, Special Publications 206, 93-130.
Fitzsimons, I.C.W., 2000b. A review of tectonic events in the East Antarctic Shield and their implications for Gondwana and earlier supercontinents. Journal of African Earth Sciences 31, 3-23.
Flood, R., Shaw, S., 1977. Two “S-type” granite suites with low initial 87 Sr/86 Sr ratios from the New England Batholith, Australia. Contributions to Mineralogy and Petrology 61, 163-173.
Foden, J., Elburg, M.A., Dougherty-Page, J., Burtt, A., 2006. The timing and duration of the Delamerian orogeny: Correlation with the Ross Orogen and implications for Gondwana assembly. Journal of Geology 114, 189-210.
Foden, J., Elburg, M.A., Turner, S., Sandiford, M., O'Callaghan, J., Mitchell, S., 2002. Granite production in the Delamerian orogen, South Australia. Journal of the Geological Society 159, 557-575.
Foley, E.K., Henderson, R., Roberts, E., Kemp, A., Todd, C., Knutsen, E., Fisher, C., Wainman, C., Spandler, C., 2021. Jurassic Arc: Reconstructing the Lost World of eastern Gondwana. Geology 49, 1391-1396.
Foster, D.A., Gray, D.R., 2000. Evolution and structure of the Lachlan Fold Belt (Orogen) of eastern Australia. Annual Review of Earth and Planetary Sciences 28, 47-80.
Fretzdorff, S., Worthington, T.J., Haase, K.M., Hekinian, R., Franz, L., Keller, R.A., Stoffers, P., 2004. Magmatism in the Bransfield basin: rifting of the South Shetland Arc? Journal of Geophysical Research: Solid Earth 109.
Fritz, H., Abdelsalam, M., Ali, K., Bingen, B., Collins, A., Fowler, A., Ghebreab, W., Hauzenberger, C., Johnson, P., Kusky, T., 2013. Orogen styles in the East African Orogen: a review of the Neoproterozoic to Cambrian tectonic evolution. Journal of African Earth Sciences 86, 65-106.
Ganade de Araujo, C.E., Rubatto, D., Hermann, J., Cordani, U.G., Caby, R., Basei, M.A.S., 2014. Ediacaran 2,500-km-long synchronous deep continental subduction in the West Gondwana Orogen. Nature Communications 5, 5198.
Gauthiez-Putallaz, L., Rubatto, D., Hermann, J., 2016. Dating prograde fluid pulses during subduction by in situ U–Pb and oxygen isotope analysis. Contributions to Mineralogy and Petrology 171, 15.
Gibson, G.M., Nutman, A.P., 2004. Detachment faulting and bimodal magmatism in the Palaeoproterozoic Willyama Supergroup, south-central Australia: keys to recognition of a multiply deformed Precambrian metamorphic core complex. Journal of the Geological Society 161, 55-66.
Gilotti, J.A., Nutman, A.P., Brueckner, H.K., 2004. Devonian to Carboniferous collision in the Greenland Caledonides: U-Pb zircon and Sm-Nd ages of high-pressure and ultrahigh-pressure metamorphism. Contributions to Mineralogy and Petrology 148, 216-235.
Glen, R., 2005. The Tasmanides of eastern Australia. Special Publication-Geological Society of London 246, 23.

Glen, R., 2013. Refining accretionary orogen models for the Tasmanides of eastern Australia. Australian Journal of Earth Sciences 60, 315-370.
Glen, R.A., Fitzsimons, I.C.W., Griffin, W.L., Saeed, A., 2017. East Antarctic sources of extensive Lower–Middle Ordovician turbidites in the Lachlan Orogen, southern Tasmanides, eastern Australia. Australian Journal of Earth Sciences 64, 143-224.
Goleby, B.R., Huston, D.L., Lyons, P., Vandenberg, L., Bagas, L., Davies, B.M., Jones, L.E.A., Gebre-Mariam, M., Johnson, W., Smith, T., English, L., 2009. The Tanami deep seismic reflection experiment: An insight into gold mineralization and Paleoproterozoic collision in the North Australian Craton. Tectonophysics 472, 169-182.
Goodenough, K., Lusty, P., Roberts, N., Key, R., Garba, A., 2014. Post-collisional Pan-African granitoids and rare metal pegmatites in western Nigeria: age, petrogenesis, and the 'pegmatite conundrum'. Lithos 200, 22-34.
Goodge, J.W., Fanning, C.M., Norman, M.D., Bennett, V.C., 2012. Temporal, Isotopic and Spatial Relations of Early Paleozoic Gondwana-Margin Arc Magmatism, Central Transantarctic Mountains, Antarctica. Journal of Petrology 53, 2027-2065.
Goodge, J.W., Williams, I.S., Myrow, P., 2004. Provenance of Neoproterozoic and lower Paleozoic siliciclastic rocks of the central Ross orogen, Antarctica: Detrital record of rift-, passive-, and active-margin sedimentation. Geological Society of America Bulletin 116, 1253-1279.
Goodwin, A.M., 1996. Principles of Precambrian geology. Elsevier.
Gray, D., Foster, D., 2004. Tectonic evolution of the Lachlan Orogen, southeast Australia: historical review, data synthesis and modern perspectives. Australian Journal of Earth Sciences 51, 773-817.
Gray, D.R., Foster, D.A., Meert, J.G., Goscombe, B.D., Armstrong, R., Trouw, R.A.J., Passchier, C.W., 2008. A Damara orogen perspective on the assembly of southwestern Gondwana. Geological Society, London, Special Publications 294, 257-278.
Green, T., 1982. Anatexis of mafic crust and high pressure crystallization of andesite. American Society of Mechanical Engineers (Paper), 465-487.
Griffin, W.L., Pearson, N.J., Belousova, E., Jackson, S.E., van Achterbergh, E., O'Reilly, S.Y., Shee, S.R., 2000. The Hf isotope composition of cratonic mantle: LAM-MC-ICPMS analysis of zircon megacrysts in kimberlites. Geochim. Cosmochim. Acta 64, 133-147.
Griffin, W.L., Wang, X., Jackson, S.E., Pearson, N.J., O'Reilly, S.Y., Xu, X.S., Zhou, X.M., 2002. Zircon chemistry and magma mixing, SE China: In-situ analysis of Hf isotopes, Tonglu and Pingtan igneous complexes. Lithos 61, 237-269.
Guitreau, M., Boyet, M., Paquette, L., Gannoun, A., Konc, Z., Benbakkar, M., Suchorski, K., Henot, J.M., 2019. Hadean protocrust reworking at the origin of the Archean Napier Complex (Antarctica). Geochemical Perspectives Letters 12, 7-11.
Hand, M., Reid, A., Jagodzinski, L., 2007. Tectonic Framework and Evolution of the Gawler Craton, Southern Australia. Economic Geology 102, 1377-1395.
Hansberry, R., 2011. Tectonic evolution of the Arkaroola Basin: implications for the development of the Adelaide Rift Complex.
Hao, H., Campbell, I.H., Park, J.-W., 2022. Nd-Hf isotopic systematics of the arc mantle and their implication for continental crust growth. Chemical Geology 602, 120897.
Hao, H.D., Campbell, I.H., Richards, J.P., Nakamura, E., Sakaguchi, C., 2019. Platinum-Group Element Geochemistry of the Escondida Igneous Suites, Northern Chile: Implications for Ore Formation. Journal of Petrology 60, 487-514.
Harley, S.L., Black, L.P., 1997. A revised Archaean chronology for the Napier Complex, Enderby Land, from SHRIMP ion-microprobe studies. Antarctic Science 9, 74-91.
Harley, S.L., Kelly, N.M., 2007. Chapter 3.2 Ancient Antarctica: The Archaean of the East Antarctic Shield, Earth's Oldest Rocks, pp. 149-186.

Hathway, B., Lomas, S.A., 1998. The Upper Jurassic Lower Cretaceous Byers Group, South Shetland Islands, Antarctica: revised stratigraphy and regional correlations. Cretaceous Research 19, 43-67.
Hawkesworth, C., Cawood, P., Dhuime, B., 2013. Continental growth and the crustal record. Tectonophysics 609, 651-660.
Hawkesworth, C., Cawood, P.A., Dhuime, B., 2019. Rates of generation and growth of the continental crust. Geoscience Frontiers 10, 165-173.
Hawkesworth, C.J., Dhuime, B., Pietranik, A.B., Cawood, P.A., Kemp, A.I.S., Storey, C.D., 2010. The generation and evolution of the continental crust. Journal of the Geological Society 167, 229-248.
Hawkesworth, C.J., Kemp, A.I.S., 2006a. Evolution of the continental crust. Nature 443, 811-817.
Hawkesworth, C.J., Kemp, A.I.S., 2006b. Using hafnium and oxygen isotopes in zircons to unravel the record of crustal evolution. Chemical Geology 226, 144-162.
Hiess, J., Bennett, V.C., 2016. Chondritic Lu/Hf in the early crust-mantle system as recorded by zircon populations from the oldest Eoarchean rocks of Yilgarn Craton, West Australia and Enderby Land, Antarctica. Chemical Geology 427, 125-143.
Hill, R., Campbell, I., Compston, W., 1989. Age and origin of granitic rocks in the Kalgoorlie-Norseman region of Western Australia: implications for the origin of Archaean crust. Geochim. Cosmochim. Acta 53, 1259-1275.
Hoatson, D., Jaireth, S., Whitaker, A., Champion, D., Claoué-Long, J., 2009. Guide to using the Australian Archean mafic-ultramafic magmatic events map. Geoscience Australia Record 41, 131.
Hocking, R., Preston, W., 1998. Western Australia: Phanerozoic geology and mineral resources. AGSO Journal of Australian Geology and Geophysics 17, 245-260.
Hoffman, P., 1997. Tectonic genealogy of North America. Earth structure: An introduction to structural geology and tectonics., 459-464.
Hoffman, P.F., Kaufman, A.J., Halverson, G.P., Schrag, D.P., 1998. A neoproterozoic snowball earth. Science 281, 1342-1346.
Holland, H.D., 2002. Volcanic gases, black smokers, and the Great Oxidation Event. Geochim. Cosmochim. Acta 66, 3811-3826.
Hollis, J.A., Carson, C.J., Glass, L.M., 2009. SHRIMP U–Pb zircon geochronological evidence for Neoarchean basement in western Arnhem Land, northern Australia. Precambrian Res. 174, 364-380.
Hollis, J.A., Wygralak, A.S., 2012. A review of the geology and uranium, gold and iron ore deposits of the Pine Creek Orogen. Episodes 35, 264-272.
Hoskin, P., Black, L., 2000. Metamorphic zircon formation by solid ‐ state recrystallization of protolith igneous zircon. Journal of metamorphic Geology 18, 423-439.
Hoskin, P.W., Ireland, T.R., 2000. Rare earth element chemistry of zircon and its use as a provenance indicator. Geology 28, 627-630.
Hoskin, P.W.O., Schaltegger, U., 2003. The composition of zircon and igneous and metamorphic petrogenesis. Rev Mineral Geochem 53, 27-62.
Howard, K.E., Hand, M., Barovich, K.M., Payne, J.L., Belousova, E.A., 2011. U–Pb, Lu–Hf and Sm–Nd isotopic constraints on provenance and depositional timing of metasedimentary rocks in the western Gawler Craton: Implications for Proterozoic reconstruction models. Precambrian Res. 184, 43-62.
Hurley, P.M., Rand, J.R., 1969. Pre-drift continental nuclei. Science 164, 1229-1242.
Huston, D.L., Blewett, R.S., Champion, D.C., 2012. Australia through time: a summary of its tectonic and metallogenic evolution. Episodes 35, 23-43.
Ickert, R.B., Hiess, J., Williams, I.S., Holden, P., Ireland, T.R., Lanc, P., Schram, N., Foster, J.J., Clement, S.W., 2008. Determining high precision, in situ, oxygen isotope

ratios with a SHRIMP II: Analyses of MPI-DING silicate-glass reference materials and zircon from contrasting granites. Chemical Geology 257, 114-128.
Iizuka, T., Campbell, I.H., Allen, C.M., Gill, J.B., Maruyama, S., Makoka, F., 2013. Evolution of the African continental crust as recorded by U-Pb, Lu-Hf and O isotopes in detrital zircons from modern rivers. Geochim. Cosmochim. Acta 107, 96-120.
Iizuka, T., Hirata, T., 2005. Improvements of precision and accuracy in in situ Hf isotope microanalysis of zircon using the laser ablation-MC-ICPMS technique. Chemical Geology 220, 121-137.
Iizuka, T., Hirata, T., Komiya, T., Rino, S., Katayama, I., Motoki, A., Maruyama, S., 2005. U-Pb and Lu-Hf isotope systematics of zircons from the Mississippi River sand: Implications for reworking and growth of continental crust. Geology 33, 485-488.
Iizuka, T., Komiya, T., Rino, S., Maruyama, S., Hirata, T., 2010. Detrital zircon evidence for Hf isotopic evolution of granitoid crust and continental growth. Geochim. Cosmochim. Acta 74, 2450-2472.
Iizuka, T., Yamaguchi, T., Itano, K., Hibiya, Y., Suzuki, K., 2017. What Hf isotopes in zircon tell us about crust-mantle evolution. Lithos 274, 304-327.
Ireland, T.R., 1992. Crustal evolution of New Zealand: evidence from age distributions of detrital zircons in Western Province paragneisses and Torlesse greywacke. Geochim. Cosmochim. Acta 56, 911-920.
Ireland, T.R., Gibson, G., 1998. SHRIMP monazite and zircon geochronology of high‐grade metamorphism in New Zealand. Journal of metamorphic geology 16, 149-167.
Itano, K., Iizuka, T., Chang, Q., Kimura, J.-I., Maruyama, S., 2016. U–Pb chronology and geochemistry of detrital monazites from major African rivers: constraints on the timing and nature of the Pan-African Orogeny. Precambrian Res. 282, 139-156.
Jacobs, J., Fanning, C.M., Henjes-Kunst, F., Olesch, M., Paech, H.-J., 1998. Continuation of the Mozambique Belt into East Antarctica: Grenville-age metamorphism and polyphase Pan-African high-grade events in central Dronning Maud Land. The Journal of Geology 106, 385-406.
Jacobs, J., Thomas, R.J., 2004. Himalayan-type indenter-escape tectonics model for the southern part of the late Neoproterozoic–early Paleozoic East African–Antarctic orogen. Geology 32, 721-724.
Jacobsen, S.B., Dymek, R.F., 1988. Nd and Sr isotope systematics of clastic metasediments from Isua, West Greenland: Identification of pre‐3.8 Ga Differentiated Crustal Components. Journal of Geophysical Research: Solid Earth 93, 338-354.
Jeon, H., Williams, I.S., 2018. Trace inheritance—Clarifying the zircon O-Hf isotopic fingerprint of I-type granite sources: Implications for the restite model. Chemical Geology 476, 456-468.
Jessop, K., Daczko, N., Piazolo, S., 2020. Metamorphism in the New England Orogen, eastern Australia: a review. Australian Journal of Earth Sciences 67, 453-478.
Johnson, P.R., 2014. An expanding Arabian-Nubian Shield geochronologic and isotopic dataset: defining limits and confirming the tectonic setting of a Neoproterozoic accretionary orogen. The Open Geology Journal 8.
Johnson, R.W., Johnson, R.W., Knutson, J., Taylor, S.R., 1989. Intraplate volcanism: in eastern Australia and New Zealand. Cambridge University Press.
Johnson, T.E., Brown, M., Gardiner, N.J., Kirkland, C.L., Smithies, R.H., 2017. Earth's first stable continents did not form by subduction. Nature 543, 239-242.
Jongens, R., Bradshaw, J.D., Fowler, A.P., 2003. The Balloon Melange, northwest Nelson: origin, structure, and emplacement. New Zealand Journal of Geology and Geophysics 46, 437-448.
Jordan, T.A., Ferraccioli, F., Leat, P.T., 2017. New geophysical compilations link crustal block motion to Jurassic extension and strike-slip faulting in the Weddell Sea Rift System of West Antarctica. Gondwana Research 42, 29-48.

Jordan, T.A., Riley, T.R., Siddoway, C.S., 2020. The geological history and evolution of West Antarctica. Nature Reviews Earth & Environment 1, 117-133.
Kemp, A.I., Hawkesworth, C.J., Paterson, B.A., Kinny, P.D., 2006. Episodic growth of the Gondwana supercontinent from hafnium and oxygen isotopes in zircon. Nature 439, 580-583.
Kemp, A.I.S., Wilde, S.A., Hawkesworth, C.J., Coath, C.D., Nemchin, A., Pidgeon, R.T., Vervoort, J.D., DuFrane, S.A., 2010. Hadean crustal evolution revisited: New constraints from Pb-Hf isotope systematics of the Jack Hills zircons. Earth and Planetary Science Letters 296, 45-56.
Kinny, P., Williams, I., Froude, D., Ireland, T., Compston, W., 1988. Early Archaean zircon ages from orthogneisses and anorthosites at Mount Narryer, Western Australia. Precambrian Res. 38, 325-341.
Kirkland, C.L., Spaggiari, C.V., Pawley, M., Wingate, M., Smithies, R.H., Howard, H., Tyler, I., Belousova, E.A., Poujol, M., 2011. On the edge: U–Pb, Lu–Hf, and Sm–Nd data suggests reworking of the Yilgarn craton margin during formation of the Albany-Fraser Orogen. Precambrian Res. 187, 223-247.
Korsch, R.J., Huston, D.L., Henderson, R.A., Blewett, R.S., Withnall, I.W., Fergusson, C.L., Collins, W.J., Saygin, E., Kositcin, N., Meixner, A.J., Chopping, R., Henson, P.A., Champion, D.C., Hutton, L.J., Wormald, R., Holzschuh, J., Costelloe, R.D., 2012. Crustal architecture and geodynamics of North Queensland, Australia: Insights from deep seismic reflection profiling. Tectonophysics 572-573, 76-99.
Kowalewski, M., Rimstidt, J.D., 2003. Average lifetime and age spectra of detrital grains: toward a unifying theory of sedimentary particles. The Journal of geology 111, 427-439.
Król, P., Kusiak, M.A., Dunkley, D.J., Wilde, S.A., Yi, K., Lee, S., Kocjan, I., 2020. Diversity of Archean crust in the eastern Tula Mountains, Napier Complex, East Antarctica. Gondwana Research 82, 151-170.
Kump, L.R., 2008. The rise of atmospheric oxygen. Nature 451, 277-278.
Kusiak, M.A., Dunkley, D.J., Wirth, R., Whitehouse, M.J., Wilde, S.A., Marquardt, K., 2015. Metallic lead nanospheres discovered in ancient zircons. Proceedings of the National Academy of Sciences 112, 4958-4963.
Kusiak, M.A., Whitehouse, M.J., Wilde, S.A., Dunkley, D.J., Menneken, M., Nemchin, A.A., Clark, C., 2013. Changes in Zircon Chemistry during Archean Uht Metamorphism in the Napier Complex, Antarctica. American Journal of Science 313, 933-966.
Lancaster, P.J., Storey, C.D., Hawkesworth, C.J., Dhuime, B., 2011. Understanding the roles of crustal growth and preservation in the detrital zircon record. Earth and Planetary Science Letters 305, 405-412.
Lee, C.-T.A., Yeung, L.Y., McKenzie, N.R., Yokoyama, Y., Ozaki, K., Lenardic, A., 2016. Two-step rise of atmospheric oxygen linked to the growth of continents. Nature Geoscience 9, 417-424.
Lee†, J.K.W., Williams, I.S., Ellis, D.J., 1997. Pb, U and Th diffusion in natural zircon. Nature 390, 159-162.
LeMasurier, W., 2013. Shield volcanoes of Marie Byrd Land, West Antarctic rift: oceanic island similarities, continental signature, and tectonic controls. Bulletin of Volcanology 75, 726.
Li, Z.-X., Bogdanova, S., Collins, A., Davidson, A., De Waele, B., Ernst, R., Fitzsimons, I., Fuck, R., Gladkochub, D., Jacobs, J., 2008. Assembly, configuration, and break-up history of Rodinia: a synthesis. Precambrian Res. 160, 179-210.
Liu, F., Gerdes, A., Liu, P., 2012. U–Pb, trace element and Lu–Hf properties of unique dissolution–reprecipitation zircon from UHP eclogite in SW Sulu terrane, eastern China. Gondwana Research 22, 169-183.
Livermore, R., Nankivell, A., Eagles, G., Morris, P., 2005. Paleogene opening of Drake Passage. Earth and Planetary Science Letters 236, 459-470.

London, D., 1992. Phosphorus in S-type magmas: the P2O5 content of feldspars from peraluminous granites, pegmatites, and rhyolites. American Mineralogist 77, 126-145.
Madey, T.E., 1986. Electron-and photon-stimulated desorption: probes of structure and bonding at surfaces. Science 234, 316-322.
Maher, K., Chamberlain, C., 2014. Hydrologic regulation of chemical weathering and the geologic carbon cycle. science 343, 1502-1504.
Maidment, D.W., Hand, M., Williams, I.S., 2013. High grade metamorphism of sedimentary rocks during Palaeozoic rift basin formation in central Australia. Gondwana Research 24, 865-885.
Maidment, D.W., Williams, I.S., Hand, M., 2007. Testing long-term patterns of basin sedimentation by detrital zircon geochronology, Centralian Superbasin, Australia. Basin Research 19, 335-360.
McArthur, J., Howarth, R., Shields, G., 2012. Strontium isotope stratigraphy. The geologic time scale 1, 127-144.
McCulloch, M., 1987. Sm‐Nd isotopic constraints on the evolution of Precambrian crust in the Australian continent. Proterozic Lithospheric Evolution 17, 115-130.
McCulloch, M.T., Wasserburg, G.J., 1978. Sm-nd and rb-sr chronology of continental crust formation. Science 200, 1003-1011.
McNair, A., 1961. The Half-Life of long-lived lutetium-176. The Philosophical Magazine: A Journal of Theoretical Experimental and Applied Physics 6, 851-856.
Meert, J.G., 2003. A synopsis of events related to the assembly of eastern Gondwana. Tectonophysics 362, 1-40.
Meert, J.G., Lieberman, B.S., 2008. The Neoproterozoic assembly of Gondwana and its relationship to the Ediacaran-Cambrian radiation. Gondwana Research 14, 5-21.
Meert, J.G., Pandit, M.K., Pivarunas, A., Katusin, K., Sinha, A.K., 2017. India and Antarctica in the Precambrian: a brief analysis. Geological Society, London, Special Publications 457, 339-351.
Mitchell, R.N., Zhang, N., Salminen, J., Liu, Y., Spencer, C.J., Steinberger, B., Murphy, J.B., Li, Z.-X., 2021. The supercontinent cycle. Nature Reviews Earth & Environment 2, 358-374.
Moecher, D.P., Samson, S.D., 2006. Differential zircon fertility of source terranes and natural bias in the detrital zircon record: Implications for sedimentary provenance analysis. Earth and Planetary Science Letters 247, 252-266.
Montgomery, D.R., Brandon, M.T., 2002. Topographic controls on erosion rates in tectonically active mountain ranges. Earth and Planetary Science Letters 201, 481-489.
Mortimer, N., van den Bogaard, P., Hoernle, K., Timm, C., Gans, P.B., Werner, R., Riefstahl, F., 2019. Late Cretaceous oceanic plate reorganization and the breakup of Zealandia and Gondwana. Gondwana Research 65, 31-42.
Mory, A.J., Redfern, J., Martin, J.R., 2008. A review of Permian–Carboniferous glacial deposits in Western Australia. Geological Society of America Special Papers 441, 29-40.
Moyen, J.-F., Stevens, G., Kisters, A.F.M., Belcher, R.W., 2007. Chapter 5.6 TTG Plutons of the Barberton Granitoid-Greenstone Terrain, South Africa, Earth's Oldest Rocks, pp. 607-667.
Müller, R., Dutkiewicz, A., Seton, M., Gaina, C., 2013. Seawater chemistry driven by supercontinent assembly, breakup, and dispersal. Geology 41, 907-910.
Murray, C., 2007. Devonian supra-subduction zone setting for the Princhester and Northumberland Serpentinites: implications for the tectonic evolution of the northern New England Orogen. Australian Journal of Earth Sciences 54, 899-925.
Myers, J.S., Shaw, R.D., Tyler, I.M., 1996. Tectonic evolution of Proterozoic Australia. Tectonics 15, 1431-1446.
Na, L., Kiessling, W., 2015. Diversity partitioning during the Cambrian radiation. Proc Natl Acad Sci U S A 112, 4702-4706.

Nance, R.D., Murphy, J.B., 2019. Supercontinents and the case for Pannotia. Geological Society, London, Special Publications 470, 65-86.
Nebel, O., Campbell, I.H., Sossi, P.A., Van Kranendonk, M.J., 2014. Hafnium and iron isotopes in early Archean komatiites record a plume-driven convection cycle in the Hadean Earth. Earth and Planetary Science Letters 397, 111-120.
Nogi, Y., Jokat, W., Kitada, K., Steinhage, D., 2013. Geological structures inferred from airborne geophysical surveys around Lützow-Holm Bay, East Antarctica. Precambrian Res. 234, 279-287.
Norvick, M., Smith, M., 2001. Mapping the plate tectonic reconstruction of southern and southeastern Australia and implications for petroleum systems. The APPEA Journal 41, 15-35.
Nutman, A.P., 2001. On the scarcity of > 3900 Ma detrital zircons in >= 3500 Ma metasediments. Precambrian Res. 105, 93-114.
Nutman, A.P., Friend, C.R.L., Horie, K., Hidaka, H., 2007. Chapter 3.3 The Itsaq Gneiss Complex of Southern West Greenland and the Construction of Eoarchaean Crust at Convergent Plate Boundaries, Earth's Oldest Rocks, pp. 187-218.
O'Hara, M.J., Fry, N., Prichard, H.M., 2001. Minor phases as carriers of trace elements in non-modal crystal–liquid separation processes II: Illustrations and bearing on behaviour of REE, U, Th and the PGE in igneous processes. Journal of Petrology 42, 1887-1910.
O'Reilly, S.Y., Zhang, M., 1995. Geochemical characteristics of lava-field basalts from eastern Australia and inferred sources: connections with the subcontinental lithospheric mantle? Contributions to Mineralogy and Petrology 121, 148.
Offler, R., Fergusson, C.L., 2016. Proto-Pacific-margin source for the Ordovician turbidite submarine fan, Lachlan Orogen, southeast Australia: Geochemical constraints. Sedimentary Geology 334, 53-65.
Oliveira, E.P., Bueno, J.F., McNaughton, N.J., Silva Filho, A.F., Nascimento, R.S., Donatti-Filho, J.P., 2015. Age, composition, and source of continental arc-and syn-collision granites of the Neoproterozoic Sergipano Belt, Southern Borborema Province, Brazil. Journal of South American Earth Sciences 58, 257-280.
Orejana, D., Martínez, E.M., Villaseca, C., Andersen, T., 2015. Ediacaran–Cambrian paleogeography and geodynamic setting of the Central Iberian Zone: constraints from coupled U–Pb–Hf isotopes of detrital zircons. Precambrian Res. 261, 234-251.
Oriolo, S., Oyhantçabal, P., Wemmer, K., Siegesmund, S., 2017. Contemporaneous assembly of Western Gondwana and final Rodinia break-up: implications for the supercontinent cycle. Geoscience Frontiers 8, 1431-1445.
Page, R., 1974. Implications of new geochronological data in the Alligator Rivers area, Northern Territory, BMR Symposium Canberra.
Page, R., 1976. Geochronology of Archaean and Lower Proterozoic rocks in the Rum Jungle-Alligator River area, Northern Territory, Australia, 25th Int. Geol. Congr., Sydney, Abstr., p. 18.
Page, R., Sun, S., 1994. Evolution of the Kimberley region, WA and adjacent Proterozoic inliers—new geochronological constraints, Geological Society of Australia Abstracts, pp. 332-333.
Palfreyman, W.D., Adkins, J., 1984. Guide to the Geology of Australia. Unknown.
Pankhurst, R.J., Rapela, C.W., Fanning, C., Márquez, M., 2006. Gondwanide continental collision and the origin of Patagonia. Earth-Science Reviews 76, 235-257.
Pankhurst, R.J., Riley, T.R., Fanning, C.M., Kelley, S.P., 2000. Episodic silicic volcanism in Patagonia and the Antarctic Peninsula: Chronology of magmatism associated with the break-up of Gondwana. Journal of Petrology 41, 605-625.
Patchett, P., Tatsumoto, M., 1981. A routine high-precision method for Lu-Hf isotope geochemistry and chronology. Contributions to Mineralogy and Petrology 75, 263-267.

Paton, C., Hellstrom, J., Paul, B., Woodhead, J., Hergt, J., 2011. Iolite: Freeware for the visualisation and processing of mass spectrometric data. Journal of Analytical Atomic Spectrometry 26, 2508-2518.
Paulsen, T., Deering, C., Sliwinski, J., Bachmann, O., Guillong, M., 2017a. New detrital zircon age and trace element evidence for 1450 Ma igneous zircon sources in East Antarctica. Precambrian Res. 300, 53-58.
Paulsen, T., Deering, C., Sliwinski, J., Valencia, V., Bachmann, O., Guillong, M., 2017b. Detrital zircon ages and trace element compositions of Permian-Triassic foreland basin strata of the Gondwanide orogen, Antarctica. Geosphere 13, 2085-2093.
Payne, J.L., Hand, M., Pearson, N.J., Barovich, K.M., McInerney, D.J., 2015. Crustal thickening and clay: Controls on O isotope variation in global magmatism and siliciclastic sedimentary rocks. Earth and Planetary Science Letters 412, 70-76.
Payne, J.L., McInerney, D.J., Barovich, K.M., Kirkland, C.L., Pearson, N.J., Hand, M., 2016. Strengths and limitations of zircon Lu-Hf and O isotopes in modelling crustal growth. Lithos 248, 175-192.
Pearson, D.G., Parman, S.W., Nowell, G.M., 2007. A link between large mantle melting events and continent growth seen in osmium isotopes. Nature 449, 202-205.
Pell, S.D., 1994. The provenance of the Australian continental dunefields.
Pell, S.D., Williams, I.S., Chivas, A.R., 1997a. The use of protolith zircon-age fingerprints in determining the protosource areas for some Australian dune sands. Sedimentary Geology 109, 233-260.
Pell, S.D., Williams, I.S., Chivas, A.R., 1997b. The use of protolith zircon-age fingerprints in determining the protosource areas for some Australian dune sands. Sedimentary Geology 109, 233-260.
Peucat, J., Hirata, T., Nesbitt, R., 1995. REE fractionation (ICPMS LASER) evidence in metamorphic zircons during granulite facies metamorphism and anatectic processes, Terra Abstracts, p. 346.
Phillips, G., Wilson, C.J.L., Campbell, I.H., Allen, C.M., 2006. U-th-pb detrital zircon geochronology from the southern Prince Charles Mountains, East Antarctica - Defining the Archaean to Neoproterozoic Ruker Province. Precambrian Res. 148, 292-306.
Pidgeon, R.T., Wilde, S.A., 1990. The Distribution of 3.0-Ga and 2.7-Ga Volcanic Episodes in the Yilgarn Craton of Western-Australia. Precambrian Res. 48, 309-325.
Pierce, E.L., Hemming, S.R., Williams, T., van de Flierdt, T., Thomson, S.N., Reiners, P.W., Gehrels, G.E., Brachfeld, S.A., Goldstein, S.L., 2014. A comparison of detrital U–Pb zircon, 40Ar/39Ar hornblende, 40Ar/39Ar biotite ages in marine sediments off East Antarctica: Implications for the geology of subglacial terrains and provenance studies. Earth-Science Reviews 138, 156-178.
Piper, J.D., 2015. The Precambrian supercontinent Palaeopangaea: two billion years of quasi-integrity and an appraisal of geological evidence. International Geology Review 57, 1389-1417.
Pisarevsky, S.A., Wingate, M.T., Powell, C.M., Johnson, S., Evans, D.A., 2003. Models of Rodinia assembly and fragmentation. Geological Society, London, Special Publications 206, 35-55.
Pons, M.L., Fujii, T., Rosing, M., Quitte, G., Telouk, P., Albarede, F., 2013. A Zn isotope perspective on the rise of continents. Geobiology 11, 201-214.
Poupinet, G., Shapiro, N.M., 2009. Worldwide distribution of ages of the continental lithosphere derived from a global seismic tomographic model. Lithos 109, 125-130.
Preiss, W.V., 2000. The Adelaide Geosyncline of South Australia and its significance in Neoproterozoic continental reconstruction. Precambrian Res. 100, 21-63.
Puetz, S.J., Condie, K.C., Pisarevsky, S., Davaille, A., Schwarz, C.J., Ganade, C.E., 2017. Quantifying the evolution of the continental and oceanic crust. Earth-Science Reviews 164, 63-83.

Pujol, M., Marty, B., Burgess, R., Turner, G., Philippot, P., 2013. Argon isotopic composition of Archaean atmosphere probes early Earth geodynamics. Nature 498, 87-90.
Queensland, G.S.o., 2011. North-west Queensland Mineral and Energy Province Report. Department of Employment, Economic Development and Innovation.
Reid, A.J., Hand, M., 2012. Mesoarchean to mesoproterozoic evolution of the southern Gawler Craton, South Australia. Episodes 35, 216-225.
Reinhard, C.T., Planavsky, N.J., Gill, B.C., Ozaki, K., Robbins, L.J., Lyons, T.W., Fischer, W.W., Wang, C., Cole, D.B., Konhauser, K.O., 2017. Evolution of the global phosphorus cycle. Nature 541, 386-389.
Rignot, E., Mouginot, J., Scheuchl, B., 2011. Ice flow of the Antarctic ice sheet. Science 333, 1427-1430.
Riley, T.R., Burton-Johnson, A., Flowerdew, M.J., Whitehouse, M.J., 2018. Episodicity within a mid-Cretaceous magmatic flare-up in West Antarctica: U-Pb ages of the Lassiter Coast intrusive suite, Antarctic Peninsula, and correlations along the Gondwana margin. Geological Society of America Bulletin 130, 1177-1196.
Riley, T.R., Flowerdew, M.J., Whitehouse, M.J., 2012. U-Pb ion-microprobe zircon geochronology from the basement inliers of eastern Graham Land, Antarctic Peninsula. Journal of the Geological Society 169, 381-393.
Rino, S., Komiya, T., Windley, B.F., Katayama, I., Motoki, A., Hirata, T., 2004. Major episodic increases of continental crustal growth determined from zircon ages of river sands; implications for mantle overturns in the Early Precambrian. Physics of the Earth and Planetary Interiors 146, 369-394.
Rino, S., Kon, Y., Sato, W., Maruyama, S., Santosh, M., Zhao, D., 2008. The Grenvillian and Pan-African orogens: World's largest orogenies through geologic time, and their implications on the origin of superplume. Gondwana Research 14, 51-72.
Roberts, N.M.W., Spencer, C.J., 2015. The zircon archive of continent formation through time. Geological Society, London, Special Publications 389, 197-225.
Rogers, J.J., 1993. India and Ur. Journal of Geological Society of India (Online archive from Vol 1 to Vol 78) 42, 217-222.
Roy, M., van de Flierdt, T., Hemming, S.R., Goldstein, S.L., 2007. 40Ar/39Ar ages of hornblende grains and bulk Sm/Nd isotopes of circum-Antarctic glacio-marine sediments: Implications for sediment provenance in the southern ocean. Chemical Geology 244, 507-519.
Rubatto, D., 2002. Zircon trace element geochemistry: partitioning with garnet and the link between U-Pb ages and metamorphism. Chemical Geology 184, 123-138.
Rubatto, D., 2017. Zircon: The Metamorphic Mineral. Reviews in Mineralogy and Geochemistry 83, 261-295.
Rubatto, D., Hermann, J., 2003. Zircon formation during fluid circulation in eclogites (Monviso, Western Alps): implications for Zr and Hf budget in subduction zones. Geochim. Cosmochim. Acta 67, 2173-2187.
Rubatto, D., Hermann, J., Buick, I.S., 2006. Temperature and bulk composition control on the growth of monazite and zircon during low-pressure anatexis (Mount Stafford, central Australia). Journal of Petrology 47, 1973-1996.
Rudnick, R.L., 1995. Making Continental-Crust. Nature 378, 571-578.
Rudnick, R.L., Gao, S., 2003. Composition of the Continental Crust, in: Holland, H.D., Turekian, K.K. (Eds.), Treatise on Geochemistry. Pergamon, Oxford, pp. 1-64.
Rudnick, R.L., Gao, S., 2014. Composition of the Continental Crust, Treatise on Geochemistry, pp. 1-51.
Sawka, W.N., Banfield, J.F., Chappell, B.W., 1986. A weathering-related origin of widespread monazite in S-type granites. Geochim. Cosmochim. Acta 50, 171-175.

Schaltegger, U., Fanning, C.M., Günther, D., Maurin, J.C., Schulmann, K., Gebauer, D., 1999. Growth, annealing and recrystallization of zircon and preservation of monazite in high-grade metamorphism: conventional and in-situ U-Pb isotope, cathodoluminescence and microchemical evidence. Contributions to Mineralogy and Petrology 134, 186-201.
Scheinert, M., Ferraccioli, F., Schwabe, J., Bell, R., Studinger, M., Damaske, D., Jokat, W., Aleshkova, N., Jordan, T., Leitchenkov, G., 2016. New Antarctic gravity anomaly grid for enhanced geodetic and geophysical studies in Antarctica. Geophysical Research Letters 43, 600-610.
Schmidt, M.W., Jagoutz, O., 2017. The global systematics of primitive arc melts. Geochemistry, Geophysics, Geosystems 18, 2817-2854.
Scotese, C.R., 2009. Late Proterozoic plate tectonics and palaeogeography: a tale of two supercontinents, Rodinia and Pannotia. Geological Society, London, Special Publications 326, 67-83.
Scrimgeour, I.R., Kinny, P.D., Close, D.F., Edgoose, C.J., 2005. High-T granulites and polymetamorphism in the southern Arunta Region, central Australia: Evidence for a 1.64 Ga accretional event. Precambrian Res. 142, 1-27.
Sepulveda, F.A., Palma-Heldt, S., Herve, F., Fanning, C.M., 2010. Permian depositional age of metaturbidites of the Duque de York Complex, southern Chile: U-Pb SHRIMP data and palynology. Andean Geology 37, 375-397.
Shaw, R., Tyler, I., Griffin, T., Webb, A., 1992. New K-Ar constraints on the onset of subsidence in the Canning Basin, Western Australia. BMR Journal of Australian Geology and Geophysics 13, 31-35.
Shaw, R., Wellman, P., Gunn, P., Whitaker, A., Tarlowski, C., Morse, M., 1995. Australian crustal elements map. AGSO Res. Newslett 23, 1-3.
Shaw, S.E., Flood, R.H., 1981. The New England Batholith, Eastern Australia - Geochemical Variations in Time and Space. Journal of Geophysical Research 86, 530-544.
Sheppard, S., Page, R., Griffin, T., Rasmussen, B., Fletcher, I., Tyler, I., Kirkland, C., Wingate, M., Hollis, J., Thorne, A., 2012. Geochronological and isotopic constraints on the tectonic setting of the c. 1800 Ma Hart Dolerite and the Kimberley and Speewah Basins, northern Western Australia. Geological Survey of Western Australia Record 7, 1-28.
Shields, G., Veizer, J., 2002. Precambrian marine carbonate isotope database: Version 1.1. Geochemistry, Geophysics, Geosystems 3, 1 of 12-12 of 12.
Shirey, S.B., Richardson, S.H., 2011. Start of the Wilson cycle at 3 Ga shown by diamonds from subcontinental mantle. Science 333, 434-436.
Siddoway, C.S., Fanning, C.M., 2009. Paleozoic tectonism on the East Gondwana margin: Evidence from SHRIMP U-Pb zircon geochronology of a migmatite-granite complex in West Antarctica. Tectonophysics 477, 262-277.
Silva, T.R., Ferreira, V.P., Lima, M.M.C., Sial, A.N., 2016. Two stage mantle-derived granitic rocks and the onset of the Brasiliano orogeny: Evidence from Sr, Nd, and O isotopes. Lithos 264, 189-200.
Smithies, R., Howard, H., Evins, P., Kirkland, C., Kelsey, D., Hand, M., Wingate, M., Collins, A., Belousova, E., Allchurch, S., 2010. Geochemistry, geochronology and petrogenesis of Mesoproterozoic felsic rocks in the west Musgrave Province, Central Australia, and implications for the Mesoproterozoic tectonic evolution of the region. Geological Survey of Western Australia.
Söderlund, U., Patchett, P.J., Vervoort, J.D., Isachsen, C.E., 2004. The 176Lu decay constant determined by Lu–Hf and U–Pb isotope systematics of Precambrian mafic intrusions. Earth and Planetary Science Letters 219, 311-324.

Speer, J.A., Cooper, B.J., 1982. Crystal structure of synthetic hafnon, HfSiO4, comparison with zircon and the actinide orthosilicates. American Mineralogist 67, 804-808.
Spencer, C.J., Cawood, P.A., Hawkesworth, C.J., Prave, A.R., Roberts, N.M.W., Horstwood, M.S.A., Whitehouse, M.J., Eimf, 2015. Generation and preservation of continental crust in the Grenville Orogeny. Geoscience Frontiers 6, 357-372.
Spencer, C.J., Cawood, P.A., Hawkesworth, C.J., Raub, T.D., Prave, A.R., Roberts, N.M.W., 2014. Proterozoic onset of crustal reworking and collisional tectonics: Reappraisal of the zircon oxygen isotope record. Geology 42, 451-454.
Squire, R., Campbell, I., Allen, C., Wilson, C., 2006. Did the Transgondwanan Supermountain trigger the explosive radiation of animals on Earth? Earth and Planetary Science Letters 250, 116-133.
Stacey, J.S., Kramers, J.D., 1975. Approximation of terrestrial lead isotope evolution by a two-stage model. Earth and Planetary Science Letters 26, 207-221.
Stein, J.L., Hutchinson, M.F., Stein, J.A., 2014. A new stream and nested catchment framework for Australia. Hydrol. Earth Syst. Sci. 18, 1917-1933.
Stein, M., Hofmann, A.W., 1994. Mantle Plumes and Episodic Crustal Growth. Nature 372, 63-68.
Stepanov, A.S., Hermann, J., Rubatto, D., Rapp, R.P., 2012. Experimental study of monazite/melt partitioning with implications for the REE, Th and U geochemistry of crustal rocks. Chemical Geology 300-301, 200-220.
Stern, R.J., 2005. Evidence from ophiolites, blueschists, and ultrahigh-pressure metamorphic terranes that the modern episode of subduction tectonics began in Neoproterozoic time. Geology 33, 557-560.
Stüwe, K., Oliver, R., 1989. Geological history of Adélie Land and King George V Land, Antarctica: evidence for a polycyclic metamorphic evolution. Precambrian Res. 43, 317-334.
Szpunar, M., Hand, M., Barovich, K., Jagodzinski, E., Belousova, E., 2011. Isotopic and geochemical constraints on the Paleoproterozoic Hutchison Group, southern Australia: Implications for Paleoproterozoic continental reconstructions. Precambrian Res. 187, 99-126.
Tang, M., Erdman, M., Eldridge, G., Lee, C.A., 2018. The redox "filter" beneath magmatic orogens and the formation of continental crust. Sci Adv 4, eaar4444.
Tang, M., Ji, W.-Q., Chu, X., Wu, A., Chen, C., 2021. Reconstructing crustal thickness evolution from europium anomalies in detrital zircons. Geology 49, 76-80.
Taylor, R., Harley, S., Hinton, R., Elphick, S., Clark, C., Kelly, N., 2015. Experimental determination of REE partition coefficients between zircon, garnet and melt: A key to understanding high‐T crustal processes. Journal of Metamorphic Geology 33, 231-248.
Taylor, S.R., 1967. The origin and growth of continents. Tectonophysics 4, 17-34.
Taylor, S.R., Mclennan, S.M., 1995. The Geochemical Evolution of the Continental-Crust. Reviews of Geophysics 33, 241-265.
Thirlwall, M.F., Anczkiewicz, R., 2004. Multidynamic isotope ratio analysis using MC-ICP-MS and the causes of secular drift in Hf, Nd and Pb isotope ratios. International Journal of Mass Spectrometry 235, 59-81.
Tingey, R.J., 1991. The geology of Antarctica. Oxford University Press.
Touret, J., Santosh, M., Huizenga, J., 2016. High-temperature granulites and supercontinents. Geoscience Frontiers 7, 101-113.
Trendall, A.F., Compston, W., Nelson, D.R., De Laeter, J.R., Bennett, V.C., 2004. SHRIMP zircon ages constraining the depositional chronology of the Hamersley Group, Western Australia. Australian Journal of Earth Sciences 51, 621-644.
Tyler, I.M., Hocking, R.M., Haines, P.W., 2012. Geological evolution of the Kimberley region of Western Australia. Episodes 35, 298-306.

Valley, J.W., 2003. Oxygen Isotopes in Zircon. Reviews in Mineralogy and Geochemistry 53, 343-385.
Valley, J.W., Kinny, P.D., Schulze, D.J., Spicuzza, M.J., 1998. Zircon megacrysts from kimberlite: oxygen isotope variability among mantle melts. Contributions to Mineralogy and Petrology 133, 1-11.
Valley, J.W., Lackey, J.S., Cavosie, A.J., Clechenko, C.C., Spicuzza, M.J., Basei, M.A.S., Bindeman, I.N., Ferreira, V.P., Sial, A.N., King, E.M., Peck, W.H., Sinha, A.K., Wei, C.S., 2005. 4.4 billion years of crustal maturation: oxygen isotope ratios of magmatic zircon. Contributions to Mineralogy and Petrology 150, 561-580.
Van Kranendonk, M.J., 2006. Volcanic degassing, hydrothermal circulation and the flourishing of early life on Earth: A review of the evidence from c. 3490-3240 Ma rocks of the Pilbara Supergroup, Pilbara Craton, Western Australia. Earth-Science Reviews 74, 197-240.
Van Kranendonk, M.J., Hickman, A.H., Smithies, R.H., Nelson, D.R., Pike, G., 2002. Geology and tectonic evolution of the archean North Pilbara terrain, Pilbara Craton, Western Australia. Economic Geology 97, 695-732.
Van Kranendonk, M.J., Kirkland, C.L., Cliff, J., 2015. Oxygen isotopes in Pilbara Craton zircons support a global increase in crustal recycling at 3.2 Ga. Lithos 228-229, 90-98.
Veevers, J.J., 2006. Updated gondwana (Permian-Cretaceous) earth history of Australia. Gondwana Research 9, 231-260.
Veevers, J.J., 2007. Pan-Gondwanaland post-collisional extension marked by 650-500 Ma alkaline rocks and carbonatites and related detrital zircons: A review. Earth-Science Reviews 83, 1-47.
Veevers, J.J., 2015. Beach sand of SE Australia traced by zircon ages through Ordovician turbidites and S-type granites of the Lachlan Orogen to Africa/Antarctica: a review. Australian Journal of Earth Sciences 62, 385-408.
Vermeesch, P., 2018. IsoplotR: A free and open toolbox for geochronology. Geoscience Frontiers 9, 1479-1493.
Vervoort, J.D., Blichert-Toft, J., 1999. Evolution of the depleted mantle: Hf isotope evidence from juvenile rocks through time. Geochim. Cosmochim. Acta 63, 533-556.
Vervoort, J.D., Kemp, A.I.S., 2016. Clarifying the zircon Hf isotope record of crust-mantle evolution. Chemical Geology 425, 65-75.
Villaseca, C., Romera, C.M., De la Rosa, J., Barbero, L., 2003. Residence and redistribution of REE, Y, Zr, Th and U during granulite-facies metamorphism: behaviour of accessory and major phases in peraluminous granulites of central Spain. Chemical Geology 200, 293-323.
Voice, P.J., Kowalewski, M., Eriksson, K.A., 2011. Quantifying the Timing and Rate of Crustal Evolution: Global Compilation of Radiometrically Dated Detrital Zircon Grains. Journal of Geology 119, 109-126.
Wade, B.P., Barovich, K.M., Hand, M., Scrimgeour, I.R., Close, D.F., 2006. Evidence for early Mesoproterozoic arc magmatism in the Musgrave Block, central Australia: Implications for Proterozoic crustal growth and tectonic reconstructions of Australia. Journal of Geology 114, 43-63.
Walter, M., Veevers, J., 1997. Australian Neoproterozoic palaeogeography, tectonics, and supercontinental connections. AGSO Journal of Australian Geology and Geophysics 17, 73-92.
Walter, M.R., Veevers, J.J., Calver, C.R., Grey, K., 1995. Neoproterozoic Stratigraphy of the Centralian Superbasin, Australia. Precambrian Res. 73, 173-195.
Walternberg, K., Bull, K., Blevin, P., Cronin, D., Armistead, S., 2016. New SHRIMP U-Pb Zircon Ages from the Lachlan Orogen and the New England Orogen, New South Wales: Mineral Systems Projects, July 2015-June 2016. Geoscience Australia.

Wang, C.Y., Campbell, I.H., Allen, C.M., Williams, I.S., Eggins, S.M., 2009. Rate of growth of the preserved North American continental crust: Evidence from Hf and O isotopes in Mississippi detrital zircons. Geochim. Cosmochim. Acta 73, 712-728.
Wang, C.Y., Campbell, I.H., Stepanov, A.S., Allen, C.M., Burtsev, I.N., 2011. Growth rate of the preserved continental crust: II. Constraints from Hf and O isotopes in detrital zircons from Greater Russian Rivers. Geochim. Cosmochim. Acta 75, 1308-1345.
Waschbusch, P., Korsch, R., Beaumont, C., 2009. Geodynamic modelling of aspects of the Bowen, Gunnedah, Surat and Eromanga Basins from the perspective of convergent margin processes. Australian Journal of Earth Sciences 56, 309-334.
Watson, E.B., Harrison, T.M., 1983. Zircon saturation revisited: temperature and composition effects in a variety of crustal magma types. earth and planetary science letters 64, 295-304.
White, A.J.R., Chappell, B.W., 2011. Some supracrustal (S-type) granites of the Lachlan Fold Belt. Earth and Environmental Science Transactions of the Royal Society of Edinburgh 79, 169-181.
Wielandt, D., Bizzarro, M., 2011. A TIMS-based method for the high precision measurements of the three-isotope potassium composition of small samples. Journal of Analytical Atomic Spectrometry 26, 366-377.
Wilde, S.A., Valley, J.W., Peck, W.H., Graham, C.M., 2001. Evidence from detrital zircons for the existence of continental crust and oceans on the Earth 4.4 Gyr ago. Nature 409, 175-178.
Willcox, J., Stagg, H., 1990. Australia's southern margin: a product of oblique extension. Tectonophysics 173, 269-281.
Williams, H., Hoffman, P.F., Lewry, J.F., Monger, J.W., Rivers, T., 1991. Anatomy of North America: thematic geologic portrayals of the continent. Tectonophysics 187, 117-134.
Williams, I., Compston, W., Black, L., Ireland, T., Foster, J., 1984. Unsupported radiogenic Pb in zircon: a cause of anomalously high Pb-Pb, U-Pb and Th-Pb ages. Contributions to Mineralogy and Petrology 88, 322-327.
Williams, I., Goodge, J., Myrow, P., Burke, K., Kraus, J., 2002. Large scale sediment dispersal associated with the late Neoproterozoic assembly of Gondwana [abs], 16th Australian Geological Convention Adelaide. Adelaide, Australia 67, 238.
Williams, I., Pulford, A., 2008. The contribution of geochronology to understanding the Paleozoic geological history of Australia. Australian Journal of Earth Sciences 55, 821-848.
Williams, I.S., 2001. Response of detrital zircon and monazite, and their U-Pb isotopic systems, to regional metamorphism and host-rock partial melting, Cooma Complex, southeastern Australia. Australian Journal of Earth Sciences 48, 557-580.
Williams, I.S., Collins, W.J., 1990. Granite-Greenstone Terranes in the Pilbara Block, Australia, as Coeval Volcano-Plutonic Complexes - Evidence from U-Pb Zircon Dating of the Mount Edgar Batholith. Earth and Planetary Science Letters 97, 41-53.
Williamson, P., Swift, M., O'Brien, G., Falvey, D., 1990. Two-stage Early Cretaceous rifting of the Otway Basin margin of southeastern Australia: Implications for rifting of the Australian southern margin. Geology 18, 75-78.
Woodhead, J.D., Hergt, J.M., 2005. A preliminary appraisal of seven natural zircon reference materials for in situ Hf isotope determination. Geostandards and Geoanalytical Research 29, 183-195.
Worden, K., Carson, C., Scrimgeour, I., Lally, J., Doyle, N., 2008. A revised Palaeoproterozoic chronostratigraphy for the Pine Creek Orogen, northern Australia: Evidence from SHRIMP U–Pb zircon geochronology. Precambrian Res. 166, 122-144.
Worsley, T., Nance, R., Moody, J., 1982. Plate tectonic episodicity: a deterministic model for periodic “Pangeas”. Eos, Transactions of the American Geophysical Union 65, 1104.

Wyche, S., 2007. Chapter 2.6 Evidence of Pre-3100 Ma Crust in the Youanmi and South West Terranes, and Eastern Goldfields Superterrane, of the Yilgarn Craton, Earth's Oldest Rocks, pp. 113-123.
Yakymchuk, C., Brown, C.R., Brown, M., Siddoway, C.S., Fanning, C.M., Korhonen, F.J., 2015. Paleozoic evolution of western Marie Byrd Land, Antarctica. Geological Society of America Bulletin 127, 1464-1484.
Yang, J., Gao, S., Chen, C., Tang, Y.Y., Yuan, H.L., Gong, H.J., Xie, S.W., Wang, J.Q., 2009. Episodic crustal growth of North China as revealed by U-Pb age and Hf isotopes of detrital zircons from modern rivers. Geochim. Cosmochim. Acta 73, 2660-2673.
Young, G.M., 2013. Precambrian supercontinents, glaciations, atmospheric oxygenation, metazoan evolution and an impact that may have changed the second half of Earth history. Geoscience Frontiers 4, 247-261.
Zhang, L., Ren, Z.Y., Xia, X.P., Li, J., Zhang, Z.F., 2015. IsotopeMaker: A Matlab program for isotopic data reduction. International Journal of Mass Spectrometry 392, 118-124.
Zhao, G.C., Sun, M., Wilde, S.A., Li, S.Z., 2004. A Paleo-Mesoproterozoic supercontinent: assembly, growth and breakup. Earth-Science Reviews 67, 91-123.
Zhao, Y.J., Wu, Y.B., Liu, X.C., Gao, S., Wang, H., Zheng, J.P., Yang, S.H., 2016. Distinct zircon U–Pb and O–Hf–Nd–Sr isotopic behaviour during fluid flow in UHP metamorphic rocks: evidence from metamorphic veins and their host eclogite in the Sulu Orogen, China. Journal of Metamorphic Geology 34, 343-362.
Zhu, Z., Campbell, I.H., Allen, C.M., Brocks, J.J., Chen, B., 2022. The temporal distribution of Earth's supermountains and their potential link to the rise of atmospheric oxygen and biological evolution. Earth and Planetary Science Letters 580, 117391.
Zhu, Z., Campbell, I.H., Allen, C.M., Burnham, A.D., 2020. S-type granites: Their origin and distribution through time as determined from detrital zircons. Earth and Planetary Science Letters 536, 116140.
Zhuravlev, A.Y., Wood, R.A., 2018. The two phases of the Cambrian Explosion. Scientific Reports 8, 16656.